

Contents

Preface	5
Summary	7
IR. S. H. BRUNEKREEF	
1 The behaviour of partially prestressed concrete beams loaded in pure bending	9
1.1 Introduction	9
1.2 Definitions	9
1.3 The design method	10
1.4 The experiments	14
1.5 Conclusions	17
IR. J. C. WALRAVEN	
2 Tests on partially prestressed T-beams subjected to shear and bending	18
2.1 Introduction	18
2.2 Experimental investigation	19
2.3 Instrumentation and testing arrangement	21
2.4 Crack development during loading	23
2.5 Analysis of vertical equilibrium during the loading process	27
2.5.1 Analysis techniques	27
2.5.2 Results of analysis	28
2.5.3 Some considerations concerning the shear-carrying capacity of the concrete compression flange	29
2.6 Discussion of design formulas with respect to the test results	31
2.7 Conclusions	35
PROF. IR. A. S. G. BRUGGELING	
3 The redistribution of stresses in axially compressed reinforced concrete column	36
3.1 Introduction	36
3.2 Methods of analysis	36
3.2.1 Rate of creep methods	36
3.2.2 Effective modulus method	40
3.2.3 Comparison of the various methods of analysis	42
3.2.4 Formulas	43
3.3 The experiments	44
3.3.1 Specimens to be tested	44
3.3.2 Test series	45
3.3.3 Concreting – concrete quality	48

3.4	Experimental results	49
3.5	Analysis of experimental results	51
3.5.1	Behaviour on macro and micro scale	51
3.5.2	Relationship.	54
3.5.3	Formulas to calculate the shrinkage shortening of longitudinally reinforced concrete specimens	55
3.5.4	Comparison of results of calculations with formulas and measured values	57
3.5.5	Calculation values given in the recommendations.	59
3.5.6	Deformations after unloading	60
3.6	Conclusions	60
	Acknowledgements	62

PROF. IR. A. S. G. BRUGGELING

4	Time-dependent deflection of partially prestressed concrete beams	63
4.1	Description of time-dependent behaviour in general.	63
4.1.1	Plain concrete	63
4.1.2	Reinforced concrete structures	63
4.1.3	Uncracked reinforced tendons under uniform distributed tensile stresses	64
4.1.4	Cracked reinforced concrete tendon	66
4.1.5	Reinforced concrete beam in bending	67
4.1.6	Influence of prestress on the deformation	70
4.2	Information from literature	70
4.3	The experiments	74
4.4	Analysis of experimental results	76
4.4.1	Deflections at midspan under short term loading	76
4.4.2	Increase in deflection at midspan under sustained load	77
4.4.3	Deformation of the tensile zone under sustained load	78
4.5	Summary of experimental results	80
4.6	Conclusions	80
5	References	82
6	Notation	84
7	Appendices	87

Preface

In the Stevin-Laboratory of Delft University of Technology, a series of investigations started some years ago on the behaviour of partially prestressed concrete. That was, because this type of concrete seemed to be a versatile method which could be applied to many sorts of structures. Unfortunately, there was a lack of knowledge and experience which did not allow to use this method immediately in practice.

In the mean time, the programme has been finished and before a new series begins based on the results of the investigation, a need was felt to publish the results in order to get in discussion with the colleagues of this special field. The FIP-Congress 1978, held in London, was a very suitable facility for this purpose. We would be pleased if we could receive comments and further suggestions.

Besides the authors, most of the members of the Stevin-Laboratory, department for concrete structures, have contributed to the work which is reported here.

Especially the efforts and help of dr. ing. H. W. Reinhardt, ir. J. A. den Uyl and ing. G. Timmers for preparing this edition of Heron are thankfully acknowledged.

Delft, february 1978

The editor

Summary

This publication over partially prestressed concrete contains four parts, two of them dealing with calculation methods and the short time behaviour and two of them considering the long time behaviour of partially prestressed concrete. All four subjects are treated partly theoretically and partly experimentally.

The first part presents a new method, based on the use of a reference force, for the design and analysis of cross-sections of partially prestressed concrete structures loaded in pure bending. The influence of relaxation, shrinkage and creep is taken into account in the reference force.

The method is also useful when mixed reinforcements are used. In the tests the cross-section of the reinforcement and the prestressing steel was varied. The influence of this variation on the behaviour and cracking of partially prestressed concrete beams was studied. The experiments have shown that this design method and the method for crack control is safe and sufficiently accurate.

The second part deals with an investigation into the behaviour of nine partially prestressed concrete T-beams. The variables in this series were the level of prestressing, the transverse reinforcement ratio and the longitudinal reinforcement ratio, the latter being obtained by varying the amounts of prestressing and reinforcing steel. The concrete cube strength was 50 N/mm^2 . All the beams had the same cross-section and the same loading arrangement with a shear span to effective depth ration of 3.1. A great number of strain measurements were performed on the longitudinal and transverse reinforcement, on the top and the bottom face of the beam and at some points on the cracks, so that not only information on the ultimate load state was obtained, but the whole stress development and redistribution could be observed and analysed. The development of the individual load-carrying components, such as transverse reinforcement, compression zone, dowel action and aggregate interlock, was analysed. The stress distribution in the compression flange is compared with results of investigations on biaxially loaded concrete. Design methods are discussed with reference to the test results.

In the third part, a special aspect of time dependent behaviour is considered, namely the redistribution of forces from concrete to reinforcement in an axially compressed reinforced concrete column. This phenomenon can be explained by the influence of shrinkage and creep deformation of concrete.

Bonded reinforcement will partly restrain this deformation. As a result of this restraint, the shrinkage forces and the axial load on the column will be carried by the reinforcement. Thus the part of this load carried by the reinforcement will increase in course of time, and the compressive stresses on the concrete section will relax in course of time.

This mechanism also operates in the tensile zone of partially prestressed concrete

beams when, under sustained load, compressive stresses are acting in the (reinforced) tensile zone. In this tensile zone the redistribution of stresses causes a reduction of the compressive stresses in the concrete. This phenomenon therefore influences the cracking moment and the bending moment of decompression (or neutralisation) of the stresses in the concrete at the centre of the reinforcement and prestressing steel. This is explained in part 4. To check the results of existing design methods, used in practice, with the real behaviour of axial compressed reinforced concrete columns experiments are carried out.

In this report the tests are described and the results analysed. It must be realised that in this case it was possible to calculate the time dependent redistribution of stresses with the “real” values of Young’s modulus, creep and shrinkage. In practice in the design calculation only the values can be used which are expected in the actual structure. Therefore also the sensitivity of the design method and the effect of its parameters on the result, in relationship to values obtained in practice, is of importance.

The fourth part deals with another aspect of time dependent behaviour, these are the time dependent deflections of concrete structures loaded in bending. They must be considered in various types of structure, e.g. in floor slabs of buildings or cantilevered bridges.

The prediction of these time dependent deflections is normally not very easy, because of lack of information based on scientific studies and on experiments. In this respect prestressed concrete structures cause no problems, however the behaviour of uncracked homogeneous sections under the influence of creep and shrinkage of concrete, and the relaxation of steel stressed, are relatively well-known. In reinforced concrete structures, however, the cracked tensile zone complicates this behaviour. Therefore the prediction of deflections is more difficult.

In partially prestressed concrete with a partly cracked tensile zone, the problems of prestressing and cracking are mixed and therefore rather complex. In this report the influences causing deformations of concrete structures will be qualitatively treated. Experiments have shown what influences are important. The results of these experiments will be analysed. Because of the complexity of the problem this report cannot yet give design rules for the various types of concrete structures.

1 The behaviour of partially prestressed concrete beams loaded in pure bending

1.1 Introduction

In the Netherlands and many other countries the use of partially prestressed concrete is not yet allowed. Some reasons for this can be mentioned:

1. A good design method was not available.
2. The discussion about cracking of prestressed structures under service loads is not yet finished.
3. The knowledge in this field obtained by experiments was not sufficient.

In the mean time a new design method was developed at the Delft University of Technology and experimentally tested in the Stevin Laboratory of this University.¹⁾ For these tests two programs were carried out:

Program 1: Partially prestressed concrete (p.p.c.) loaded in pure bending,

Program 2: P.p.c. loaded in pure bending and loaded in bending plus shear.

The aim of this paper is to report on the design method and the tests in which the variation of the reinforcement and the prestressing steel was studied.

This paper describes the tests on p.p.c. loaded in pure bending; the tests on p.p.c. loaded in bending plus shear are described in the paper by J. Walraven.

1.2 Definitions

- Structures in partially prestressed concrete (p.p.c.):
“Prestressed concrete structures in which under certain circumstances tension or limited cracking due to bending moments is allowed”.
- Prestressing force:
“The total normal force in a concrete section”

$$N = A_{st} \cdot \sigma_t + A_{sp} \cdot \sigma_p$$

- Reference force:
“The force at the elastic centre of gravity of both reinforcements ($A_{st} + A_{sp}$), when the concrete stress due to bending moments or tensile forces in that elastic centre of gravity is zero”.
- Degree of prestressing:
“The quotient of the force on the prestressing steel when the 0,2% proof stress is reached and the force in both reinforcements when the reinforcement yields or the 0,2% proof stress is reached. The symbol of the degree of prestressing is λ ”.

¹⁾ The contribution of CUR-Committee C 22 is gratefully acknowledged.

$$\lambda = \frac{A_{sp} \cdot f_{0,2}}{A_{sl} \cdot f_y + A_{sp} \cdot f_{0,2}}$$

- Decompression moment:
“The moment M_0 due to which the stress in the outmost “concrete fibre” of the precompressed tension zone is zero”.
- Cracking moment:
“The moment M_r due to which an accepted risk of cracking occurs”.

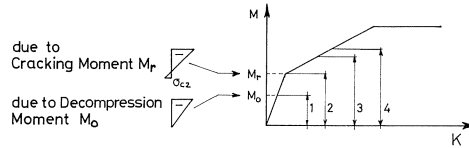


Fig. 1.1. Definition of M_r and M_0 in a moment-curvature diagram.

1.3 The design method

This method is valid for class 1, 2 and 3 in Fig. 1.2.

class	1	2	3	4		
$M_{perm.} + M_{long\ duration}$						
$M_{max.}$						
	prestres. concrete	partially prestressed concrete		reinforced concrete		

Fig. 1.2. Classes of reinforced and prestressed concrete according to CEB.

The design method developed at the Delft University of Technology makes use of the reference force F_{Rt} , in which the influence of relaxation, shrinkage and creep is incorporated on basis of the Dischinger differential equation which is actually only valid for a constant state of stress [43, 44]. Nevertheless, the Dischinger method is still used here for the benefit of simplicity [1, 4].

$$F_{Rt} = F_{R0} \cdot e^{-\eta} + \left(\frac{M \cdot e}{I_c} + \frac{\varepsilon_{cs\infty} \cdot E_c}{\varphi_\infty} \right) \frac{A_c}{\xi} (1 - e^{-\eta}) \quad (1)$$

Where:

$$F_{R0} = A_{sp}(\sigma_{p0} - \Delta\sigma)$$

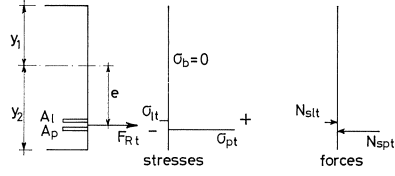


Fig. 1.3. Reference force F_{Rt} .

$$\eta = \frac{n \cdot \omega \cdot \xi \phi_t}{1 + n \omega \xi}$$

$$F_{Rt} = N_{stl} + N_{spt}$$

$$A_s = A_{sl} + A_{sp}$$

$$\sigma_{lt} = (F_{Rt} - F_{R0}) / A_s$$

$$\sigma_{pt} = \left(F_{Rt} + F_{R0} \frac{\omega_e}{\omega_p} \right) / A_s$$

In a cross-section affected only by the imaginary force F_{Rt} all concrete stresses are zero (Fig. 1.3).

Now a reference moment M_{Rt} is defined in such a way that the concrete stresses at the elastic centre of gravity of the reinforcing steel $A_l + A_p$ are zero if the cross-section is only affected by this imaginary moment M_{Rt} .

This moment must be:

$$M_{Rt} = F_{Rt} \cdot e \frac{\xi}{\xi - 1}$$

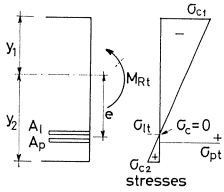


Fig. 1.4.
Reference moment M_{Rt} .

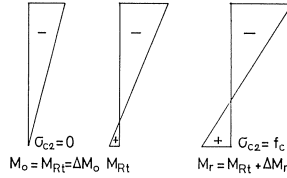


Fig. 1.5.
Stresses due to M_o , M_{Rt} and M_r .

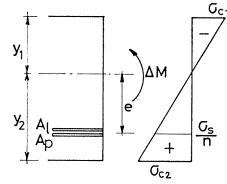


Fig. 1.6.
Stresses due to ΔM .

$$\sigma_{c1} = - \frac{F_{Rt}(y_1 + e)}{A_c e}$$

$$\sigma_{c2} = \frac{F_{Rt}(y_2 - e)}{A_c e}$$

$$\sigma_{lt} = \frac{F_{Rt} - F_{R0}}{A_s}$$

$$\sigma_{pt} = \frac{F_{Rt} + F_{R0} \frac{\omega_l}{\omega_p}}{A_s}$$

$$A_s = A_{sl} + A_{sp}$$

$$\kappa_{Rt} = \frac{(F_{Rt} - F_{R0})e}{E_c \cdot I_c n \omega \xi} + \frac{M(1 - e^{-\eta})}{E_c I_c n \omega \xi^2}$$

Using M_{Rt} makes it easy to calculate the stresses in a cross-section due to a bending moment in the linear elastic state, when the structure is not cracked or the bending moment is smaller than M_0 .

Otherwise it is possible to relate the decompression moment M_0 and the cracking moment M_r at F_{Rt} by means of M_{Rt} . Then we get:

$$M_0 = \frac{F_{Rt} \cdot e}{\xi - 1} \frac{y_2 + y_2 \xi + e}{y_2 + n\omega(y_2 - e)} = F_{Rt} \cdot y_2 \frac{e + k'}{y_2 + n\omega(y_2 - e)} \quad (3)$$

$$M_r = M_0 + f_c \frac{I_c(1 + n\omega \xi)}{y_2 + n\omega(y_2 - e)} \quad (4)$$

The stresses and curvature due to a moment M in the linear elastic state, when the structure is not cracked or the moment is smaller than M_0 , can be calculated by superposition of the stresses and curvature of M_{Rt} and of a moment $\Delta M = M - M_{Rt}$.

The stresses and curvature due to a bending moment ΔM are:

$$\sigma_{c1} = - \frac{\Delta M}{I_c} \frac{y_1 + n\omega(y_1 + e)}{1 + n\omega \xi}$$

$$\sigma_{c2} = \frac{\Delta M}{I_c} \frac{y_2 + n\omega(y_2 - e)}{1 + n\omega \xi}$$

$$\sigma_s = \frac{\Delta M}{I_c} \frac{ne}{1 + n\omega \xi}$$

$$\kappa = \frac{\Delta M}{E_c I_c} \frac{1 + n\omega}{1 + n\omega \xi} \quad (5)$$

In the linear elastic state, when the structure is cracked, the stresses can be calculated with F_{Rt} (Fig. 1.7). The depth of the compression zone h_x can be calculated with formula 6.

$$\frac{M}{F_{Rt}} = \frac{A_{cx} \cdot y_x (h - h_x + y_x + k'_x)}{A_{cx} \cdot y_x - n A_s (h - h_x)} \quad (6)$$

M/F_{Rt} can be calculated with a certain bending moment M .

The true value of h_x can be determined by trying some values of h_x in formula 6 and linear interpolation (Fig. 1.8).

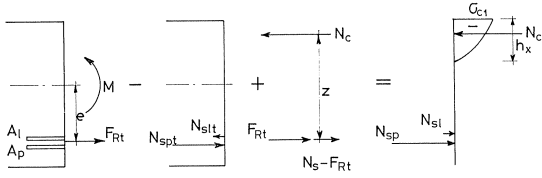


Fig. 1.7. Stresses when the structure is cracked.

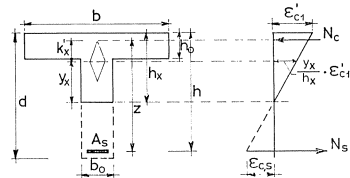


Fig. 1.8. Strains after cracking.

$$\begin{aligned}\sigma_{c1} &= \frac{M h_x}{A_{cx} y_x (h - h_x + y_x + k'_x)} \\ \sigma_{sl} &= \frac{M}{A_s (h - h_x + y_x + k'_x)} - \frac{F_{R0}}{A_s} \\ \sigma_{sp} &= \sigma_{sl} + \frac{F_{R0}}{A_{sp}} \\ \varkappa &= \frac{1}{\nu} \varkappa_{Rt} + \frac{1}{h_x} \varepsilon'_{c1}\end{aligned}\quad (7)$$

A relation between the increase of the stress in the reinforcement and the crack width, formulated at the E.T.H. (Federal Technological University) in Zürich, will be checked [3, 4].

This relation is:

$$\begin{aligned}\text{if } \Delta\sigma_s = 150 \text{ N/mm}^2 &\text{ then } w_{\max} < 0.15 \text{ mm} \\ \Delta\sigma_s = 200 \text{ N/mm}^2 &\quad w_{\max} < 0.24 \text{ mm} \\ \Delta\sigma_s = 240 \text{ N/mm}^2 &\quad w_{\max} < 0.36 \text{ mm}\end{aligned}\quad (8)$$

Where:

$$\Delta\sigma_s = \frac{M}{A_s (h - h_x + y_x + k'_x)} - \frac{F_{Rt}}{A_s}$$

The formula for crack width control in the Netherlands code V.B. 1974 part. E.508 will also be checked [5].

$$\omega_{\max} = 0,8 \Delta\sigma \left(2c + 2,5 \frac{d}{\omega_0} 10^{-5} \right) \text{ mm}\quad (9)$$

Where: d = average diameter

$$\omega_0 = \frac{A_s}{b_0 \cdot h} 100$$

The failure moment can be calculated with:

$$M_u = z_u(A_t f_y + A_p \cdot f_{0,2}) \quad (10)$$

There, the size of the lever arm z_u depends on the geometry of the cross-section.

1.4 The experiments [5]

In order to check the theory, 10 T-section beams were tested in program 1 and 9 beams in program 2.

All the beams were statically loaded in a four point loading test (Fig. 1.9).

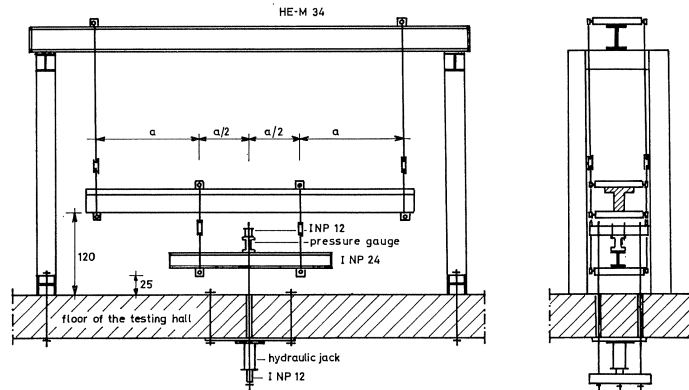


Fig. 1.9. Testing frame.

The cross-sections of the beams of program 1 were all the same, the degree of prestressing λ was varied: $0.64 \leq \lambda \leq 1.00$.

The amount of normal reinforcing steel varied between 0 and 452 mm^2 , whereas the prestressing steel was the same for all beams and consisted in two $\frac{1}{2}$ " strands (see Appendix 1 Table 1).

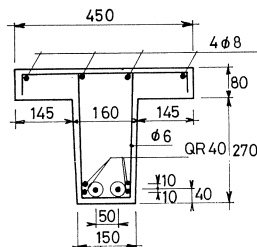


Fig. 1.10.
Cross-section of the beams
of program 1.

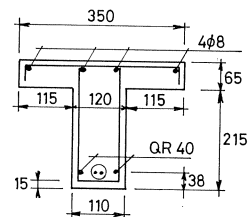


Fig. 1.11.
Cross-section of the beams
of program 2.

The concrete quality was B 30 (average cube strength at 28 days was about 38 N/mm² (Appendix 1 Table 2)).

The cross-sections of the beams of program 2 were all the same, the degree of prestressing was varied: $0 \leq \lambda \leq 0.90$.

The amount of normal reinforcing steel and of prestressing steel both varied according to Table 1: The prestressing tendons were also $\frac{1}{2}$ " strands.

The concrete quality was B45 (average cube strength at 21 days more than 52 N/mm² (Table 2)).

Program 1 will be described here. Where there is a major difference between program 1 and program 2 the value of program 2 will be added in parentheses.

After 3(4) days of hardening of the concrete, the beams were prestressed. After 3(2) weeks the ducts were grouted. The tests were carried out after 4(3) weeks of hardening.

One of the main problems was that of measuring the shrinkage and creep. Normally, shrinkage and creep tests were carried out under the same conditions as the hardening conditions of the beams.

This was impossible in this case, because the testing equipment for shrinkage and creep tests was installed in a special climate-controlled room which was too small for the beams.

Therefore the beams hardened in the testing hall with an average temperature

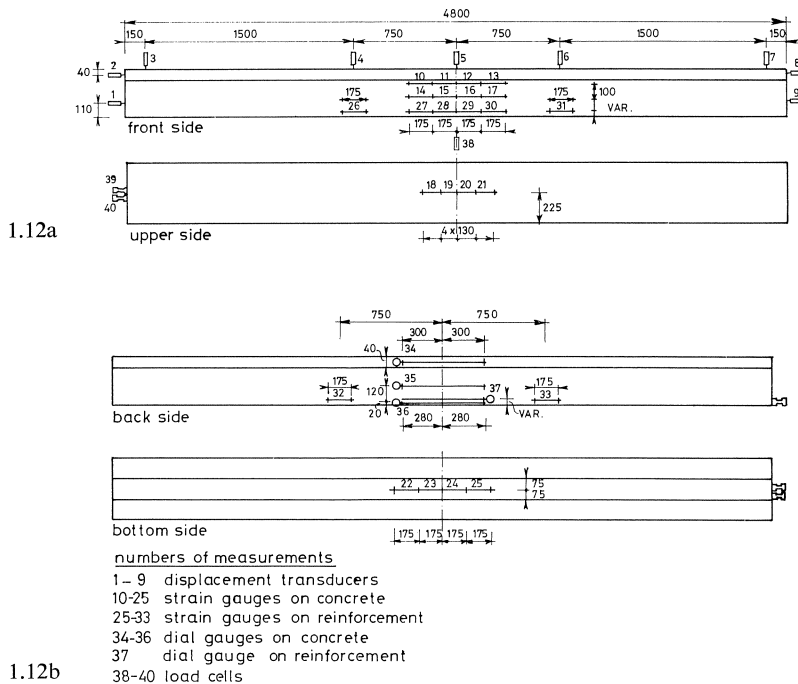


Fig. 1.12. Measuring scheme of programme 1.

of 20°C and relative humidity of 40%, but with considerable fluctuations in temperature and relative humidity.

In order to get the values of shrinkage and creep an indirect determination method was used which will be described now: First, the strains at different levels of the depth of the beams and the force in the strands were measured during the hardening period by dial gauges and pressure gauges, respectively (Fig. 1.12 (1.13) nrs. 34–37 (44–46) and 39 + 40 (41 + 42)).

Before grouting the ducts the force in the strands was changing as a result of relaxation, shrinkage and creep. This was measured with the pressure gauges no.'s (39 + 40 (41 + 42)).

After grouting, the force in the pressure gauges did not change any more because the anchorage of the strands was taken over by bond.

The change in the force in the strands is identical with the change in curvature, so that force F after grouting of the strands can be determined by extrapolation (Fig. 1.14), assuming that no significant relaxation has taken place.

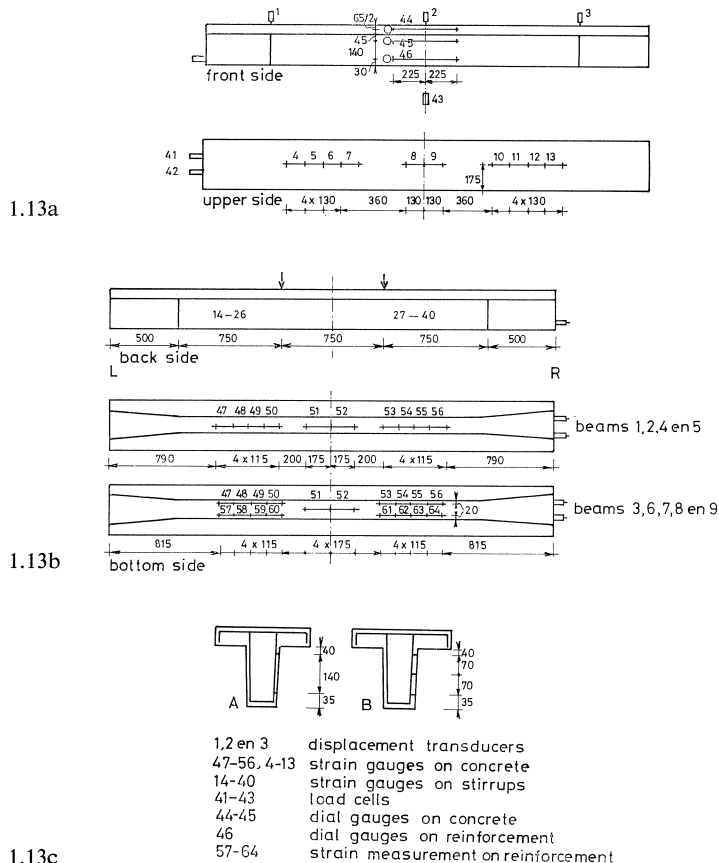


Fig. 1.13. Measuring scheme of programme 2.

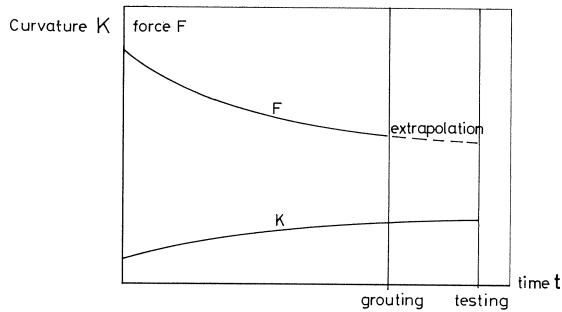


Fig. 1.14. Variation of curvature and force in the prestressing steel, with time, schematically.

The following were measured in the tests:

- the load
- the deflections
- the concrete and reinforcement strains
- the crackwidth (Figs. 1.12 and 1.13).

With the stress-strain relation of the concrete, which was measured on the day of testing, the stresses in the beams in the uncracked and the cracked stage could be calculated and compared with the theoretical results.

The comparison of the results given in the appendix shows that the method described in this paper is sufficiently accurate. It also emerged that the crack widths can be very satisfactorily calculated according to the Netherlands codes for concrete (formula 9).

1.5 Conclusions

Cross-sections of partially prestressed concrete structures can be designed fairly easily with the method described in this paper. It is based on the use of the reference force F_{Rt} in which all the time-dependent losses are taken into account.

The experiments have shown this method to be sufficiently accurate. The method for crack control of the E.T.H. in Zürich is very safe; the more complex Dutch formula is also safe, but does describe the experimental results more accurately.

The calculation of the moment of failure given in this paper gives safe results.

It is also possible to use this method for limit state design.

2 Tests on partially prestressed T-beams subjected to shear and bending

2.1 Introduction

To prevent shear failure in partially prestressed beams it is necessary, as in the case of reinforced and fully prestressed beams, to prevent every possible failure mode.

In principle, four modes of shear failure are distinguished:

a. Web shear failure.

This type of failure occurs when, within the region of the structural span not affected by flexural cracks, the tensile strength of the concrete is reached, resulting in a diagonal crack. In beams of normal proportions, if no shear reinforcement is provided, failure may occur immediately upon the appearance of the shear crack. In this respect partial prestressing would give an increase in strength in relation to a reinforced beam, because the shear cracking load is delayed as a result of the axial compressive stresses.

b. Web crushing failure.

This type of failure may occur in a structural member which is overreinforced in shear; crushing in the inclined concrete struts appears before the yielding stress in the stirrups is reached. This type of failure only occurs in thin webbed beams. It can be demonstrated that a prestressing force has a positive influence on the web crushing strength. In Fig. 2.1. a prestvertical cross-section of a beam with vertical stirrups is considered. If the ultimate concrete compressive strength is given as $\alpha f'_c$ it can be calculated that the vertical component of the web compression forces is equal to

$$V_u = \alpha \cdot f'_{cp} \cdot b_w \cdot z \cdot \cot \theta \cdot \sin^2 \theta$$

The minimum value for this expression is obtained for $\theta = 45^\circ$, being the inclination in a non-prestressed element. Members subjected to an axial compression force show smaller values; hence, partial prestressing leads to a higher web crushing resistance. This subject is dealt with, interalia, in [12].

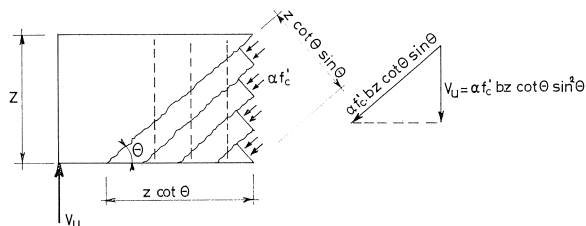


Fig. 2.1. Forces in the case of web crushing.

c. Bond failure.

Bond failure may occur when the longitudinal reinforcement has been designed regardless of the shear influence. Due to the inclined cracking in the shear region the longitudinal reinforcement is subjected to an additional tensile force which may lead to deficient bond when this phenomenon is not considered.

d. Bending shear failure.

This type of failure may occur in regions of the span where flexural cracks have appeared. The failure development usually means an extension of diagonal cracks originating from the flexural cracks from the lower part of the beam up to the compression flange. The final collapse is caused either by crushing or splitting of the concrete compression area above the crack, after yielding of the stirrup reinforcement.

This failure type is the most important one and also the one most frequently discussed.

The study of this failure type in partially prestressed beams is the subject of this article.

2.2 Experimental investigation

Nine beams were tested, in which the effect of the following principal variables was investigated; percentage of web reinforcement, percentage of longitudinal reinforcement and average prestress in the concrete. The dimensions of all beams were the same and are indicated in Fig. 2.2.

The series can be subdivided into three groups with different prestressing levels. Beam 1 was not prestressed, beams 2–5 were prestressed in such a way that the flexural cracking moment would correspond to $M_{f1,cr} = 22,5$ kNm and the corresponding shear force to $V_{f1,cr} = 30$ kN, and beams 6–9 were so prestressed that $M_{f1,cr} = 34$ kNm and $V_{f1,cr} = 45$ kN.

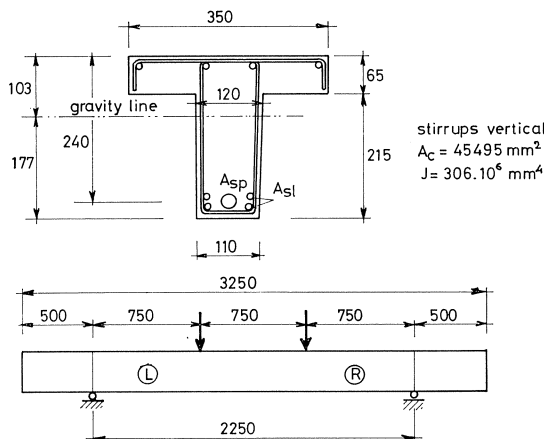


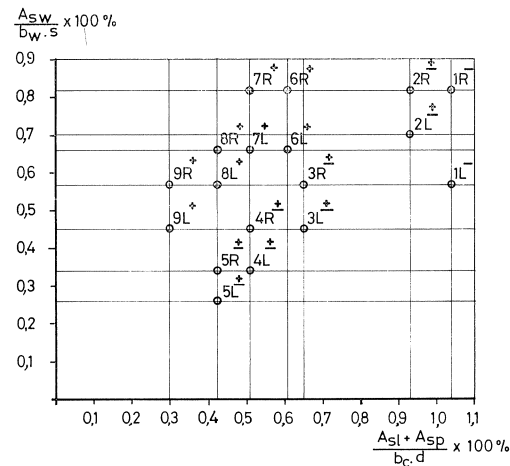
Fig. 2.2. Dimensions of the test beams.

Table 2.1. Details of mechanical and geometrical properties of beams.

specimen	web reinforcement				longitudinal reinforcement						concrete strength			
	left/ right	diam-s mm-mm	A_s/b_{ws} perc.	f_{yw} N/mm ²	A_{sl}		A_{sp} (prestressed)		f_{ypst} N/mm ²	σ_{pe}	$\frac{A_{sp} + A_{sl}}{b_c d} 100\%$	f'_{cem} N/mm ²	f_{cm} N/mm ²	$V_{cr,fl}$ (theor) kN
					nr-diam mm	f_{yls} N/mm ²	$(\frac{1}{8}'' = 93 \text{ mm}^3)$	σ_{pe}						
1	L	Ø5-60	0.57	301	5 Ø16	402	0	1840	-	1.04	47.9	3.3	15	
	R	Ø6-60	0.82	290	4 Ø16	403	$\frac{1}{8}''$	1840	1180	0.93	54.5	3.8	30	
2	L	Ø6-70	0.70	290	4 Ø16	403	$\frac{1}{8}''$	1840	1180	0.93	54.5	3.8	30	
	R	Ø6-60	0.82	290	4 Ø16	403	$\frac{1}{8}''$	1840	1180	0.93	54.5	3.8	30	
3	L	Ø5-75	0.45	301	2 Ø12 + 2 Ø14	444 410	$\frac{1}{8}''$	1840	1142	0.65	50.8	3.9	30	
	R	Ø5-60	0.57	301	2 Ø14	410	$\frac{1}{8}''$	1840	1030	0.51	51.7	3.6	30	
4	L	Ø4-65	0.34	318	2 Ø16	407	$\frac{1}{8}''$	1840	1030	0.51	51.7	3.6	30	
	R	Ø5-75	0.45	301	2 Ø16	407	$\frac{1}{8}''$	1840	1030	0.51	51.7	3.6	30	
5	L	Ø4-85	0.26	318	2 Ø14	410	$\frac{1}{8}''$	1840	913	0.42	56.5	3.5	30	
	R	Ø4-65	0.34	318	2 Ø14	410	$\frac{1}{8}''$	1840	913	0.42	56.5	3.5	30	
6	L	Ø6-75	0.66	290	2 Ø16	423	$2 \times \frac{1}{8}''$	1840	948	0.61	50.8	3.8	45	
	R	Ø6-60	0.82	290	2 Ø16	423	$2 \times \frac{1}{8}''$	1840	948	0.61	50.8	3.8	45	
7	L	Ø6-75	0.66	290	2 Ø14	405	$2 \times \frac{1}{8}''$	1840	916	0.51	52.6	3.8	45	
	R	Ø6-60	0.82	290	2 Ø14	405	$2 \times \frac{1}{8}''$	1840	916	0.51	52.6	3.8	45	
8	L	Ø5-60	0.57	301	2 Ø12	444	$2 \times \frac{1}{8}''$	1840	804	0.43	53.5	3.9	45	
	R	Ø6-75	0.66	290	2 Ø12	444	$2 \times \frac{1}{8}''$	1840	804	0.43	53.5	3.9	45	
9	L	Ø5-75	0.45	301	2 Ø8	442	$2 \times \frac{1}{8}''$	1840	693	0.30	53.2	4.1	45	
	R	Ø5-60	0.57	301	2 Ø8	442	$2 \times \frac{1}{8}''$	1840	693	0.30	53.2	4.1	45	

Within each group the amount of reinforcing steel was varied, while in each individual beam the left (L) and right (R) side contained different amounts of stirrup reinforcement.

Details of the mechanical and geometrical properties are listed in Table 2.1.



- no prestress
- ± average prestress
- + high prestress

Fig. 2.3. Scheme of parameter variation.

Comparison table

variable	constant	comparable beam sides
A_{sl}	A_{sp}	5R-4L
		4R-2L
		9R-8L
		8R-7L
$M_{u,fl}$	$M_{cr,fl}$	7L-6L
		8R-6L
		7R-6R
$A_{sw}/b_w s$	A_{sl}, A_{sp} $M_{cr}, M_{u,fl}$	9 Beams
		L-R
$M_{cr,fl}$	$\frac{A_s}{b_w s}$	3L-9L
		3R-9R
$A_{sl} + A_{sp}$	$M_{u,fl}$	1L-9R
		1L-3R
		2R-7R

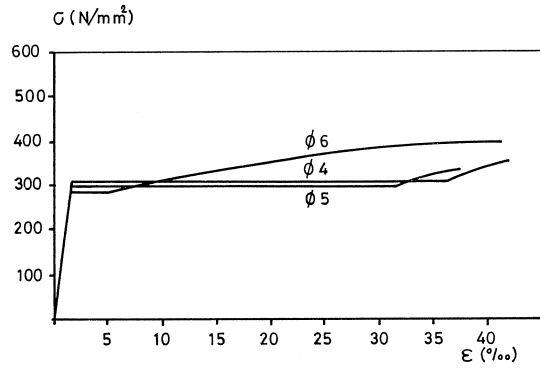
Fig. 2.3 gives a general survey of parameter variation and shows the combinations of beams that have to be compared to study the effect of the parameter variation. The Figs. 2.4a-c give the stress-strain relationships for the types of steel used.

After casting, the beams were covered with plastics sheets. The prestress in beams 2-9 was applied 5 days later, by either one or two $\frac{1}{2}$ " strands, tensioned from one end, while the force in the steel at the other end was measured by a load cell. The strands were anchored individually. The ducts were injected with cement grout 14 days after casting. The tests were carried out 21 days after casting.

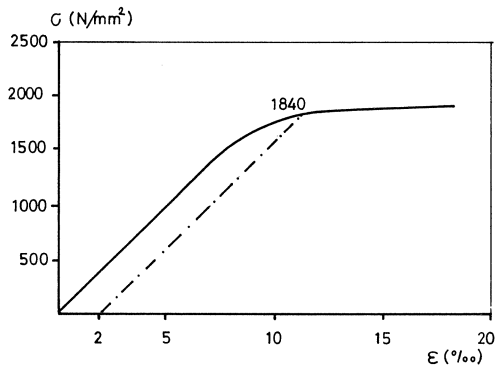
2.3 Instrumentation and testing arrangement

The beams were all simply-supported over a span of 2250 mm and loaded with two symmetrically positioned concentrated loads (Fig. 2.5).

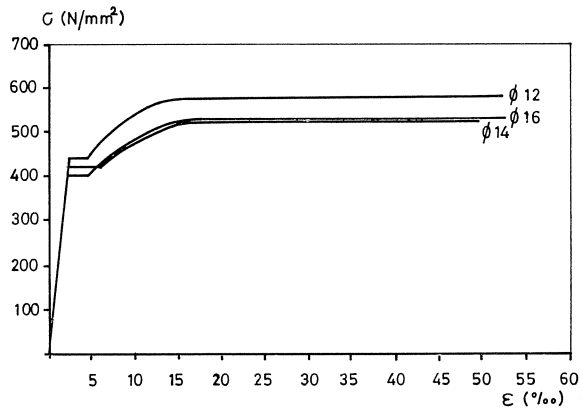
The shear span was 750 mm for all beams, giving a shear span to effective depth ratio of 3.1. The deflection was measured at three points by electrical transducers (Fig. 2.6). The strain in each stirrup was measured by either one or two strain gauges, directly affixed to the stirrup surface. The longitudinal strain distribution at the top of the beam was measured by 10 strain gauges on the surface of the concrete. The strain of the longitudinal reinforcement was directly measured on the steel by 18



a. Stirrups



b. Longitudinal steel



c. Prestressing steel

Fig. 2.4. Stress-strain curves for different steel qualities used.

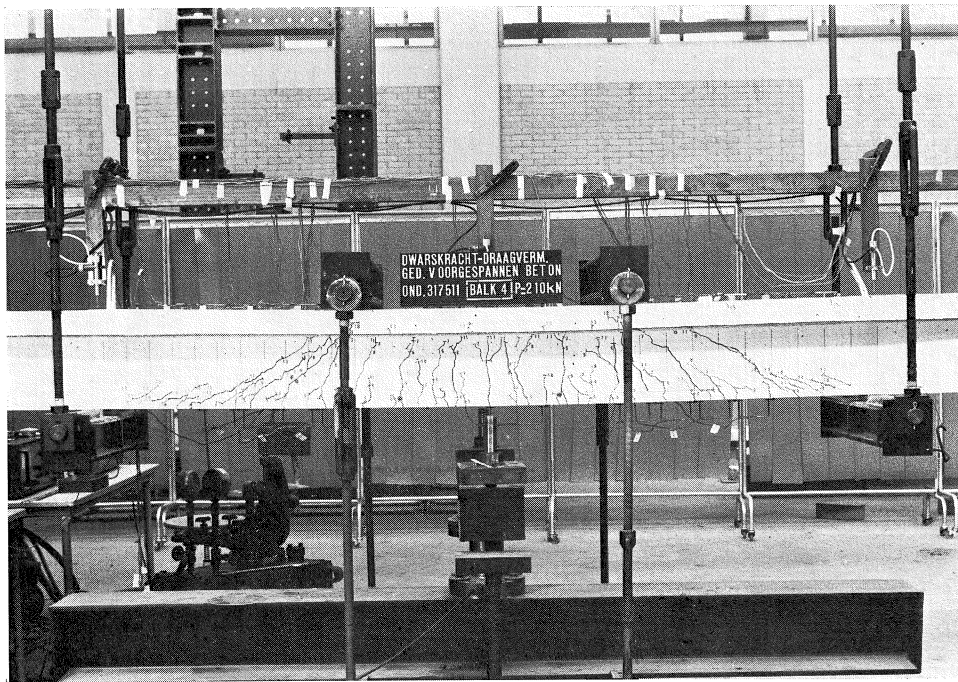


Fig. 2.5. Beam during loading.

strain gauges. Details of the measurements are given in Fig. 2.6. The beams were all loaded incrementally in steps of 20 kN. In interesting loading stages (first shear crack, ultimate load), this step was reduced to 10 kN. After failure of the weaker side of the beam the test was ended, in view of the fact that the other side was also near to failure and no additional information was expected.

2.4 Crack development during loading

During loading four main ranges of crack development can be distinguished.

1. The uncracked loading range.

The first cracks that develop follow the principal stress trajectories. Hence prestressing leads to more flatly inclined cracks.

2. The inclined cracking range.

When both the transverse and the longitudinal reinforcement have been activated, an anisotropic stress situation arises. New cracks appear, having a different inclination. This inclination is influenced by the amounts of transverse and longitudinal steel. A greater amount of transverse steel leads to more steeply inclined cracks. A greater amount of longitudinal steel leads to flatter cracks.

For each beam at both sides the average crack inclination in the web between two sections at distances $\frac{1}{2}d - \frac{3}{4}d$ has been determined, just before the onset of yielding.

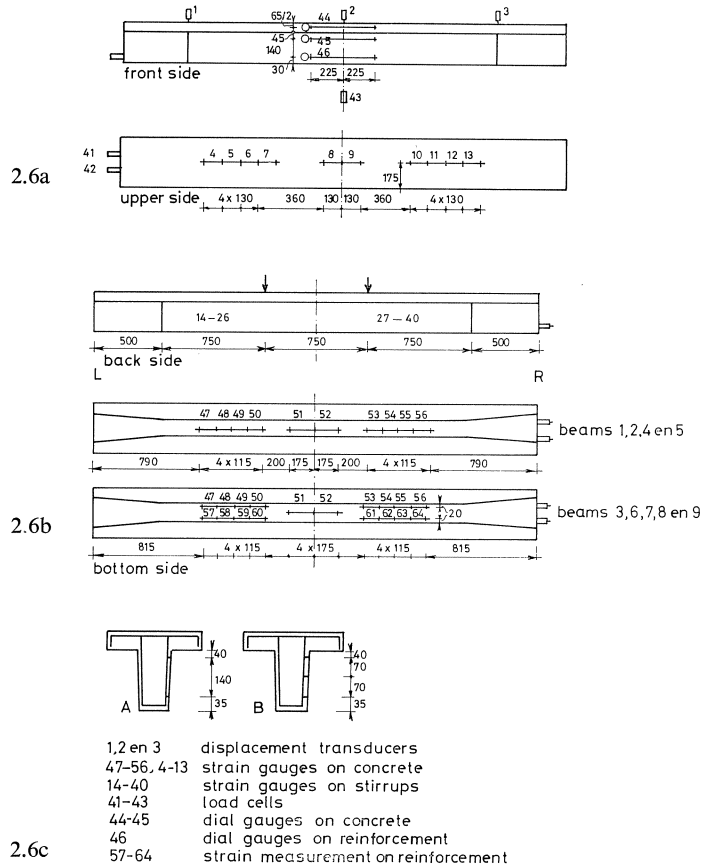


Fig. 2.6. System of measurements.

Only the cracks intersecting the web at mid-depth have been taken into account
 The results are listed in Tables 2.2a and 2.2b.

Table 2.2-a. Measured average crack inclination before stirrup yielding, related to varying amounts of stirrup reinforcement (other parameters constant)

beam	crack incl. (degr.)	transv. reinforcement (%)
1L-1R	40.3-45.3	0.66-0.95
2L-2R	36.7-39.6	0.81-0.95
3L-3R	31.3-41.5	0.52-0.66
4L-4R	36.5-38.3	0.39-0.52
5L-5R	32.7-44.8	0.30-0.39
6L-6R	36.1-36.0	0.76-0.95
7L-7R	34.3-39.3	0.76-0.95
8L-8R	33.5-38.0	0.66-0.76
9L-9R	37.9-38.8	0.52-0.66

Table 2.2-b. Measured average crack inclination before stirrup yielding, related to varying amounts of longitudinal reinforcement, the other parameters being constant

beam	crack incl. (degr.)	long reinforcement (%)
8R-6L	38.0-36.1	0.43-0.61
9R-8L	38.8-33.5	0.30-0.43
4R-3L	38.3-31.3	0.51-0.65
5R-4L	44.8-36.5	0.42-0.51
7R-6R	39.3-36.0	0.51-0.61
8R-7L	38.0-34.3	0.43-0.51

3. The stirrup yielding range.

Yielding of the stirrups did not immediately lead to failure. Due to the fact that the concrete compression flange had a considerable reserve capacity, the load could be greatly increased (Table 2.3). No change in crack inclination was observed in this range.

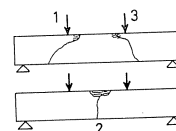


Table 2.3 Summary of test results

specimen	shear force at flexural cracking $V_{cr,fl}$ (kN)	shear force at inclined cracking $V_{cr,s}$ (kN)	shear force at first stirrup yielding (kN)	shear force at failure V_u (kN)	failure place	failure type
1	17	42.5	77.5 (L) 117.5 (R)	126	1	FI (FI)*
2	27	57.5	95 (L) 117.5 (R)	154	2	FI (FI)
3	27	57.5 (L) 67.5 (R)	75 (L) 95 (R)	127	1	C (FI)
4	32	57.5	70 (L) 72.5 (R)	116	1,3	C (C)
5	27	57.5	61.5 (L) 66.5 (R)	100	1,3	C (C)
6	47	77.5	112.5 (L) 122.5 (R)	167	1,3	C (C)
7	47	82.5	107.5 (L) 107.5 (R)	151	1	C (C)
8	42	75	92.5 (L) 96 (R)	145	1	C (C)
9	47	77.5	81 (L) 86.5 (R)	126	1	C (FI)

* In parentheses: expected failure type of the strongest beam-side

4. The ultimate loading range.

In all the beams yielding of the main reinforcement was reached. The crack patterns of all beams in this stage are represented in Fig. 2.8.

The failure mode, as was generally observed, is represented in Fig. 2.7.

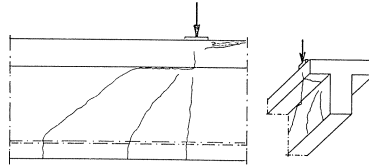


Fig. 2.7. Generally observed failure mode.

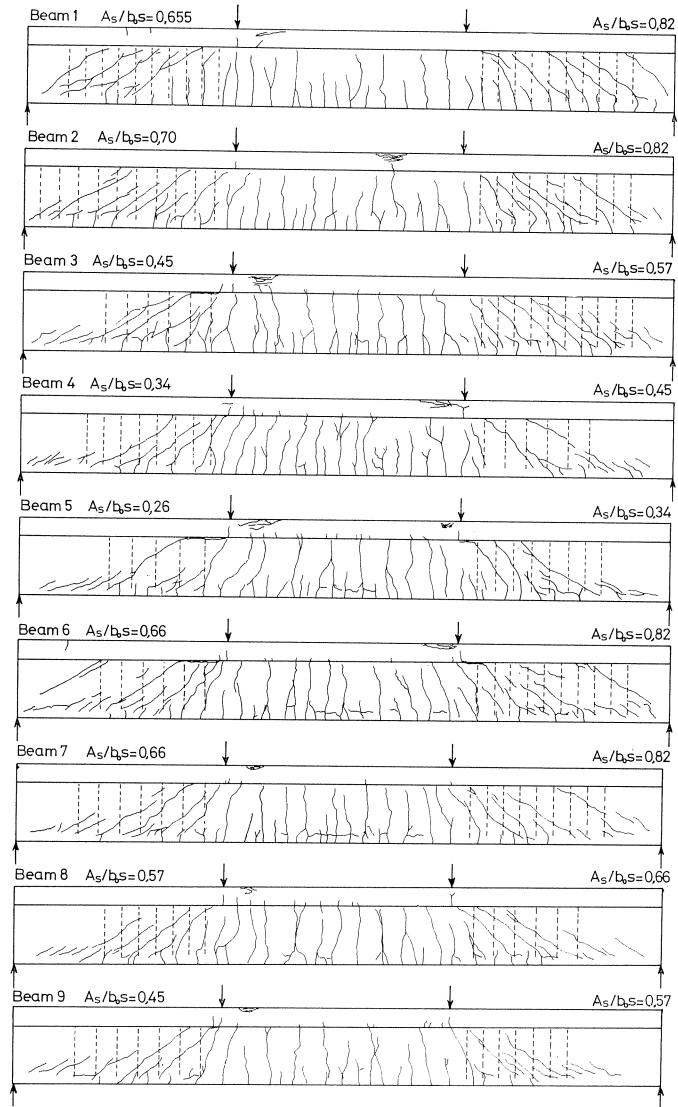


Fig. 2.8. Crack patterns just before failure.

After reaching the compression flange, the inclined crack continued along the edge of the flange, and passed the directly loaded area. In some of the beams the crack continued in the lower part of the compression flange. At the other side of the loading plate the compression zone was reduced and concrete compression failure occurred. This failure mode is indicated as C(ombined) in Table 2.3.

Only beam 2 reached its ultimate load in consequence of “straight” flexural bending failure, in the middle of the constant moment region.

2.5 Analysis of vertical equilibrium during the loading process

2.5.1 Analysis techniques

After inclined cracking has occurred, the shear force is transferred by four components (Fig. 2.9).

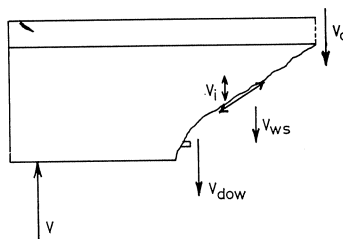


Fig. 2.9. Components providing the internal equilibrium.

V_{dow} = dowel action of the longitudinal reinforcement

V_i = vertical component of aggregate interlock in crack plane

V_{ws} = contribution of the transverse reinforcement across the crack

V_c = contribution of the uncracked compression area.

The determination of the dowel action has been based on a study by Baumann [22], giving expressions for the dowel cracking load and the contribution of the dowel action after a dowel crack is formed.

The contribution of aggregate interlock was determined by a method previously used by Jungwirth [14], comparing the measured crack displacements with the result of interlock tests carried out by Fenwick [20] and Houde/Mirza [21].

The contribution of the transverse reinforcement was determined directly from measurements on the stirrup. A complication is that the stirrup stress is greater than the measured strain multiplied by the steel elasticity modulus, this being due to bond between stirrups and concrete.

The calculation has also been based on the technique of [14], taking these effects into account. As a result of their pronounced yield range, it was possible to determine the contribution of the stirrups after yielding with a fair degree of accuracy.

The contribution of the uncracked concrete compression zone was found by subtracting the three above-mentioned contributions from the total external shear force.

2.5.2 Results of analysis

For all the beams the distribution of forces over the single components was determined. For the beams 1L, 3R, 8L, 9R the distribution is represented in Fig. 2.10.

These beams all contained the same transverse reinforcement, but different longitudinal reinforcement ratios, and different prestressing levels; beam 1 was not prestressed, beam 3 had an average level of prestressing, and beams 8 and 9 a high one.

It can be seen that aggregate interlock affects only the redistribution of forces during the loading process, but does not contribute in general to the ultimate load resistance. However, aggregate interlock plays an important part before the ultimate load stage is reached, as the slope of the inclined cracks can only be influenced by the proportions of transverse and main reinforcement by virtue of this phenomenon.

As can be expected, dowel action increased with increasing amount of longitudinal reinforcement.

Due to the fact that aggregate interlock and dowel action are more pronounced when the longitudinal reinforcement is higher, the increase in stirrup stress is less steep (Fig. 2.11).

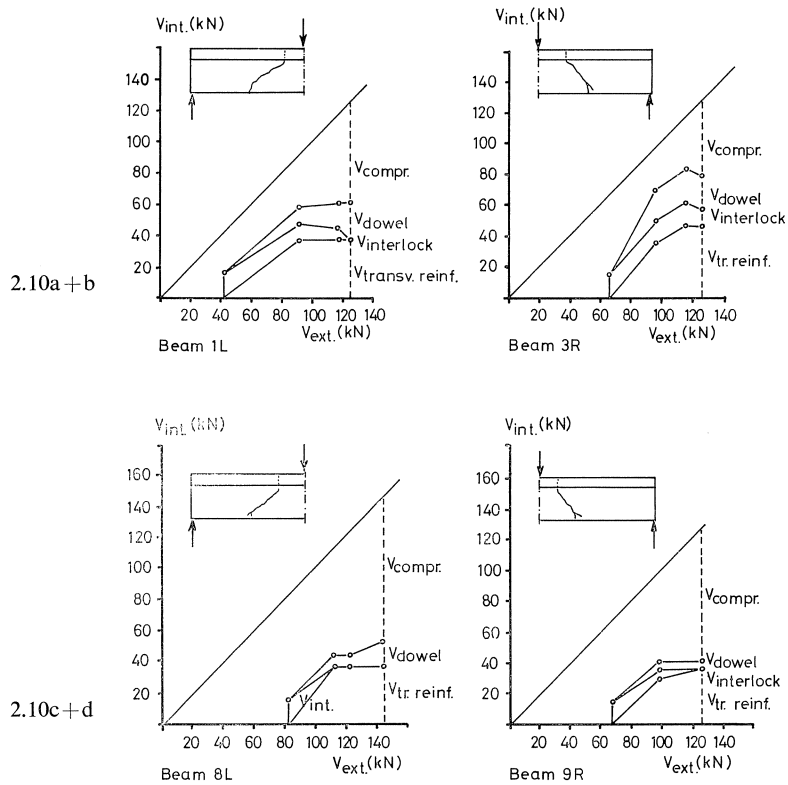


Fig. 2.10. Distribution of the shear force over the individual load carrying components for beams 1L, 3R, 8L, 9R.

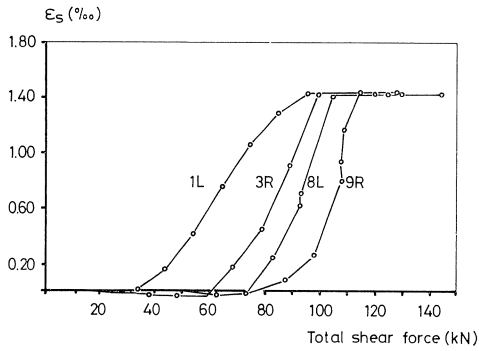


Fig. 2.11. Development of stirrup stresses in beams 1L, 3R, 8L, 9R for stirrup No. 20 and 33 (Fig. 2.6).

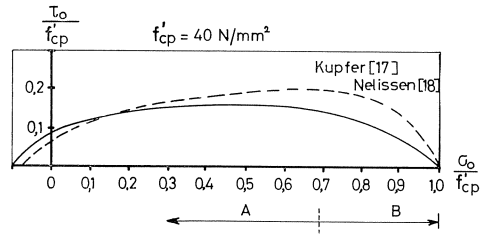


Fig. 2.12. Failure envelopes according to measurements by KUPFER and NELISSEN.

After yielding, the stirrup strain could pass through a considerable deformational range before failure occurred. During this process the shear-carrying component of the uncracked compression area increased substantially, absorbing almost the entire load increase. Data concerning the distribution of forces in the other beams are given in appendix A 2.

2.5.3 Some considerations concerning the shear-carrying capacity of the concrete compression flange

In the ultimate load state the contribution of the concrete compression area varied from 65 to 108 kN (beam 6). As was calculated from the deflection, only about 10 kN could have been carried by secondary bending of the flange.

For the analysis of the stress situation in the compression area the concrete failure criteria experimentally stated by Kupfer [17] and Nelissen [18] were used. From these criteria, giving combinations of ultimate principal stresses, with the aid of Mohr's circle, envelopes were derived, giving the ultimate shear stress as a function of the normal compression stress (Fig. 2.12).

To obtain information about the stress situation in the compression flange, the distribution of forces in the shear region of a beam is discussed on the basis of the model, represented in Fig. 2.13, where a vertical section is considered.

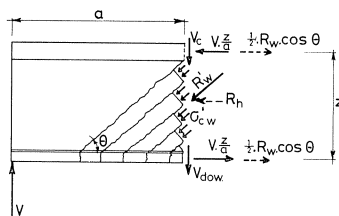


Fig. 2.13. Forces in the shear region.

Flexural moment equilibrium is provided by forces in the compression flange and in the tension flange. Vertical equilibrium is provided by the component of the compression area (V_c), the dowel action (V_{dow}), and the vertical component of the web stresses $R'_w \cdot \sin \theta$. To maintain equilibrium, however, a horizontal component is needed (R_h), which can only be developed by the compression and tension flanges. This leads to the conclusion that the compression area is partially unloaded, while the tension flange is subjected to an additional load. This phenomenon can also be observed by considering the strain measurements (Fig. 2.14).

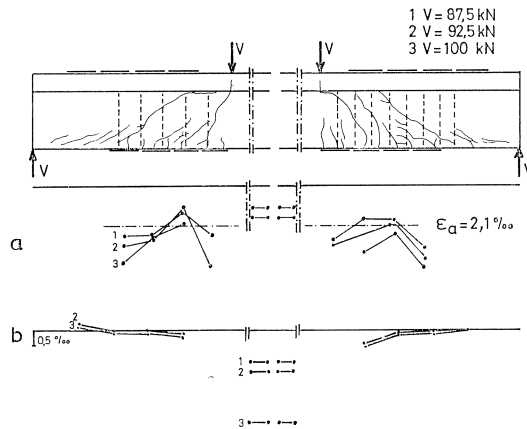


Fig. 2.14. Strain measurements on longitudinal reinforcement (a) and compression flange (b) (Beam 5).

Hence a favourable stress situation in the compression flange is obtained. Due to the force $\frac{1}{2}R_h$ the normal stresses remain in the region A (Fig. 2.12), where a relatively large shear stress can be resisted, even if in the constant moment region the normal compressive stresses reach almost the critical value at the end of zone B

$$\left(\frac{\sigma_0}{f'_{cp}} = 1.0 \right)$$

However, the great shear-bearing capacity of the compression flange cannot be explained by the occurrence of this favourable stress situation alone. Only if that

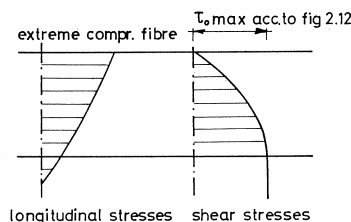


Fig. 2.15. Presumed normal- and shear stress distribution in the compression flange.

part of the compression flange which is active in transferring shear extends over a substantial portion of the width can satisfying agreement with the experimentally found shear component be obtained.

When a shear stress distribution as indicated in Fig. 2.15 is presumed, nearly the whole compression flange must have contributed to obtaining the calculated shear resistance.

In the literature more data are found confirming these observations. Leonhardt et al. [13] are led by their experiments to the conclusion that the effective flange width in carrying shear is at least equal to twice the web width.

Thürlimann et al. [2] basing themselves on their tests on partially prestressed concrete beams, also report a large reserve capacity of the compression flange.

Placas and Regan [15] report tests on simply supported T-beams with variable flange width and constant longitudinal and transverse reinforcement.

An increase in strength was observed for flange widths up to about twice the web width.

Cederwall et al. [16] report test series on partially prestressed beams with rectangular cross-section and deduce statistical formulas to predict the average shear bearing capacity of this type of beams. Comparing our own test results with these formulas it is found that the T-beams have an excess capacity of 60%.

2.6 Discussion of design formulas with respect to the test results

Many formulas predicting the shear capacity are based on the addition principle. In these methods the ultimate load-bearing capacity is based on the improved truss analogy. For reinforced concrete structural elements the shear bearing capacity is expressed as the sum of two terms;

$$V_u = V_c + V_{ws} \quad (1)$$

where V_{ws} is the contribution of the web reinforcement and is calculated on the basis of the Mörsh truss-analogy, assuming a crack angle of 45 deg., while V_c is “the contribution of the concrete” to the ultimate shear resistance.

This is visualised in Fig. 2.16a, giving the development of stirrup stress (solid line) as a function of the shear force according to observations in numerous experiments. The dotted line gives the theoretical relation between the stirrup stress and the shear force according to the Mörsh truss analogy. For the load V the actual stirrup stress corresponds to point A. In a perfectly functioning truss this stress would have resulted in a contribution of the shear reinforcement V_{ws} corresponding to BC. The difference between V and V_{ws} (line AB) which is to be attributed to the shear resistance of the compression zone, etc. is approximately constant after inclined cracking. The contribution of the concrete V_c in (1) is based on experimental observations.

In the case of prestressed concrete, however, the stirrup stresses develop later due to the fact that inclined cracking is delayed by prestressing. Further on the line is

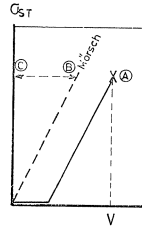


Fig. 2.16a

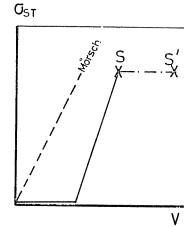


Fig. 2.16b

Fig. 2.16. Stirrup stress development as a function of the load for reinforced (a) and prestressed concrete beams (b).

steeper that the line corresponding to the Mörsh truss, which can be attributed to the smaller amount of longitudinal steel in the case of prestressed beams. As a result, the concrete contribution decreases after inclined cracking. The remaining part at the onset of yielding is believed still to be greater than the concrete contribution in a non-prestressed beam. As the corresponding load was generally accepted as the basis for the design formulation, a positive influence has been attributed to the prestressing influence. This is expressed in an additional term V_p

$$V_u = V_{ws} + V_c + V_p$$

where V_p is a function of the prestressing force (the term V_p has to be distinguished from the term $V_{incl.}$ which has to be added in the case of inclined tendons to take account of the vertical component of the prestressing force).

The test on which the term V_p is based are, however, in the author's opinion, not fully representative of prestressed or partially prestressed beams. With the aim to get shear failures in any case, a lot of tests have been carried out on fully or partially reinforced beams without a compression flange (no reserve capacity) and unrealistically low transverse reinforcement ratios. As a result, shear failures soon occurred, immediately after yielding of the stirrups. Hence the great reserve capacity which practical prestressed and partially prestressed beams have at their disposal is not taken into account.

The second type of design formulas is based on the plasticity principle, as formulated by Braestrup [10], Nielsen and Braestrup [8–9], and Thürlimann et al. [6–7]. Those models have the advantage that they are no longer based on the stirrup yielding load, but make use of the redistribution range after stirrup yielding (Fig. 2.16b, line SS).

The theoretical model developed by Thürlimann has been adopted in the CEB-model code [19] and is therefore compared with the present author's own test results.

The basis of the model is a plastic truss in which the possible distribution of forces is formulated as a lower bound criterion, considering admissible stress fields not exceeding the plastic limit forces. Hence more solutions are available, which means that the direction of the diagonal compressive struts can be chosen arbitrarily over a great range of values.

This range is restricted by kinematic conditions; a redistribution of forces is only possible if sufficient aggregate interlock is available. As a result, the inclination of the concrete compression struts may be chosen freely between the limits

$$0.5 \leq \tan \gamma \leq 2.0$$

So the structural member is considered to develop into a plastic truss in which the longitudinal forces are restricted to the upper and lower chords and the shear forces to the web. The web resistance is therefore formulated as

$$V_{ws} = \frac{A_{sw}}{s} \cdot 0.9 \cdot d \cdot f_{swy} \cdot (\cot \gamma + \cot \alpha) \cdot \sin \alpha$$

α = being the inclination of the transverse reinforcement, and

γ = being the chosen inclination of the compression struts between the mentioned limits.

As the longitudinal reinforcement has to endure a greater tensile force due to shear action, the model can only be applied when an additional amount of longitudinal steel, prescribed in the code, has been added.

The most economical choice for the inclination leads to $\gamma = 30^\circ$. As has been observed in the experiments, the full plastic truss action can be reached only after a redistribution of stresses in the web. The loading range between inclined cracking and full truss action is characterised as the “transition range”. In this range an additional shear resistance may be taken into account:

$$\begin{aligned} \text{if } V_{u,fl} \leq 0.60f_{ct}b_wd \text{ then } V_c &= 0.60f_{ct}b_wd && \text{(uncracked stage)} \\ \text{if } V_{u,fl} \geq 1.80f_{ct}b_wd \text{ then } V_c &= 0 && \text{(full truss action)} \end{aligned} \quad (2)$$

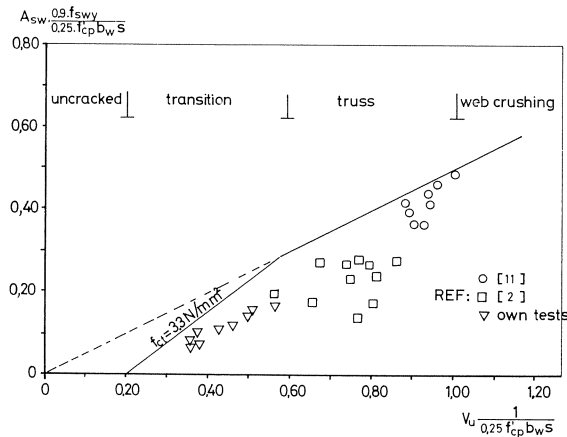


Fig. 2.17. Comparison of test results with CEB-model code (refined method).

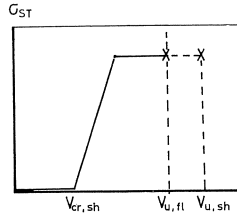


Fig. 2.18. Stirrup stress development as a function of the load as observed in the author's own test beams (idealised), indicating that the shear resistance was not completely exhausted when yielding of the longitudinal reinforcement occurred.

For intermediate values (transition range) V_c is determined by interpolation.

This means that all ranges that possibly can be passed through are present in the formulation.

The results of the present author's own experiments give values in the transition range.

In Fig. 2.17a comparison is made between the design formula and a selection of results of tests on partially prestressed concrete beams.

In this comparison the web crushing strength, presumed to be equal to $0.25f'_c b_w d$, has been used as a reference value.

Considering the present author's own tests it must be realised that, although the stirrup strains passed through a considerable yielding range in fact the shear resistance

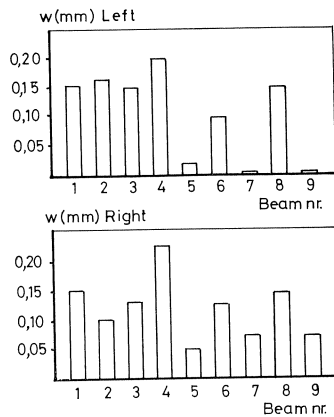


Fig. 2.19. Measured inclined crack widths in the serviceability limit state.

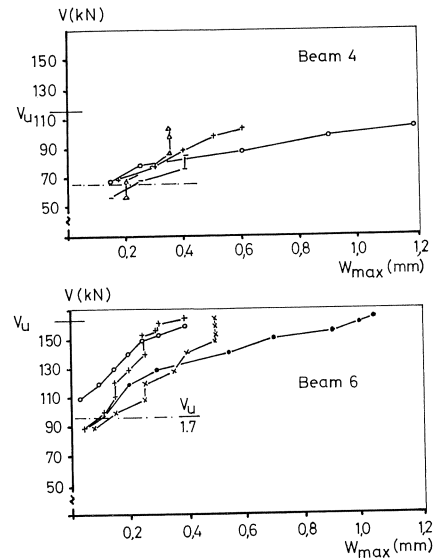


Fig. 2.20. Inclined crack width development for beams 4 and 6 (other beams in appendix A2).

of the element was not exhausted (Fig. 2.18); in each beam yielding of the main reinforcement gave rise to failure. This means that the same ultimate load could have been reached with a reduced transverse reinforcement. Therefore the value of the additional term in the transition range (2) could seem to be too conservative. However, as an increase of this term leads to a reduction of the transverse reinforcement, the crack width in the serviceability state could become the critical factor for design. Fig. 2.19 represents the maximum measured crack widths in the serviceability limit state, which is assumed to be equal to the ultimate load, divided by 1.7. Fig. 2.20 gives the crack development as a function of the load for beams 4 and 6. From these figures it can be concluded that an increase of the concrete contribution in the design formula would probably not have the desired effect.

2.7 Conclusions

- After yielding of the transverse reinforcement the load could be increased considerably, because of the high load-bearing capacity of the concrete compression flange.
- Comparing the stress combination in the concrete compression flange with the results of investigations on the properties of biaxially loaded concrete [Kupfer, Nelissen] it can be concluded that nearly the whole compression flange must have contributed to shear transfer.
- The development of stresses and deformations in the test beams did not proceed so far that full plastic truss action could be reached.
The slope of the inclined cracks, and as a result the contribution of the stirrups to shear transfer in this loading state, appeared to be influenced by the transverse- and longitudinal reinforcement ratios and the prestressing stresses.
- The design principle as formulated by Thürlimann, based on the mathematical theory of plasticity with a transition range to be applied when full plastic truss action is not yet reached, seems to be a physically correct and reliable method to design partially prestressed beams with regard to bending-shear behaviour.

Acknowledgements

The experimental work has been executed by Mr. F. Kopp, as a research project to obtain his degree in civil engineering, under supervision of the writer.

3 The redistribution of stresses in axially compressed reinforced concrete columns

3.1 Introduction

In the method of analysis for the limit states (cracking moment, admissible crack width) of structures in partially prestressed concrete, which methods have been developed by the author, the redistribution of compressive stresses due to creep and shrinkage is taken into account. The magnitude of redistribution is, of course, very important for the cracking load and the load at which the admissible crack width is reached.

This method is based on Dischinger's method but, more generally, developed for sections loaded with eccentric compressive forces. In the preceding paper 1 this method of analysis has been briefly described. In this method the introduction of a reference value of the prestressing force is explained.

The description makes it clear that the method is relatively simple and takes into account all the relevant parameters.

Because this method basically uses the results of the stress redistribution, it is important to know if this calculated redistribution of stresses is really in accordance with the actual behaviour of the structure.

To check this, long-term loading tests on columns and prisms were carried out. In these tests several parameters were varied, such as the magnitude of the compressive stress and the percentage of bonded reinforcement. Both will influence the creep and shrinkage behaviour of the concrete.

The concrete quality of the test specimen and the climate conditions were kept constant during the tests. In this paper the tests are described and the results assessed in comparison with methods of analysis.

3.2 Methods of analysis

Birkenmaier [33] published an interesting paper on methods for determining the redistribution of stresses in concrete structures due to creep and shrinkage of concrete. In this paper a comparison is given between the results of calculations with several methods. Because that paper is not only up to date but also very clear and complete, its conclusions will be summarised here as far as they are of interest for the analysis of our experiments.

More information on these methods can be found in that paper.

3.2.1 *Rate of creep methods*

3.2.1.1 Dischinger's method – axially compressed reinforced concrete columns [33 page 18, 41]

Dischinger's method is interesting because it offers the possibility of arriving at closed-form solutions obtained from differential equations. Although this method is strictly speaking only valid for constant stress [43, 44] it is here used for the benefit of its simplicity as a basis for more general methods for partially prestressed concrete (compression and bending).

The following assumptions are made by Dischinger:

1. Plane sections remain plane
2. The reinforcement is fully bonded to the concrete.
Therefore always $\varepsilon'_{ct} = \varepsilon'_{st}$.
3. The development of shrinkage deformations in time is the same as the development of creep deformations in time.
Therefore it is assumed:

$$\frac{\varepsilon'_{cst}}{\varepsilon'_{cct}} = \text{constant} = \frac{\varepsilon'_{cst}}{\varphi_t} = \frac{\varepsilon'_{cs\infty}}{\varphi_\infty}$$

Or

$$\varepsilon'_{cst} = \frac{\varphi_t}{\varphi_\infty} \cdot \varepsilon'_{cs\infty}$$

As will be shown later on, the experiments to be described here gave no support to this assumption. The quotient $\varepsilon'_{cst}/\varphi_t$ increased considerably in time. See appendix A 3.7.

4. Young's modulus is constant in time.
It is well known that this modulus increases with time.
With the given assumption we can write:

$$\sigma'_{ct} = \sigma'_{c0} - \left[\sigma'_{c0} + \frac{\varepsilon'_{cs\infty}}{\varphi_\infty} \cdot E_c \right] (1 - e^{-\eta})$$

- In which $\eta = \alpha \cdot \varphi_t$

$$\alpha = \frac{n\omega}{1 + n\omega}$$

- In which $n = E_s/E_c$.

In principle, for E_c the value E_{c0} on loading has to be taken into consideration.

Because of the delay of shrinkage with regard to creep (increase of $\varepsilon'_{cst}/\varphi_t$ in time) it may be better to use a higher value of E_c , for example $E_c = 1,3E_{c0}$.

- $\omega = \frac{A_s}{A_c}$

In this case the net area of the concrete section has to be taken into consideration. All formulas are derived with this ω value.

The total area of the section of a concrete column is therefore $(A_s + A_c)$.

Dischinger writes:

$$\sigma'_{st} - \sigma'_{s0} = -\frac{1}{\omega} (\sigma'_{ct} - \sigma'_{c0})$$

or

$$\varepsilon'_{st} - \varepsilon_{s0} = -\frac{1}{\omega \cdot E_s} (\sigma'_{ct} - \sigma'_{c0})$$

Because $\varepsilon'_{st} = \varepsilon'_{ct}$ and $\varepsilon'_{s0} = \varepsilon'_{c0}$ we can write:

$$\varepsilon'_{ct} = \varepsilon'_{c0} + \frac{1}{\omega \cdot E_s} \left[\sigma'_{c0} + \frac{\varepsilon'_{cs\infty} \cdot E_c}{\varphi_\infty} \right] (1 - e^{-\eta})$$

or

$$\varepsilon'_{ct} = \varepsilon'_{c0} + \frac{1}{n\omega} \left[\varepsilon'_{c0} + \frac{\varepsilon'_{cs\infty}}{\varphi_\infty} \right] (1 - e^{-\eta})$$

In this expression, in which we know the real values measured on test specimens, we can also use the measured values of $\varepsilon'_{cst}/\varphi_t$ instead of $\varepsilon'_{cst}/\varphi_\infty$ (Fig. 3.1).

As can be seen in the formulas for ε'_{ct} , the value of ε'_{ct} is only determined by the value of $\eta = \alpha \cdot \varphi_t$. It means that not the relationship $\varphi_t - t$ is important, but only the φ_t value under consideration, assuming that shrinkage and creep are concordant.

The value for the maximum deformation after stabilisation ($\varepsilon'_{c\infty}$) can be written as

$$\varepsilon'_{c\infty} = \varepsilon'_{c0} + (\varphi_\infty \cdot \varepsilon'_{c0} + \varepsilon'_{cs\infty}) \frac{1 - e^{-\eta_\infty}}{n\omega \cdot \varphi_\infty}$$

or with introduction of

$$\alpha = \frac{n\omega}{1 + n\omega}$$

$$\varepsilon'_{c\infty} = \varepsilon'_{c0} + (\varphi_\infty \cdot \varepsilon'_{c0} + \varepsilon'_{cs\infty}) \frac{1 - \alpha}{\alpha \varphi_\infty} (1 - e^{-\alpha \cdot \varphi_\infty})$$

It is possible to introduce into the rate of creep method a calculation method with intervals. In that case the relationship of creep with time and shrinkage with time must be known.

3.2.1.2 In Dischinger's approach it is questionable whether the shrinkage shortening has been correctly introduced into the derivation of the formulas.

In fact, a shrinkage force due to full restraint (without creep) is assumed.

At an interval dt this shrinkage force is

$$\frac{dN_{cs}}{dt} = \frac{d\varepsilon'_{cst}}{dt} \cdot A_c E_c$$

This shrinkage force is released and then acts as a compressive force on the reinforced concrete section.

Therefore

$$\frac{d\sigma'_{ct}}{dt} = \frac{1}{A_c(1+n\omega)} \cdot \frac{dN_{cs}}{dt} = \frac{1}{1+n\omega} \cdot \frac{d\varepsilon'_{cst}}{dt} \cdot E_c$$

In the derivation of his formula Dischinger has written:

$$\frac{d\varepsilon'_{cst}}{dt} \cdot E_c$$

Therefore in our method a revised Dischinger formula is used:

$$\varepsilon'_{ct} = \varepsilon'_{c0} + \frac{1}{\omega \cdot E_s} \left[\sigma'_{c0} + \frac{\varepsilon'_{cs\infty} \cdot E_c}{\varphi_\infty(1+n\omega)} \right] (1 - e^{-\eta})$$

With the introduction of the value α (see 3.2.1.1) the shrinkage term is written:

$$(1 - \alpha) \frac{\varepsilon'_{cs\infty} \cdot E_c}{\varphi_\infty}$$

$$\sigma'_{ct} = \sigma'_{c0} - \left[\sigma'_{c0} + \frac{\varepsilon'_{cs\infty} \cdot E_c}{\varphi_\infty(1+n\omega)} \right] (1 - e^{-\eta})$$

3.2.1.3 Trost's method

The rate of creep method can also be used by introducing a reduction factor ϱ .

In that case one can write for the stress distribution after stabilisation [33 page 25].

$$\sigma'_{c\infty} - \sigma'_{c0} = - \left[\sigma'_{c0} + \frac{\varepsilon'_{cs\infty} \cdot E_c}{\varphi_\infty} \right] \frac{n\omega \cdot \varphi_\infty}{1 + n\omega(1 + \varrho \cdot \varphi_\infty)}$$

$$\varepsilon'_{s\infty} - \varepsilon'_{s0} = \varepsilon'_{c\infty} - \varepsilon'_{c0} = - \frac{1}{\omega \cdot E_s} (\sigma'_{c\infty} - \sigma'_{c0}) = - \frac{1}{n\omega \cdot E_{c0}} (\sigma'_{c\infty} - \sigma'_{c0})$$

$$\varepsilon'_{c\infty} = \varepsilon'_{c0} + (\varphi_\infty \cdot \varepsilon'_{c0} + \varepsilon'_{cs\infty}) \frac{1}{1 + n\omega(1 + \varrho \cdot \varphi_\infty)}$$

or on introducing α

$$\varepsilon'_{c\infty} = \varepsilon'_{c0} + (\varphi_\infty \cdot \varepsilon'_{c0} + \varepsilon'_{cs\infty}) \frac{1 - \alpha}{1 + \varrho \cdot \alpha \cdot \varphi_\infty}$$

For ϱ we can write

$$\varrho = 0,5 + \frac{\varphi_\infty}{20}$$

Trost proposes the following values for the reduction factor ϱ [33 page 40].

a. $\varrho = 0,5 + \frac{1}{4f(t)}$ – calculation of redistribution of stresses

t	7	14	28	90	360 days
$f(t)$	1,4	1,2	1,0	0,75	0,5
ϱ	0,68	0,71	0,75	0,83	1,0

b. $\varrho = 0,85$ – relaxation of stresses.

3.2.1.4 Rüsç's method

Rüsç developed with Jungwirth a method for the calculation of creep deformation, based on Dischinger's approach [33 page 26].

But in this method a delayed elastic deformation at release is introduced.

The equations used by Rüsç are the same as those already discussed in 3.2.1.1.

Instead of the initial compressive stress σ'_{c0} Rüsç introduces the values.

a. $\bar{\sigma}'_{c0} = \sigma'_{c0} \frac{1+n\omega}{1+\bar{n}\omega}$

$$\bar{n} = n(1 + \varphi_{vt})$$

φ_{vt} is a factor related to the delayed elastic deformation.

b. $\bar{n} = \varphi_{ft} \frac{n\omega}{1+\bar{n}\omega}$

φ_{ft} is a factor related to the creep flow.

The original creep coefficient φ_t is the sum of $\varphi_v + \varphi_{ft} = \varphi_t$.

Experiments and studies by Bázant et al. [39] have shown that Rüsç's method, adopted in the current C.E.B. recommendations, is questionable for concrete.

3.2.2 Effective modulus method

This method considers in fact only the end state of stress-equilibrium after stabilization and does not take into account the changing state of stress [33 page 40, 38, 40].

The effective result is that creep resulting from stress reduction due to internal stress redistribution is fully recovered.

Hence the total strain of the structure is underestimated by this method.

Shrinkage shortening is incorporated in the results on the assumption that shrinkage strains can be calculated on the basis of the end deformation due to an assumed

constant shrinkage stress-potential σ_{cs} . This tensile stress is applied to restraint-free shrinkage.

$$\sigma_{cs} = \frac{\varepsilon'_{cs\infty} \cdot E_{c0}}{1 + \varphi_{\infty}}$$

Young's (elastic) modulus E_{c0} of the concrete is assumed to be time-independent.

The elastic deformation at $t = 0$ is

$$\varepsilon'_{c0} = \frac{N'_0}{(1 + n\omega)E_{c0} \cdot A_c}$$

In the calculation the effective load is increased by the shrinkage force.

$$N' = N'_0 + \frac{\varepsilon'_{cs\infty} \cdot E_{c0}}{1 + \varphi_{\infty}} \cdot A_c$$

To calculate time-dependent creep behaviour the effective modulus

$$E_{c\text{eff}} = \frac{E_c}{1 + \varphi_{\infty}}$$

is introduced.

As a result one finds:

$$\varepsilon'_{c\infty} = \frac{N'(1 + \varphi_{\infty})}{[1 + n(1 + \varphi_{\infty})\omega]E_{c0} \cdot A_c}$$

$$\varepsilon'_{c\infty} = \frac{1}{1 + n\omega(1 + \varphi_{\infty})} (\varepsilon'_{c0}(1 + n\omega)(1 + \varphi_{\infty}) + \varepsilon'_{cs\infty})$$

This formula is used in the effective modulus method.

The stress in the concrete can then be calculated with:

$$\sigma'_{c\infty} = \frac{1}{1 + n\omega(1 + \varphi_{\infty})} (\sigma'_{c0} - \omega \cdot E_c \cdot \varepsilon'_{cs\infty})$$

For comparison with Trost's formula one can write for:

$$\varepsilon'_{c\infty} = \frac{1 + \varphi_{\infty}}{1 + n\omega + n\omega \cdot \varphi_{\infty}} \cdot \varepsilon'_{c0}(1 + n\omega) + \frac{\varepsilon'_{cs\infty}}{1 + n\omega + n\omega \cdot \varphi_{\infty}}$$

With introduction of the ratio α :

$$\begin{aligned}
\varepsilon'_{c\infty} &= \frac{1 + \varphi_\infty}{\frac{n\omega}{\alpha} + n\omega \cdot \varphi_\infty} \cdot \frac{n\omega}{\alpha} \cdot \varepsilon'_{c0} + \frac{\varepsilon'_{cs\infty}}{\frac{n\omega}{\alpha} + n\omega \cdot \varphi_\infty} \\
&= \varepsilon'_{c0} + \varepsilon'_{c0} \frac{1 - \alpha}{1 + \alpha \cdot \varphi_\infty} \cdot \varphi_\infty + \frac{1 - \alpha}{1 + \alpha \cdot \varphi_\infty} \cdot \varepsilon'_{cs} \\
\varepsilon'_{c\infty} &= \varepsilon'_{c0} + (\varphi_\infty \cdot \varepsilon'_{c0} + \varepsilon'_{cs}) \frac{1 - \alpha}{1 + \alpha \cdot \varphi_\infty}
\end{aligned}$$

3.2.3 Comparison of the various methods of analysis

All the formulas for $\varepsilon'_{c\infty}$ can be reduced to an equivalent form

$$\varepsilon'_{c\infty} = \varepsilon'_{c0} + (\varphi_\infty \cdot \varepsilon'_{c0} + \varepsilon'_{cs\infty}) \frac{1 - \alpha}{1 + \varrho \cdot \alpha \cdot \varphi_\infty}$$

– Dischinger's method.

Pauw [18] explains that by expanding

$$\frac{1 - e^{-\alpha \cdot \varphi}}{\alpha \cdot \varphi}$$

in series it can be shown that the reduction factor ϱ can approximately be written as:

$$\varrho = 0,5 + \frac{\alpha \cdot \varphi}{12} \left(1 - \frac{(\alpha \cdot \varphi)^2}{60} \right)$$

– Trost approximates with $\varrho = 0,85$.

– Effective modulus method gives the same result as Trost, but with $\varrho = 1,0$.

The values of ϱ are the lowest with Dischinger's method and the highest with the effective modulus method.

Therefore we can expect the total deformations calculated with Dischinger to give the highest and those calculated with the effective modulus to give the lowest values. As already mentioned, the effective modulus method probably underestimates the total strain. From a practical point of view the three methods do not differ very much.

Fig. 3.1 gives the relationship between $\varepsilon'_c - \omega - \varepsilon'_{cs}$ calculated with Dischinger's method with the assumptions $\varphi_\infty = 2$; $\varepsilon_{c0} = 0,5 \times 10^{-3}$ [37].

Calculations show that the differences between the three methods in this case are small.

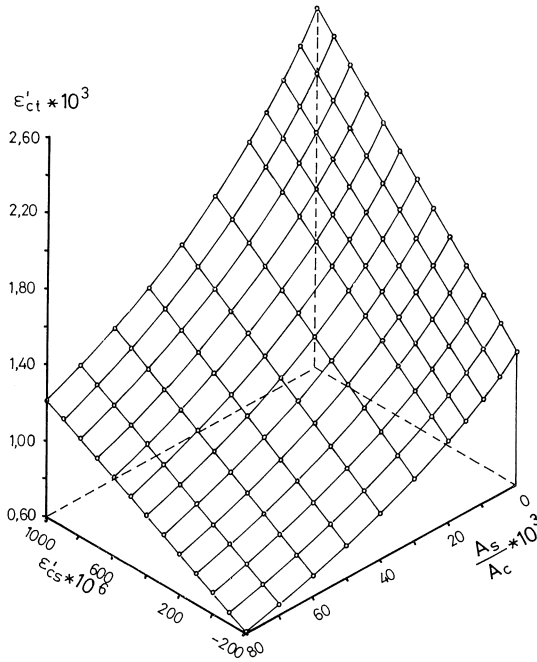


Fig. 3.1. Dischinger method with $\varphi = 2$; $\varepsilon'_{c0} = 50 \times 10^{-5}$.

3.2.4 Formulas

Deformations

Dischinger
$$\varepsilon'_{ct} = \varepsilon'_{c0} + \frac{1}{n\omega} \left(\varepsilon'_{c0} + \frac{\varepsilon'_{cs\infty}}{\varphi_\infty} \right) (1 - e^{-\eta})$$

Dischinger revised
$$\varepsilon'_{ct} = \varepsilon'_{c0} + \frac{1}{n\omega} \left(\varepsilon'_{c0} + \frac{1}{1+n\omega} \cdot \frac{\varepsilon'_{cs\infty}}{\varphi_\infty} \right) (1 - e^{-\eta})$$

Trost
$$\varepsilon'_{c\infty} = \varepsilon'_{c0} + (\varphi_\infty \cdot \varepsilon'_{c0} + \varepsilon'_{cs\infty}) \frac{1}{1+n\omega(1+\varrho \cdot \varphi_\infty)}$$

Effect. Mod.
$$\varepsilon'_{c\infty} = (\varepsilon'_{c0}(1+n\omega)(1+\varphi_\infty) + \varepsilon'_{cs\infty}) \frac{1}{1+n\omega(1+\varphi_\infty)}$$

Stresses

Dischinger
$$\sigma'_{ct} = \sigma'_{c0} - \left[\sigma'_{c0} + \frac{\varepsilon'_{cs\infty} \cdot E_{c0}}{\varphi_\infty} \right] (1 - e^{-\eta})$$

Dischinger revised
$$\sigma'_{ct} = \sigma'_{c0} - \left[\sigma'_{c0} + \frac{1}{1+n\omega} \cdot \frac{\varepsilon'_{cs\infty} \cdot E_{c0}}{\varphi_\infty} \right] (1 - e^{-\eta})$$

Trost
$$\sigma'_{c\infty} = \sigma'_{c0} - \left[\sigma'_{c0} + \frac{\varepsilon'_{cs\infty} \cdot E_c}{\varphi_\infty} \right] \frac{n\omega \cdot \varphi_\infty}{1+n\omega(1+\varrho \cdot \varphi_\infty)}$$

Effect. Mod.
$$\sigma'_{c\infty} = (\sigma'_{c0} - \omega \cdot E_c \cdot \varepsilon'_{cs\infty}) \frac{1}{1 + n\omega(1 + \varphi_\infty)}$$

Remark

It will be noted that the Trost and Effective Modulus methods only give an estimation of the total strain after stabilisation and not for other times.

3.3 The experiments

3.3.1 *Specimens to be tested*

The experiments were carried out with the following specimens:

3.3.1.1 Series K – 12 columns

Columns – dimensions 150 × 150 × 1200 mm.

The columns were reinforced longitudinally with deformed bars, grade FeB 400.

Both the top and the bottom of the columns were provided with six stirrups $\varnothing 6$ mm over 300 mm of the column height (Fig. 3.2). Concrete cover to the reinforcement was 30 mm.

Longitudinal reinforcement of the columns.

K ₀	K ₁	K ₂	K ₃	K ₄	K ₅
K ₁₀	K ₁₁	K ₁₂	K ₁₃	K ₁₄	K ₁₅
unrein.	4 \varnothing 6	4 \varnothing 8	4 \varnothing 12	8 \varnothing 12	8 \varnothing 16
0%	0,5%	0,9%	2%	4%	7%

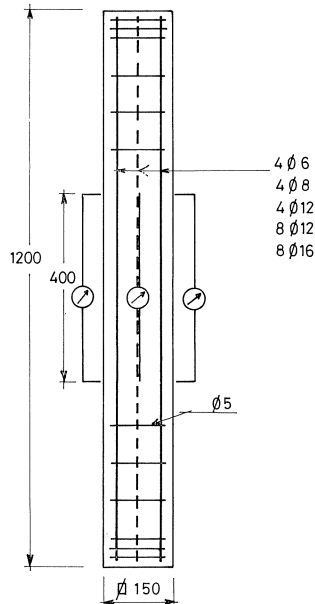


Fig. 3.2. Column reinforcement.

3.3.1.2 Series P – 40 prisms

Prisms – dimensions $150 \times 150 \times 600$ mm.

30 prisms were unreinforced.

10 prisms $P_1 \dots P_5$; $P_{11} \dots P_{15}$.

The longitudinal reinforcement of these prisms is the same as for the columns K with the same subscript (e.g., $4\varnothing 12$ reinforcement of prisms P_3 and P_{12}).

The reinforced prisms were provided with stirrups over 150 mm length at the top and the bottom.

3.3.1.3 Series P.S. – 12 prisms

Prisms – dimensions $100 \times 100 \times 300$ mm.

Unreinforced – only used in series IV.

3.3.1.4 Series C – 98 cubes

Cubes – dimensions $150 \times 150 \times 150$ mm.

3.3.2 Test series

The following experiments were performed on the specimens.

3.3.2.1 Series $K_0 \dots K_5$

These columns were loaded with a constant load between 175 kN and 240 kN.

At loading the strain for all the columns was $0,25 \times 10^{-3}$.

Test were performed in a climate-controlled room of the Stevin Laboratory.

In a test frame, 16 columns (maximum height 4000 mm) can be kept under sustained load, which can act centrally or eccentrically on the columns. The maximum load is 600 kN for one test rig.

The loads are held constant by using a system of stacked cup springs (Fig. 3.3).

A method has been developed to avoid hysteresis on applying the loads. During the tests the relative humidity was held constant at $50\% \pm 3\%$ and the temperature at $20^\circ\text{C} + \frac{1}{4}^\circ\text{C}$.

The load was applied within 30 sec.

Strain measurements were carried out on the four sides of the columns (two measurements on the concrete surface and two directly on the reinforcing bars). Gauge length 400 mm.

The strains were measured at the following intervals *after* loading.

Days 1, 2, 5, 9, 14, 20, 34, 56.

Months 3, 4, 6, 9 and 12.

Loading took place 14 days after casting the columns.

During this period the columns were cured in a room with a high value of relative humidity (95%).

At the end of the test period the columns were unloaded and strain measurements were carried out during 4 weeks.

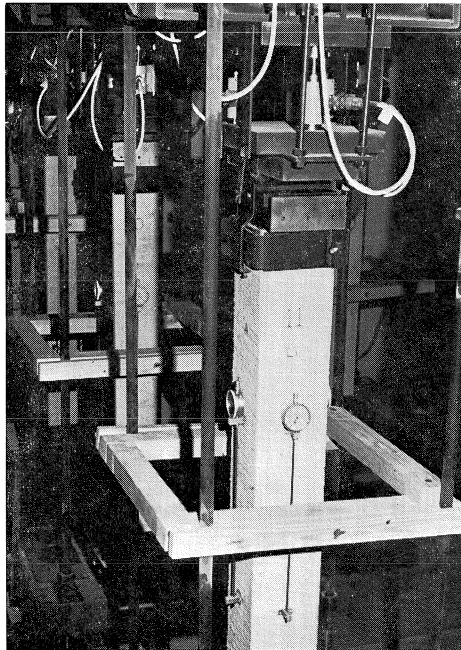


Fig. 3.3. Loading frame for column.

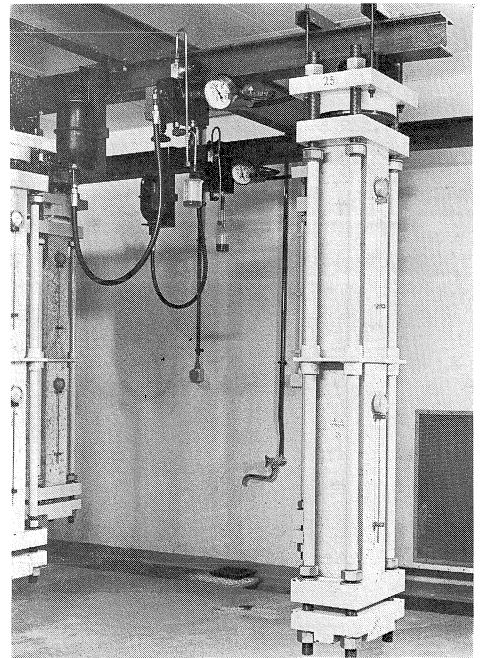


Fig. 3.4. Creep rig.

3.3.2.2 Series $K_{10} \dots K_{15}$

The test procedure for these columns was equal to series $K_0 \dots K_5$, with the exception of the strain at loading ($0,4 \times 10^{-3}$), and therefore resulting in a constant load on the columns ranging from 230 to 320 kN.

3.3.2.3 Series P

Loaded unreinforced specimen

8 prisms were tested according a standard creep test procedure to determine the relationships of the creep coefficient φ_t with time. The creep test equipment in the Stevin Laboratory consists of 30 separate hydraulic test units, each with a capacity of 1000 kN (Fig. 3.4). The loads are controlled by means of hydraulic jacks and are measured with oil pressure strain gauges.

To keep the load constant, every test unit has a nitrogen gas accumulator with a pre-pressure of 50% of the expected oil pressure in the hydraulic system. This incorporates a “gas spring” in the oil circuit, compensating for losses of pressure caused by creep deformation of the concrete. The climatological conditions of the room are controlled. The strains of the columns at the start of the tests were of the same magnitude as in the specimen series K ($0,25 \times 10^{-3}$ and $0,4 \times 10^{-3}$).

Non-loaded unreinforced specimen

These specimens were placed upright in the climate-controlled room. The upper and

lower surfaces of these prisms were coated to simulate the same surface conditions with regard to drying as in the loaded prisms.

At mid-height of these 10 prisms strain measurements on two sides were carried out for one year with an accuracy of 0,001 mm. Gauge length 300 mm.

The weight of the prisms was measured to observe the drying process. Accuracy of weight – ± 1 gram.

These measurements started 14 days after casting at the start of the creep tests on series K.

10 prisms were loaded to failure after the end of the time-dependent tests. During these tests the stress-strain diagram was determined.

Non-loaded reinforced specimens P₁ ... P₅ and P₁₁ ... P₁₅

These specimens were tested as described at 3.3.2.3.2.

3.3.2.4 Series P.S.

These prisms were compressed to failure in a testing machine and the stress-strain diagram was determined to calculate:

1. Young's modulus at zero stress (secant modulus).
2. Ultimate compressive strength.

The strain velocity during the test was held constant at $3,33 \times 10^{-3} \%$ per second.

Prisms were tested 14 days (4), 28 days (4) and 6 month's (3) after manufacture.

Remark

The results of these test showed a great scatter in the values of Young's modulus. Therefore it was decided to determine E_{c0} from the results which were obtained during the loading procedure of series K.

$$E_{c0} = \frac{\sigma'_{c0}}{\epsilon'_{c0}}; \quad \sigma'_{c0} = \frac{N' - A_s \cdot \epsilon'_{c0} \cdot E_{cs}}{A_c}$$

$$E_{c0} = \frac{N'}{A_c \cdot \epsilon'_{c0}} - \frac{A_s}{A_c} \cdot E_{cs}$$

3.3.2.5 Series C

The cubes were used to determine the compressive cube strength and splitting strength of the concrete.

Cubes were tested at various ages.

time	days			months	
	7	14	28	6	12
compressive str.	3 × 3*	4 × 5*	4 × 5*	3 × 3* + 1 × 5*	4 × 5*
tensile splitting str.	–	–	4 × 3 + 1 × 6	–	–

* Number of specimens tested.

3.3.3 Concreting – concrete quality

3.3.3.1 Concrete mix

The concrete mix contained 325 kg of class A Portland cement per m³, a water-cement-ratio of 0,58 (190,5 kg water per m³), 1830 kg sand-gravel mix per m³ with: 76% of weight > 1,4 mm grain size
24% of weight ≤ 1,4 mm grain size.

The columns were cast horizontally and the concrete was compacted by vibrating on a high-frequency vibrating table.

Three days after concreting the specimens were cured in a room with a temperature of 20°C and a high relative humidity.

3.3.3.2 Pours

The specimens were concreted in four pours.

pour	date			
I	6-11-'74	2 columns	2+6 prisms	24 cubes
II	13-11-'74	2 columns	2+8 prisms	24 cubes
III	20-11-'74	2 columns	2+8 prisms	24 cubes
IV	6- 8-'75	6 columns	2+6 prisms	26 cubes + 12 prisms P.S.

During the installation of the first test series I, II and III there was found to be too much scatter in concrete quality between the three pours. Therefore it was decided to cast the series K₁₀ ... K₁₅ prisms and cubes from one batch and to accept the difficulties of a large pour and a large number of specimens with many measurements starting simultaneously.

To prepare this work and to gather information from the test in progress, pour IV was concreted 9 months after the pours I, II and III.

3.3.3.3 Concrete quality

Information about concrete quality is given in appendix A 3.1.

This table gives the results of tests on

cube strength

prism strength

modulus of elasticity

tensile splitting strength.

3.3.3.4 Loss of weight – series P

Appendix A 3.2 gives the results of the measurements on the loss of weight of 22 prisms.

It shows that the mean loss of weight in one year is a value of 44,07 kg per m³ concrete with a variation coefficient of 8%. That means that in one year 22% of the water in the concrete mix has evaporated.

3.4 Experimental results

Appendix A 3.3

Mean values of strain measurements $P_0 \dots P_5$ and $P_{10} \dots P_{15}$. 34 days, 91 days, 182 days and 364 after loading of the test specimen series K.

In the table the strain measurements are given.

The stresses in the concrete and reinforcement can be calculated with

$$\sigma'_s = \varepsilon'_c \cdot E_s$$

$$\sigma'_c = \frac{A_s \cdot \sigma'_s}{A_c}$$

The E_s value is assumed at 210.000 N/mm².

This calculation is based on the assumption that plane sections remain plane and that in the measuring zone no bond stresses between the reinforcement and the concrete develop and therefore the stresses in this zone are constant.

It means good bond is assumed to exist between reinforcement and concrete in the top and bottom part of the column, resulting in introduction of all the compressive stresses into the reinforcement caused by (reduced) shrinkage of the concrete.

The table shows that relatively high tensile stresses in the concrete are built up in one year, especially in prisms with a high percentage of longitudinal reinforcement.

Appendix A 3.4

Mean values of strain measurements $K_0 \dots K_5$; $K_{10} \dots K_{15}$. 0 days, 34 days, 91 days, 182 days and 364 days after loading.

In this table the stresses in the concrete and reinforcement are calculated, assuming:

1. plane sections remain plane
2. modulus of elasticity of the longitudinal reinforcement $E_s = 210.000 \text{ N/mm}^2$

The concrete stress σ'_c is calculated with

$$\sigma'_c = \frac{N' - A_s \cdot \sigma'_{as}}{A_c}$$

$$\sigma'_c = \frac{N'}{A_c} - \frac{A_s}{A_c} \cdot \varepsilon'_c \cdot 210.000 \text{ N/mm}^2$$

$$E_{c0} = \frac{\sigma'_c}{\varepsilon'_c} = \frac{N'}{A_c \cdot \varepsilon'_c} - \frac{A_s}{A_c} \cdot 210.000 \text{ N/mm}^2$$

The table clearly shows the influences of the longitudinal reinforcement on the re-

distribution of stresses in the columns and the reduction of the time-dependent deformation.

This appendix also gives the strain measurements during 28 days after the unloading of the specimen.

With the decrease of strain caused by unloading, “Young’s” modulus is calculated in the same way as mentioned before.

The tensile stresses caused by the increased compression reinforcement were too high for the columns K_4 , K_5 , K_{14} and K_{15} .

These upright columns showed horizontal cracks.

For the remaining columns the tensile stresses in the concrete were calculated with the remaining compressive deformation of the reinforcement ($E_s = 210.000 \text{ N/mm}^2$).

The table shows that the maximum calculated tensile stress was nearly 3 N/mm^2 (K_3).

In Fig. 3.5 and 3.6 some results are presented graphically.

Fig. 3.7 gives the relationship between deformation and time after unloading.

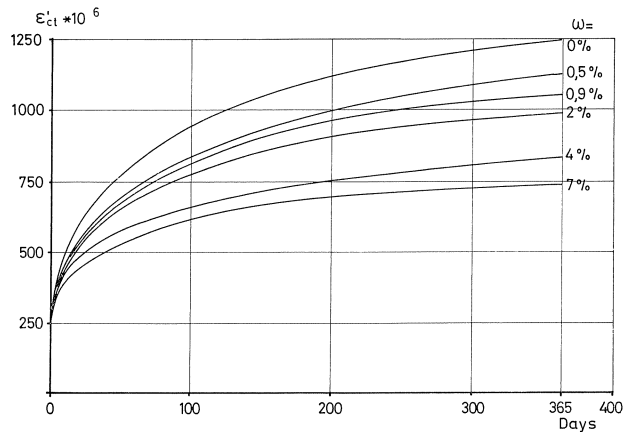


Fig. 3.5. Strain versus time.

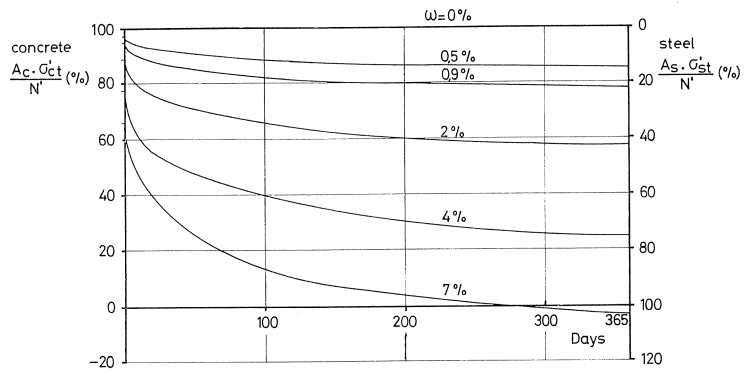


Fig. 3.6. Stresses versus time.

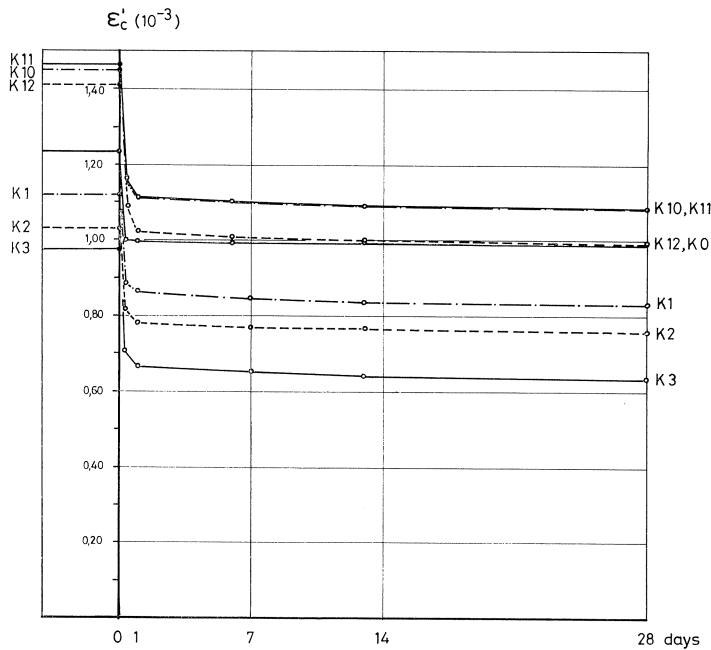


Fig. 3.7. Strain after unloading.

3.5 Analysis of experimental results

3.5.1 Behaviour on macro and micro scale

Creep and shrinkage of concrete are closely related to the conditions of humidity of the concrete itself. Therefore knowledge of the real distribution of humidity over the cross-section is very important. The time-dependent behaviour of a concrete structure – behaviour on the macro scale – therefore also depends on the distribution of humidity in the structure, already mentioned, and the time-dependent stresses and deformations of all the “fibres” involved.

Consider a fibre in a structural member (micro-scale); the moisture content of the concrete of this fibre depends on:

1. The distance between this fibre and the surface of the structure.
2. The evaporation of moisture at this surface.

Influence of the relative humidity of the atmosphere and other atmospheric conditions which influence the evaporation process (wind, temperature).

3. The porosity of the concrete between this fibre and the concrete surface.
4. The quality and humidity of the concrete in the fibres at a greater distance from the surface of the structure than the fibre under consideration.
5. The time that has elapsed after casting up to the instant when the stress distribution is observed.

All these factors affect the amount of moisture that is transported through the concrete structure and therefore affect the rate of drying of the concrete at each fibre.

The differences in the drying process of the various fibres originally cause differences between the strains at these fibres, but, because all these fibres are part of a solid concrete structure, the restraint of each fibre causes stresses – stress distribution – over the section of the structure.

Stresses and strains at all the fibres of a cross section, due to this influence of distribution of humidity – the micro process – result in the observed deformations of a structure as a whole – the macro process.

An interesting study of the micro process in relation to the macro behaviour has been carried out at the Delft University of Technology. The results of that study enable the macro behaviour to be calculated from the micro behaviour. It is mentioned because it is of considerable interest as a basis for the observations described here. It will be published separately in due course [42].

Some results of the calculation of the distribution of moisture over the cross-section of the columns of these tests are given for information.

Fig. 3.8 shows essentially the distribution of moisture over the cross-section of a column ($150 \times 150 \text{ mm}^2$) after 133 days curing in an atmosphere of 50% relative humidity and a temperature of 20°C .

The diffusion coefficient in this calculation is $10^{-10} \text{ m}^2/\text{sec}$.

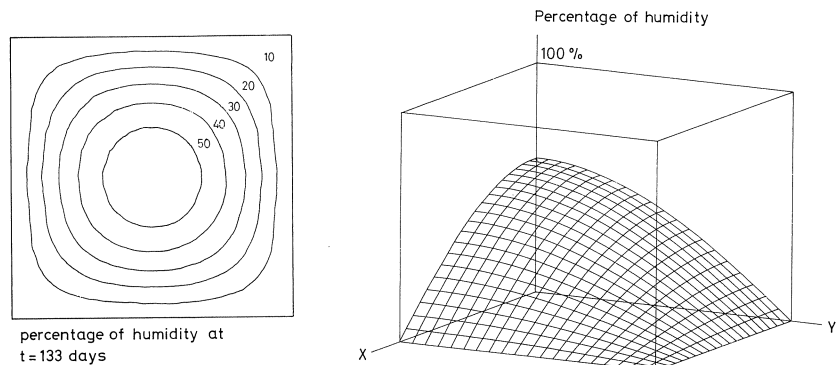


Fig. 3.8. Distribution of humidity after 133 days.

In Fig. 3.9 the concrete stresses in several fibres of the cross section are shown. This calculation is based on the assumption of purely elastic behaviour. Creep and crack formation, however, can also be taken into consideration.

Fig. 3.10 gives the calculated (macro) total shortening of a loaded and drying column, resulting from the mentioned method and the measured total shortening of a prism of pour K_0 .

The three diagrams clearly show the relationship between the micro (calculated) behaviour and the macro (observed) behaviour.

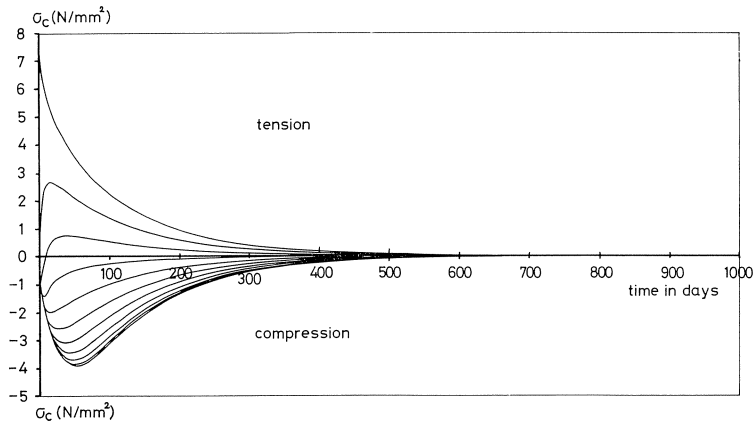


Fig. 3.9. Stresses at various points of cross-section.

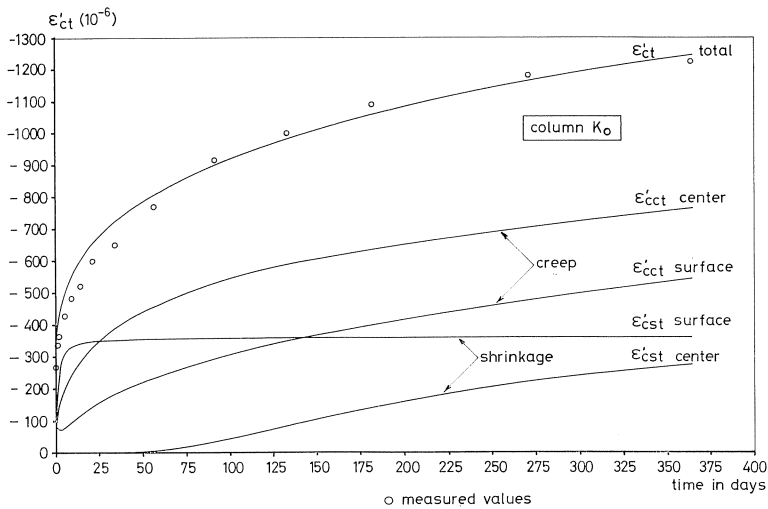


Fig. 3.10. Strains versus time.

They make us realise that the shrinkage values and the creep values used in practice are very rough estimates of the result of a rather complex process in the concrete.

The formulas of Dischinger, Trost and others must be seen in the same context.

Concrete quality (porosity), temperature, climate conditions, the shape and dimensions of the cross-section, these all are factors of importance in the real time-dependent behaviour of a structure. So it is necessary to be cautious with the conclusions drawn from certain experiments, which are described here by way of example because these conclusions in fact refer only to the results of these experiments.

Nevertheless it is of course necessary to give the designer of concrete structures more simple, but adequate, design rules based on scientific studies. The results of

these tests may therefore be of interest to see how macro behaviour can be determined with only measured macro material properties.

3.5.2 Relationship

Total deformation – shrinkage – loss of weight due to evaporation. (See calculation and Fig. 3.12 in Appendix A 3.6 and A 3.7).

In appendix A 3.7 the relative values of

$$\frac{\varepsilon'_c}{\varepsilon'_{c\ 364}}; \quad \frac{\varepsilon'_{cs}}{\varepsilon'_{cs\ 364}} \quad \text{and} \quad \frac{\text{loss of weight}}{\text{loss of weight} - 364}$$

in percentages are given as a function of the time t .

Appendix A 3.6 clearly indicates that the loss of weight ratio at a given interval is nearly the same as the total deformation ratio, but that the shrinkage ratio is lower during the first month. The shrinkage ratio increases rapidly during the second and third month. After three months the total deformation, the shrinkage and the loss of weight obey the same laws in course of time. This conclusion can also be drawn from appendix A 3.7.

This appendix shows that after three months the ratio $\varepsilon'_{cs}/\varphi_t$ is nearly constant for all the four pours observed.

It is of interest to mention that after 100 days the differences between the several internal stresses rapidly increase (see Fig. 3.9). Therefore it can be assumed that the internal state of stress in the concrete specimen greatly influences the macro deformation. During the first weeks considerable stress in the specimen is built up due to restraint of shrinkage deformations. This stress system reduces the macro observed shrinkage deformation of the specimen as a whole, because the tensile stresses on the outside are in equilibrium with compressive stresses inside the column.

The tensile stresses reduce the shortening due to shrinkage. The shrinkage in the interior of the column is small because the humidity is high.

Evidently the explanation of the macro behaviour is only possible with knowledge of the internal system of stress distribution and moisture distribution.

The observations make it clear that the third assumption in Dischinger's approach (3.2.1.1) is not correct.

On a macro scale the shrinkage deformations take place when the large creep deformations decrease i.e., $d\varphi_t/dt$ increases.

Shrinkage may therefore cause higher internal stresses than calculated with Dischinger's approach.

Dischinger assumes

$$\varepsilon'_{cs} = \frac{\varphi_t}{\varphi_\infty} \cdot \varepsilon'_{cs\infty}$$

and therefore

$$\sigma'_{cs} = \frac{\varepsilon'_{cs\infty}}{\varphi_\infty} \cdot E_c$$

If no creep of concrete would take place in the period of shrinkage, we obtain $\sigma'_{cs} = \varepsilon'_{cs\infty} \cdot E_c$.

In reality shrinkage takes place in a period with lower values of $d\varphi_t/dt$ and higher values of E_c .

Therefore in Dischinger's approach we must write

$$\sigma'_{cs} = \psi \cdot \frac{\varepsilon'_{cs\infty}}{\varphi_\infty} \cdot E_c \quad \text{with} \quad \psi > 1$$

Perhaps it is correct to express the value of ψ as a function of the reinforcement ratio ω .

A simple approach could be to use the value $\psi = (1 + n\omega)$.

In that case the term $1/(1 + n\omega)$ in Dischinger's revised formula (3.2.1.2) can be neglected.

Remark

From an investigation of shrinkage and creep data it appears that the scatter in the results of time-dependent deformation is rather large for the same concrete quality, as the following table shows.

specimens	$f'_{c\ 14}$ N/mm ²	$f'_{c\ 28}$ N/mm ²	ε'_{c0} $\times 10^{-6}$	$\varepsilon'_{c\ 364} - \varepsilon'_{c0}$ $\times 10^{-6}$	loss of weight kg/m ²	φ_{364}
K ₀ -P ₀	17,8	22,4	270	963	41,4	2,47
K ₁₀ -P ₁₀	17,2	21,1	399	1051	43,2	1,88

More research seems to be necessary to get information about the factors which cause variation in shrinkage and creep values obtained for a constant concrete strength.

It can also be concluded that "concrete quality" can be defined in several ways. In research projects relating to time-dependent behaviour a small amount of scatter of shrinkage and creep deformations of the concrete would be very important for better interpretation of the results.

3.5.3 Formulas to calculate the shrinkage shortening of longitudinally reinforced concrete specimens

To calculate the shrinkage shortening of reinforced members the formulas given before (3.2) can be used with $\varepsilon'_{c0} = 0$. They can be written as follows – for $t = \infty$ –:

$$\text{Dischinger:} \quad \varepsilon'_{ct} = \varepsilon'_{cs\infty} \left(\frac{1 - e^{-\eta}}{n\omega \cdot \varphi_\infty} \right) \quad \eta = \frac{\varphi_\infty \cdot n\omega}{1 + n\omega}$$

$$\text{revised Dischinger:} \quad \varepsilon'_{ct} = \varepsilon'_{cs\infty} \left(\frac{1 - e^{-\eta}}{(1 + n\omega)n\omega \cdot \varphi_\infty} \right)$$

$$\text{Trost:} \quad \varepsilon'_{ct} = \varepsilon'_{cs\infty} \left(\frac{1}{1 + n\omega(1 + q \cdot \varphi_{\infty})} \right) \quad q = 0,85$$

$$\text{Effective Modulus:} \quad \varepsilon'_{ct} = \varepsilon'_{cs\infty} \left(\frac{1}{1 + n\omega(1 + \varphi_{\infty})} \right)$$

These formulas can only be expected to give rough estimates of the measured values of ε'_{ct} .

The micro process, described under 1, is very complex and therefore it is impossible to calculate the restraint shrinkage deformation with these formulas very accurate.

In appendix A 3.3 the results of the calculations with the three methods are given for $t = 364$ days.

In the calculation are used:

- E_c values, calculated for each column from the instantaneous deformations.
- ε'_{cs364} and φ_{364} values, measured on the corresponding specimens.

The mean values of prisms P_1 – P_{11} , P_2 – P_{12} , etc. give the following results (after 364 days).

method	ω					
	0	0,5%	0,9%	2%	4%	7,5%
Measured	319	277	245	231	169	127×10^{-6}
Dischinger	–	278	282*	244	180	132×10^{-6}
Trost	–	270	267	228	159	114×10^{-6}
Effect. Mod.	–	267	274*	220	150	109×10^{-6}

* caused by high E_c values for K_2 in respect with K_1 .

From the different shrinkage values of series $P_1 \dots P_5$ and $P_{10} \dots P_{15}$ (see A 3.5 and A 3.6) a difference in deformations due to restraint of shrinkage is possible in both series.

The values calculated with the three methods considered do not differ very much from the measured values, especially in the range with normal percentages of reinforcement (till 2%).

The scatter in the calculated deformations in relation to the measured deformations is too large to decide whether the results of one method are in better agreement than those of another method.

It underlines the statement that the calculation methods do not take account of the complex micro system and therefore give only rough estimates.

Generally speaking, the test results show the influence of longitudinal reinforcement on the reduction of time-dependent deformations to be relatively small: 30% reduction with 2% reinforcement (Fig. 3.11).

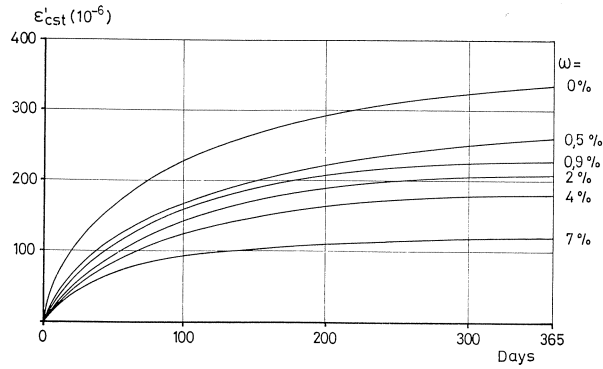


Fig. 3.11. Influence of reinforcement on time dependent deformation.

3.5.4 Comparison of results of calculations with formulas and measured values

In appendix A 3.8 the measured (M) deformations are compared with the deformations calculated with the three methods (*Dischinger, Trost, Effective Modulus*).

The deformations are calculated for several periods, and not only for the deformations after one year of creep and shrinkage assuming that to be the period after which stabilization has taken place. As mentioned in 3.2, the theories have in fact only been developed for the deformations over the period in which stabilization has taken place.

In the calculation the following values are used:

- E_c = values calculated with the use of measured deformations at loading – 14 days after concreting.
- ϵ'_{cst} = shrinkage values determined on the special test series P – creep and shrinkage test.
- φ_t = creep values determined on the special test series P.
- ϵ'_{c0} = values measured at loading – 14 days after concreting.
- ρ = 0,85 (Trost).
- E_s = 210.000 N/mm²
- n = E_s/E_c (E_c – calculated).

One has to realise that:

1. Dischinger's method is used with real values of $\epsilon'_{cst}/\varphi_t$ obtained from creep and shrinkage tests and not with $\epsilon'_{cs\infty}/\varphi_\infty$. Because $\epsilon'_{cst}/\varphi_t$ is not a constant value and independent on time (assumed by Dischinger), the calculated values of the deformation at a given time are not the same as those calculated with the original Dischinger formula.
2. In practical calculations one never has the opportunity to use the “real” values of E_c , $\epsilon'_{cs\infty}$, φ_∞ because these calculations are made *before* the structure is built. In this case of comparison experiments, however, “real” values can be used although these values are obtained from other specimens. Therefore differences

between the characteristics introduced in the calculations and these characteristics for the concrete of the specimen considered may vary.

Subject to these restrictions, the results of measurements can be compared with those of the calculations.

A comparison between measured and calculated stresses in concrete and reinforcement is not given in the appendix, because there is a clear relationship between strains and stresses.

On the other hand, it is more useful to compare *measured* values (deformations or strains) with calculated ones than values which are both calculated.

The following conclusions can be drawn from the comparison:

1. There is a remarkable scatter in the measured deformations. This can easily be seen on comparing the results of several specimens with a low percentage of reinforcement.
2. The deformations calculated with three formulas do not differ very much from the measured deformations.
3. On comparing the mean values of calculated deformations with the mean values which are measured (see appendix A 3.9) it can be concluded that the difference between the measured and the calculated values is the smallest for Dischinger's method (2–4%) and the largest for the Effective Modulus method (2–12%). The results, calculated with Trost's method are 6–10% below the measured values.
4. The calculated values are lower than the measurements, and therefore on the unsafe side.

The cause of the differences is partly explained by the *underestimation* of shrinkage in the deformations. As already mentioned, the assumption in the calculation of a "stabilized" value of ϵ'_{cs}/φ_t is not correct because the shrinkage shortening is delayed with regard to the creep deformations. This means that $d\epsilon'_{cs}/d\varphi_t$ gives a higher value than assumed.

Because lower values of the total deformation result in lower compressive stresses in the reinforcement and therefore in higher compressive stresses in the concrete, the results of the calculation methods are on the *unsafe* side.

Again these observations lead to the conclusion that higher values of stresses due to restraint shrinkage must be introduced into the calculation.

- a. Merely to show the results of introducing such higher values, the last calculations (364 days) were also carried out with $1,2\epsilon'_{cs,364}$. The calculated values are given in appendix A 3.8.

The result of the increase of $\epsilon'_{cs\infty}$ is that a smaller difference between calculated and measured deformations is found.

- b. Another alternative could be to introduce into Trost's method a value q as a function of the reinforcement.

3.5.5 Calculations with values for E_c , ε'_{cs} and φ_∞ given in the recommendations

As already mentioned, it is in practice impossible to know at the time of designing a concrete structure the real values of E_c , $\varepsilon'_{cs\infty}$ and φ_∞ of the concrete which will be used on the job.

Therefore it is important to know how values given in recommendations result in values of expected deformations which are of the same order as the real ones.

Therefore calculations were carried out with the values of E_c , $\varepsilon'_{cs\infty}$ and φ_∞ based on the CEB-FIP recommendations (version Sept. 1977 – CEB-bulletin 117, 120).

To determine these values the characteristic concrete strength of the columns is to be estimated at 30 N/mm^2 .

Relative humidity is taken as 50%.

Temperature as 20°C .

Dimensions of specimen $150 \text{ mm} \times 150 \text{ mm} \times 600 \text{ mm}$.

1. Value of E_{ct0} – CEB-FIP Recommendations art. 2.5.2.

Since the recommendations give no value for $t_0 = 14$ days, the value $t_0 = 28$ days is used, being $E_{c28} = 32.000 \text{ N/mm}^2$.

2. Creep factor

CEB-FIP Recommendations art. 2.5.4 give $\varphi_{(364-14)} = 2,7$. A more correct calculation can be carried out with appendix C of the Recommendations.

Introducing

$$\varphi_d = 0,4 ; \beta_d = 0,9$$

$$\varphi_f = 4,67 ; \beta_{f14} = 0,32 ; \beta_{f364} = 0,8$$

We find:

$$\varphi_{(364-14)} = 0,4 \times 0,9 + 4,67(0,8 - 0,32) = 2,6$$

3. Shrinkage

CEB-FIP Recommendations art. 2.5.4 give $\varepsilon'_{cs(364-14)} = 25 \times 10^{-5}$. The more correct calculation with appendix C given:

$$\varepsilon'_{cs(364-14)} = 38 \times 10^{-5}(0,83 - 0,13) = 27 \times 10^{-5}$$

This calculation takes into account that the specimens were cured (relative humidity 95%) before the tests started.

Results of the calculations with the three formulas (D, T, E) and introducing the values of E'_{c0} , $\varepsilon'_{cs\infty}$ and φ_∞ , determined with the CEB-FIP recommendations, are given in the last lines of appendix A 3.8.

In this case CEB-FIP are to be congratulated, because the differences between the calculated and measured values are relatively small, if we take into account that the calculations are based on expected characteristics of the concrete.

In the range of reinforcement percentages used in practice (0–2%) Dischinger's

method gives very small differences from the measured values for the series K_0 – K_5 and a difference of 10% to 12% on the safe side for series K_{10} – K_{15} .

Again it is found that the differences found with the Effective Modulus theory are the largest and with Dischinger's method the smallest.

Of course, no conclusions can be drawn from one case, but the results of this comparison are encouraging.

3.5.6 *Deformations after unloading*

Appendix A 3.4 gives the development of deformations after unloading of the reinforced columns.

Appendix A 3.5 gives these developments for the test prisms. The deformations of the unreinforced columns on unloading were respectively: 81%, 62%, 77% and 74% of the deformations on loading. The scatter in this percentages is rather large.

The delayed elastic deformations after 28 days are respectively 19%, 28%, 17% and 20% of the deformations on loading.

The total deformation after 28 days is 100%, 90%, 94%, and 94% of the deformation on loading.

This shows that 28 days after unloading nearly the whole elastic deformation which occurred on loading has recovered.

The reinforced concrete specimens that did not crack showed a behaviour similar to that of the unreinforced ones.

Because only the elastic deformation on loading will be recovered, the tensile stresses in the concrete caused by compressed reinforcement (due to shrinkage and creep) are considerable.

Only with low percentages of reinforcement will the concrete not crack after unloading. This in itself already well known behaviour can be of importance in concrete structures in which unloading of compressed concrete can be expected.

3.6 **Conclusions**

Long-term tests were carried out on two series of longitudinally reinforced concrete columns to determine the time-dependent deformation under centrally applied sustained load along their axes. In these test the applied loads were of such magnitude that the deformations on loading the columns of each series were more or less equal.

The percentages of longitudinal reinforcement were 0, 0,5% 0,9%, 2%, 4% and 7%.

To compare the behaviour of the loaded columns with that of unloaded ones, two series of prisms with the same longitudinal reinforcement were studied.

In these series the influence of shrinkage on the deformations of reinforced concrete members could be observed.

In other tests the creep behaviour of the concrete and the strength of concrete at different age was verified.

All the specimens were placed in a climate-controlled room at 20°C and 50% relative humidity.

The test results could be compared with the deformations calculated with three theories: Dischinger's, Trost's and the Effective Modulus theory. In this comparison the real characteristics of the concrete were introduced into the calculation.

The results were also compared with a calculation based on values given in the recent CEB-FIP recommendations.

The deformations in time of the columns under sustained load were influenced by the magnitude of the longitudinal reinforcement. In one year the time-dependent deformation of reinforced concrete was reduced by about 50% when the longitudinal reinforcement was equal to 7% of the concrete section. With a lower percentage of reinforcement this reduction was smaller. The redistribution of stresses from concrete to steel was so important that in one case with 7% reinforcement it was found that tensile stresses had been introduced into the concrete at the end of one year.

The shrinkage of reinforced specimens was also reduced by the longitudinal reinforcement. When the percentage of this reinforcement was 7%, this reduction was nearly 60% compared with the unreinforced specimens.

After unloading, the columns with a high percentage of longitudinal reinforcement (4%, 7% and one of 2%) showed transverse cracks.

The recovery of the shortening of the unreinforced specimens after one month was nearly the same as the deformation on loading.

It is to be noted that the scatter in the characteristics of the concrete used which were of importance for the observed phenomena was really large.

In one year the shrinkage varied from $0,30 \times 10^{-3}$ to $0,34 \times 10^{-3}$ and in this period the creep factor varied from 1,8 to 2,5. On loading, Young's modulus varied from 22 to 32×10^3 N/mm² if calculated from the deformations on loading.

The test prisms showed values varying from 25 to 33×10^3 N/mm².

It can be concluded that it is very important to get better control of this phenomena in tests on time-dependent behaviour.

During the tests the evaporation of water was also measured on the non-loaded prisms.

In one year the evaporation of water was 44 kg/m³ with a standard deviation of $3,3$ kg/m³ (22 specimens).

Observation of the increase of evaporation with shrinkage showed that in the first months the shrinkage was delayed in relation to the rate of evaporation. The rate of the total deformation of loaded columns as a function of time was very similar to the rate of evaporation.

Comparison of the measured deformations with those calculated with the three theories leads to the following conclusions.

Shrinkage

The mean value of the total deformation of the non-loaded reinforced concrete specimens after one year, as calculated by Dischinger's method was 6% larger than

measured. Trost's method gave a mean value 2% smaller than measured, and the Effective Modulus theory 3% smaller. The shrinkage, creep and E_c values measured on the unreinforced specimens were used in these calculations.

Shrinkage and creep

The mean value of the total deformation of the loaded reinforced concrete columns after one year was with Dischinger 3 to 4%, with Trost 5 to 10% and with the Effective Modulus theory 7 to 12% smaller than measured.

These methods are therefore on the unsafe side. It may be necessary to introduce a higher shrinkage value into the calculations to get more appropriate results.

Comparison of the predicted deformations by using recent CEB-FIP recommendations showed that for the series with the lowest level of deformations the test results were very close to the predicted values for the percentages of reinforcement normally used in practice. The series with the higher level of deformations showed calculated values which were more than 10% higher than the observed values.

It can in general be concluded that Dischinger's theory, which is used in our method of analysis for partially prestressed concrete, shows close agreement between the calculated deformations and the measured ones.

The following items are recommended for future research.

1. Study of the phenomena causing restraint shrinkage and creep by using the knowledge obtained from research on the micro system, and introducing these phenomena into the real system of a structure.
2. Research on the variation of time-dependent behaviour of several types of concretes. Development of a method to diminish the magnitude of this variation in laboratory projects.
3. It seems necessary to standardize the shrinkage and creep tests in order to compare the results of different laboratories. Exclusion of several parameters such as curing dimensions of the specimen, temperature, climatic conditions is necessary to allow comparison of results. It would be useful if the standardisation of these tests included measurements of the loss of weight of the non-loaded prisms (and, after the test, of the loaded prisms) due to evaporation of water; evaluation of test results also with the introduction of the ratio $\epsilon'_{cst}/\varphi_t$ as a function of time.

Acknowledgements

The experimental work has been carried out by Dipl.-Ing. J. Bednar during his stay at the Stevin Laboratory. His contributions are gratefully acknowledged.

4 Time dependant deflection of partially prestressed concrete beams

4.1 Description of time-dependent behaviour in general

4.1.1 Plain concrete

Concrete shows time-dependent deformations due to shrinkage and creep. The amount of shrinkage is influenced by several factors, of which the moisture content of the concrete and moisture transport in the concrete may be mentioned.

When concrete dries rapidly, the shrinkage deformations are considerable over a short period. This is the case in thin concrete structures under climatic conditions with low relative humidity.

If the concrete structure is more massive, the drying of the concrete takes place over a long period and therefore shrinkage proceeds at a slow rate. Due to differences in moisture content in the concrete, shrinkage stresses are built up in the structure, caused by partial restraint of shrinkage.

The amount of creep deformation is influenced by the compressive (or tensile) stresses acting on the concrete and by the moisture conditions of the concrete, as is shown in paper 3.

4.1.2 Reinforced concrete structures

In reinforced concrete structures the bonded reinforcement reduces the time-dependent deformations of the concrete. The steel will undergo deformations only if it is stressed. A shortening of the concrete and reinforcement in time causes compressive stresses in the steel and – as a result – a reduction of compressive stresses in the concrete (Fig. 4.1).

This “redistribution” of stresses reduces the time-dependent overall deformations compared with these deformations in unreinforced concrete. With the method originally proposed by Dischinger the change of a uniformly distributed concrete stress on a section in time can be expressed by the formula described in paper 1.

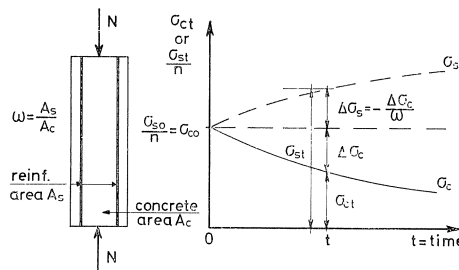


Fig. 4.1. Stresses versus time.

In paper 3 it is shown that Dischinger's method predicts the redistribution of compressive stresses in axially loaded columns very well (Fig. 4.1).

The revised Dischinger formula can be written as follows

$$\Delta\sigma_c = \left(\sigma_{c0} + \frac{\varepsilon'_{cs\infty} E_c}{\varphi_{\infty}(1+n\omega)} \right) (1 - e^{-\alpha\omega}) \quad \text{with} \quad \alpha = \frac{n\omega}{1+n\omega}$$

Because

$$A_c \Delta\sigma_c + A_s \Delta\sigma_s = 0 \quad \Delta\sigma_s = -\frac{1}{\omega} \Delta\sigma_c$$

The deformation of the reinforcement as a function of time can be calculated with the change $\Delta\sigma_c$ over the period $t=0$ to $t=t$.

$$\Delta\varepsilon_s = -\frac{1}{\omega E_s} \cdot \Delta\sigma_c = \varepsilon_{s0} - \varepsilon_{st}$$

The total deformation of the reinforcement can therefore be calculated with

$$\varepsilon_{st} = \varepsilon_{s0} + \frac{1}{\omega E_s} \Delta\sigma_c$$

With an increase $\Delta\sigma_c$ of the compressive stress in the concrete the elongation ε_{s0} of the reinforcement is reduced, and with an increase $\Delta\sigma_c$ of the tensile stress in the concrete the elongation ε_{s0} will also increase in time.

4.1.3 *Uncracked reinforced tendons under uniform distributed tensile stresses*

If a tensile force N produces concrete stresses which belong to the linear elastic part of the stress-strain diagram, at the time $t=0$, we can calculate the stresses in the steel and concrete with the formula:

$$\sigma_{c0} = \frac{N}{(1+n\omega)A_c}$$

$$\varepsilon_{c0} = \varepsilon_{s0} = \frac{\sigma_{c0}}{E_c} = \frac{\sigma_{s0}}{E_s}$$

$$\sigma_{s0} = n\sigma_{c0}$$

Over the period t we have found:

$$\varepsilon_{s0} - \varepsilon_{st} = \Delta\varepsilon_s = -\frac{1}{\omega \cdot E_s} \cdot \Delta\sigma_c$$

Therefore we can write:

$$\Delta \varepsilon_s = -\frac{1}{\omega \cdot E_s} \left(\frac{N}{(1+n\omega)A_c} + \frac{\varepsilon'_{cs\infty}}{(1+n\omega)} \cdot \frac{E_c}{\varphi_\infty} \right) (1 + e^{-\alpha\varphi})$$

$$\Delta \varepsilon_s = -\left(\varepsilon_{s0} + \frac{\varepsilon'_{cs\infty}}{\varphi_\infty} \frac{1}{1+n\omega} \right) \frac{(1 - e^{-\alpha\varphi})}{n\omega}$$

From this the following conclusions can be drawn; putting:

$$\frac{\varepsilon'_{cs\infty}}{(1+n\omega)\varphi_\infty} = \bar{\varepsilon}_{cs}$$

4.1.3.1 $\varepsilon_{st} > \varepsilon_{s0}$ gives a time-dependent elongation if $\Delta \varepsilon_s$ is negative. In this case the value $|\varepsilon_{s0} + \bar{\varepsilon}_{cs}|$ is positive.

This means that the elongation ε_{s0} is larger than the shrinkage value $|\bar{\varepsilon}_{cs}|$.

4.1.3.2 $\varepsilon_{st} < \varepsilon_{s0}$ if $|\varepsilon_{s0}| < |\bar{\varepsilon}_{cs}|$

4.1.3.3 $\varepsilon_{st} = \varepsilon_{s0}$ if $|\varepsilon_{s0}| = |\bar{\varepsilon}_{cs}|$

We can conclude that there is *no* time-dependent deformation of the uncracked tendon of the reinforced concrete tensile zone if the elongation of the steel has the same value as the shrinkage shortening $\bar{\varepsilon}_{cs}$.

A higher steel elongation causes an *elongation* in course of time. A lower steel elongation causes a *shortening* in course of time.

Example

$$\varepsilon'_{cs\infty} = -0,2 \times 10^{-3} \quad \text{and} \quad -0,4 \times 10^{-3}$$

$$\varphi_\infty = 2,5, \quad n = 8$$

Graph in Fig. 4.2

$$\omega = 0 \dots 0,05$$

$|\bar{\varepsilon}_{cs}|$ has normally a value between 0,1 and $0,2 \times 10^{-3}$.

Because the ultimate tensile strain has a value between 0,08 and $0,12 \times 10^{-3}$ it is clear that if no cracks in the concrete occur, the value of ε_{s0} must be smaller than the ultimate strain and therefore in most cases $|\bar{\varepsilon}_{cs}|$ will be larger than the ultimate strain ε_{s0} .

Therefore it can be concluded that in the cases of an uncracked reinforced tendon a *shortening* of the tendon in course of time will be observed.

The shrinkage shortening of such a tendon is only partly reduced by the creep of concrete under tension.

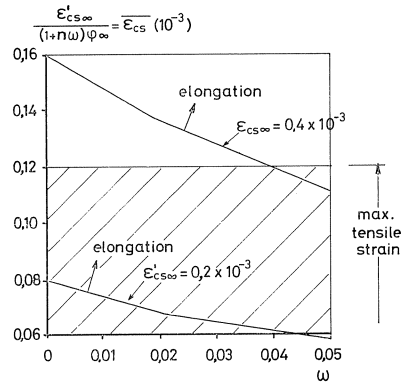


Fig. 4.2. Example.

Fig. 4.2 shows that in most cases the values of $\bar{\epsilon}_{cs}$ are high. Therefore an important reduction of these deformations by reinforcement is possible only under the following conditions:

- a high percentage of bonded reinforcement
- a low modulus of elasticity of the concrete ($n = \text{high}$)
- a high creep factor
- a low shrinkage value of the concrete.

4.1.4 Cracked reinforced concrete tendon

4.1.4.1 Assumed that there is a zone between two cracks in the tendon in which the deformations of the concrete and reinforcement are equal. In this case two zones can be distinguished in a portion of the tendon between two cracks (Fig. 4.3):

- a. Transfer zone of tensile stresses into the concrete.
At the end of this zone there is a uniformly distributed tensile stress over the section.
- b. The zone (b) with uniformly distributed tensile stress over the section.

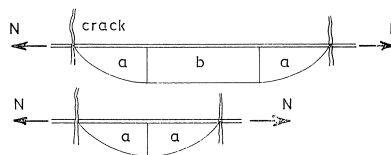


Fig. 4.3. Bond between cracks.

In this case we can use the above-mentioned approach of uncracked reinforced concrete with the introduction of a reduction factor c . In zone (b) this factor is 1. In zone (a) the tensile stresses in the steel are higher than in zone (b). The shrinkage of

concrete is only partly “resisted” by the reinforcement. Therefore the time-dependent deformation of the steel is reduced. This gives a reduction factor < 1 .

In relation to the case of an uncracked concrete tendon ($\Delta\varepsilon_{s,un}$) the deformation ($\Delta\varepsilon_{s,cr}$) is reduced in this case. We can write as an approximation

$$\Delta\varepsilon_{s,cr} = c\Delta\varepsilon_{s,un}$$

$$0,6 < c < 0,9$$

4.1.4.2 Relative displacements between reinforcement and concrete. In this case it is very difficult to calculate the time-dependent deformations of the tendon. If the stresses in the reinforcement are no longer reduced in course of time, the “tension stiffness” of the concrete is zero. This means that the steel has an elongation $N/(A_s \cdot E_s)$ at the end of this period.

If this situation is reached, the concrete is tensionless and will only shrink. Shrinkage shortening can of course partly be reduced by the reinforcement. As a limit case it can be assumed that shrinkage does not change the length of the (steel)tendon but only widens the cracks; it means that there is no influence of tension stiffening. In a cracked concrete tendon the shortening of the tendon due to shrinkage is reduced in relation to an uncracked tendon. If one considers a large distance between two cracks, a slightly reduced shortening of the tendon due to shrinkage will occur (small tensile force and low percentage of reinforcement).

In the case of small distance between two cracks the shortening in course of time can be zero, causing widening of cracks (large tensile force and high percentage of reinforcement).

To demonstrate the various cases of behaviour in Fig. 4.4 the relationship is given between the shortening of a concrete tendon and the shrinkage of concrete.

4.1.5 Reinforced concrete beam in bending

In this case there is an interaction between the reinforced concrete tendon in the tensile zone and the compression zone of a beam.

Fig. 4.5 gives the moment – curvature relationship of a section of a concrete beam.

1. Uncracked tensile zone – short-term test
2. Uncracked tensile zone – long-term test
3. Cracked tensile zone – no tension stiffening – short-term test
4. Cracked tensile zone – no tension stiffening – long-term test
5. Influence of tension stiffening – short-term test.
6. Influence of shrinkage – uncracked tensile zone.

In this case there is no influence of the bending moment on the curvature caused by shrinkage. The curvature is caused by the reduction of shrinkage shortening due to the reinforcement in the tensile zone.

7. Influence of shrinkage – no tension stiffening.

Because there is no tension stiffening the influence of shrinkage is independent of the bending moment.

8. Influence of shrinkage – influence of tension stiffening.

Increase of the bending moment causes the tension stiffening to decrease. Therefore in this case there is – indirectly – an influence of the bending moment on the curvature caused by shrinkage.

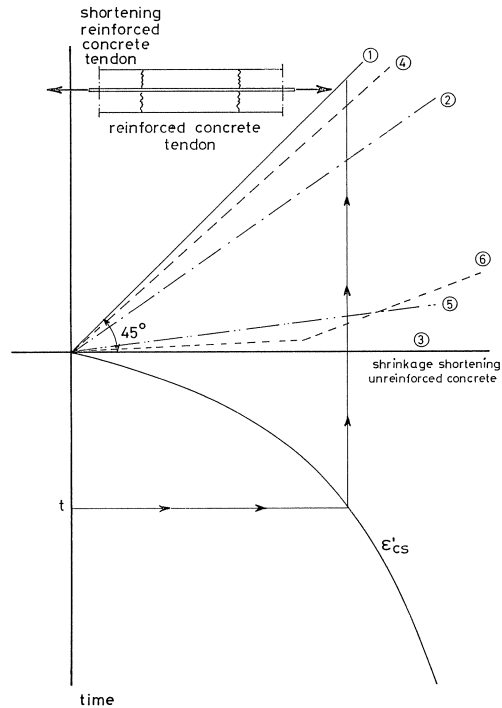


Fig. 4.4. Strain behaviour of various members.

- 1 = plain concrete
shortening = shrinkage
- 2 = reinforced uncracked concrete tendon
shortening reduced with respect to free shrinkage (influence of reinforcement)
- 3 = unreinforced cracked concrete tendon
no reinforcement; shrinkage causes only widening of cracks
Therefore no shortening of the tendon as a whole is observed
- 4 = small tensile force; low percentage of reinforcement, cracked concrete
shortening is only a slightly reduced shrinkage
- 5 = high tensile force; high percentage of reinforcement, cracked concrete
no tension stiffening – no considerable shortening of the tendon in course of time
- 6 = observed relationship for a cracked reinforced tendon in experiments
In the first period no shortening, because new cracks in the concrete appear.
Later on, influence of deformations caused by shrinkage and improved bond behaviour.

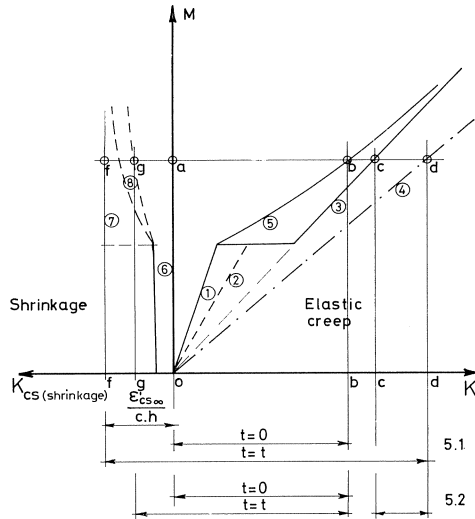


Fig. 4.5. Moment-curvature relationship.

4.1.5.1 Beam with a high percentage of reinforcement and adequate elongation of the steel, but no reinforcement in the compression zone.

In Fig. 4.5 all influences in this case on curvature of a section in bending can be clearly shown.

- M - κ -diagram – short-term test, line 1–5.
At bending moment $M = a$, $\kappa = ab$.
- Due to long-term loading the influence of tension stiffening may decrease due to bond creep and shrinkage, extra curvature $\kappa = bc$.
- Due to long-term loading the compression zone shortens due to creep – extra curvature $\kappa = cd$.
- Due to shrinkage the curvature increases with $\kappa = af$, if there is no tension stiffening. The tensile zone has a constant length. In this case, assuming there is no tension stiffening, the curvature at bending moment M increases from $\kappa = ab$ to $\kappa = fd$. The time-dependent curvatures are very important, causing considerable deflections of the concrete elements.

4.1.5.2 Beam with a small percentage of reinforcement and an adequate elongation of the steel.

- M - κ -diagram – short-term test, line 1–5.
- The influence of tension stiffening is not decreased in course of time $\kappa = \overline{ab}$.
- Due to long-term loading the compression zone shortens. $\kappa = \overline{cd}$.
- Due to shrinkage of concrete both compression zone and tensile zone are shortening and the curvature of the section by shrinkage is small.

In this case κ is, during the time of testing, increased from $\kappa = \overline{ab}$ to $\kappa = \overline{gb} + \overline{cd}$. In

comparison with case 4.1.5.1 the curvatures caused by time-dependent influences are smaller.

4.1.6 Influence of prestress on the deformations

In prestressed concrete the amount of “reinforcement” depends on the type of the structure.

If the “reinforcement” consists only of prestressing steel the percentage of reinforcement is relatively small and the compressive force on the section is high. If the tensile zone is cracked (P.P.C.) the additional tensile force caused by elongation of the concrete and cracks in the tensile zone is small.

This case can be compared with 4.1.5.2. It means that the time-dependent deflections are reduced in comparison with case 4.1.5.1. If the P.P.C. beam has a low magnitude of prestress and a high percentage of normal reinforcement the case is more connected to 4.1.5.1.

This description of the time-dependent influences shows that it is not possible to give general rules for the time-dependent deflections of partially prestressed concrete with a cracked tensile zone, without introducing parameters, related with the amount and the type of reinforcement.

Remark

1. Fully prestressed concrete (uncracked tensile zone) shows great flexural rigidity. Also, the time-dependent deflections are small because there is no curvature due to shrinkage (case 4) but only due to creep.
2. In partially prestressed concrete beams (P.P.C.) the tensile zone is cracked over only a limited length because the prestressing force normally introduces compressive stresses in the concrete which are not reduced sufficiently near the supports to produce cracks under normal loads.

4.2 Information from literature

Study of the literature causes difficulties because the definition of partially prestressed concrete (P.P.C.) as a concrete structure of Class III according to the CEB-FIP-recommendations of 1970 is rather poor.

In fact, many combinations of P.P.C.-structures are possible, all of them belonging to Class III structures.

The following methods of defining Class III structures can be mentioned:

1. Combinations of prestressing steel and normal (low-tensile) reinforcement.
2. Combinations of prestressed and non-prestressed high-tensile steel.
3. The magnitude of the average prestress in the concrete.
4. The “level” of prestressing, defined as:

$$\lambda = \frac{A_{sp} \cdot f_{0,2}}{A_{st} \cdot f_y + A_{sp} \cdot f_{0,2}}$$

5. The “level” of prestressing ψ defined as the total prestressing force at zero stress in the tensile zone related to this prestressing force for Class I prestressed concrete

$$\psi = \frac{F_{R\infty}}{F_{Rl\infty}}$$

The list of possibilities clearly shows that if P.P.C. is considered, it is necessary properly to define which type of Class III structures is envisaged.

Test by E. W. Bennett at Leeds University [25] carried out on T-beams in P.P.C. with a prestress of $1,6 \text{ N/mm}^2$, $\lambda = 0,86$, $\psi = 0,50$ showed that under sustained design load (load factor 1.8) the following can be observed:

- in 300 days the deflection of the beams, by applying symmetrical concentrated loads, increased to more than twice the initial value, while about 50% of the additional deflections occurred within the first 20 days of loading;
- recovery after unloading was only 15% in nearly 30 days;
- in the course of 300 days the crack width in the tensile zone increased from 0,10 mm to 0,13 and 0,18 mm, i.e., 130% to 180% of the original values.

These tests showed that in this case with a low prestress but a relatively high percentage of reinforcement the tension stiffening is reduced under long-term loading so that cracks, even small in width, do not close up after removal of the load.

The minimum prestress in the concrete for closure of the cracks on unloading was nearly 2 N/mm^2 .

The following test data obtained by Bennett concerning the behaviour under sustained loading call for mention:

beam	loading deflection (midspan) crack width			after 300 days sustained loading	
	at $0,55M_u$	at $0,55M_u$	M_u	deflection	crack width
B1	12,6 mm	0,08 mm	$3458 \times 10^4 \text{ Nmm}$		
S	15,0 mm	0,10 mm		33 mm	0,18 mm
B2	25,6 mm	0,16 mm	$6070 \times 10^4 \text{ Nmm}$		
S	23,0 mm	0,11 mm		49 mm	0,13 mm
B4	24,7 mm	0,08 mm	$6010 \times 10^4 \text{ Nmm}$		
S	24,0 mm	0,11 mm		54 mm	0,16 mm

* Index S beams tested under sustained loading
 M_u for these beams marginally higher than those of the other beams.

Cederwall [28] observed the time-dependent behaviour of reinforced concrete beams and several beams with prestressed reinforcing bars.

No observations on the development of cracks, etc. are reported. Only the curvatures of the zone in which the cracks appeared were calculated.

A lightweight P.P.C. beam was tested at the Federal Technological University (E.T.H.) at Zürich [27, 31].

In these beams with a concrete section of 116.500 mm^2 the compression zone was reinforced with 505 mm^2 ; the magnitude of prestress was $2,6 \text{ N/mm}^2$ and $\lambda = 0,43$; $\psi = 0,48$.

The shrinkage of concrete during the test period (2 years) was 36×10^{-5} , and the creep factor φ was 0,4 after 4 months and 1.05 after 2 years.

	days after concreting	
	3	730
time-dependent deflection (midspan)	1,3 mm	8 mm
number of cracks in the zone of constant bending moments	34	35
maximum crack width	0,15 mm	0,18–0,20 mm
mean value of tensile strain in the cracked zone	$0,9 \times 10^{-3}$	$1,3 \times 10^{-3}$

Remark: Increase in tensile strain during the first 3 months.

In a subsequent report [31] the behaviour of the beam during the next three years is discussed.

During this time the curvature of the beam increased by 2,3%. This is in agreement with the increase in total deflection by 2,6%. The width of the cracks in this beam remained unchanged during the last three years and the neutral axis was displaced downwards by about 5 mm (in the first two years by 80 mm).

In this beam a considerable amount of normal reinforcement was put into the compression zone (0,45% of total beam cross-section). This reinforcement caused a reduction of the deformation of the compression zone due to shrinkage (and creep).

The increase in the steel stress in the tensile zone after cracking was limited in the calculation to 150 N/mm^2 , according the S.I.A. standard 162.

The strain, due to loading in the zone of tensile reinforcement, was nearly constant ($1,26 - 1,37 \times 10^{-3}$).

In this case the tension-stiffening of the tensile zone was reduced. This resulted in a nearly constant length of the tensile zone and a deflection caused by shrinkage and creep of the compression zone.

Stevens [35] tested 24 pairs of reinforced concrete beams ($0,2 \times 0,385 \text{ m}$) with the following variables:

- strength of reinforcing steel
- concrete cover
- proportions of reinforcement – balanced and half balanced
- environment – controlled and natural

Tests were continued for two years.

Within the scope of this report the most important conclusions are:

During the first three months an increase in elongation at the level of the reinforcement (“crack strain”) was observed.

After a period of one year an almost constant length of the tensile zone at the centre of the reinforcement was observed.

When the time-dependent deflections were calculated with a maximum compressive strain in the concrete allowing for creep and shrinkage, the relationship was:

$$\varepsilon'_{ct} = \frac{\sigma'_{c1}}{E_c} (1 + 0,67\varphi) + \varepsilon'_{cs}$$

this method gives an average calculated deflection to estimated deflection of 1.00 with a standard deviation of 0,08.

Calculation of tension stiffening effects from the measurements showed that on an average the value of the tensile force, resisted by the concrete between the cracks was reduced to about one-third of that developed just before cracking.

The deflection of beams in two years was more important in beams with a high percentage of reinforcement in comparison with beams with a low percentage of reinforcement.

A_s/bh in %	2,3	1,4	1,1	0,8	0,6
type	A	E	B-J	F	K
deflection in time in mm	2,03	1,85	1,14 (1,60)	1,3	(1,27)
direct deflection in mm	1,93	2,29	1,02 (2,72)	1,42	(1,58)

() – very high strength steel

These phenomena can be explained with the influence of tension stiffening given at 4.1.5.1 and 4.1.5.2.

Corley and Sozen [34] tested four small reinforced concrete beams ($0,08 \times 0,18$ m and $0,08 \times 0,13$ m) and compared the results of these tests with measured deflections published by others. They propose a simple expression for the curvature caused by the creep of concrete, assuming that during the time that creep strain occurs the steel strain in the tensile zone does not change and the strain distribution remains linear.

A similar approach is proposed for the curvature caused by shrinkage, taking into account – if necessary – the compression reinforcement. In the analysis of the results of the deflections calculated with the given assumptions and the measured deflections they write:

“Where important differences between measured and computed deflections do exist the method on computation tends to overestimate the amount of deflection. This trend is most apparent in beams with low percentages of steel . . . Even when only a part of the span was considered to be cracked the computed deflection for each beam (referred to) was more than that measured . . .

As previously noted, tension in concrete becomes more significant as the steel percentage decreases”.

These phenomena can be explained with the model given in 4.1.5.1 and 4.1.5.2 where the influence of tension stiffening is described.

A perusal of the literature concerned with time-dependent behaviour gives only rather scanty information. It can be concluded that the influence of time on the behaviour of cracked P.P.C. beams with enough bonded reinforcement may be loss off tension stiffening resulting in:

1. Widening of cracks in the tensile zone;
2. Increase in deflection of the beam at midspan.

Some tests indicate that with sufficient bonded reinforcement no increase in the length of the reinforced tensile zone can be expected in course of time.

The description given of the expected behaviour of beams in P.P.C. with only a small percentage of bonded reinforcement in the tensile zone shows that none of the above mentioned experiments were carried out on such beams.

Experiments were accordingly carried out in the Stevin Laboratory with the following aims [23, 32]:

1. to control the results of experiments on a beam with a large quantity of bonded reinforcement;
2. to study the behaviour of P.P.C. beams with a cracked tensile zone and to compare this behaviour with a beam of the same type but with an uncracked tensile zone.

4.3 The experiments

Two test series were carried out, each consisting of two beams. The cross-sections of the four beams were the same. Information on the reinforcement of these four beams is given in the table below.

beam type		tensile zone	reinf. steel	prestr. steel	prestr. force start of test
serie 1	1.1. P.P.C.	uncracked	2∅6	7∅4*	109 kN
	1.2. Reinf. conc.	cracked	2∅6-1∅22		
serie 2	2.1. P.P.C.-bonded tendon	cracked	2∅6	7∅4*	65 kN
	2.2. P.C.C.-unbonded tendon	cracked	2∅6	7∅4*	70 kN

* strand

The beams 2.1 and 2.2 were loaded above the cracking load in preliminary tests, thus introducing cracks in the tensile zone. To have open cracks under the same sustained load the prestressing force was reduced in comparison with beam 1.2.

Beams 1.1 and 1.2 were precast in a factory. The beams 2.1 and 2.2 were produced in the laboratory.

The cross-section of the beams is given in Fig. 4.6.

The relevant data concerning material properties, deformations of the beams and the stress distribution are compiled in the appendix A 4.1. Material properties are summarized in Table A 4.1.

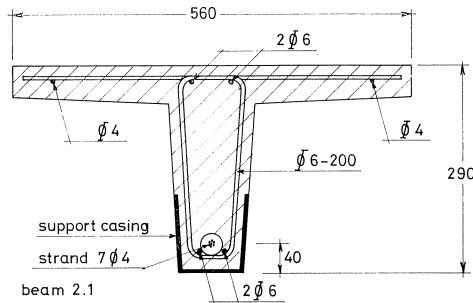


Fig. 4.6. Cross-section of test-beam.

After concreting, prestressing and precracking (beams 2.1 and 2.2) the beams were placed in a room with constant relative humidity ($50\% \pm 2\%$) and temperature ($20^\circ\text{C} \pm \frac{1}{2}^\circ\text{C}$).

The beams 1.1 and 1.2 were loaded with concrete tiles. The beams 2.1 and 2.2 were supported by pendulums connected with a steel frame and subjected to a four

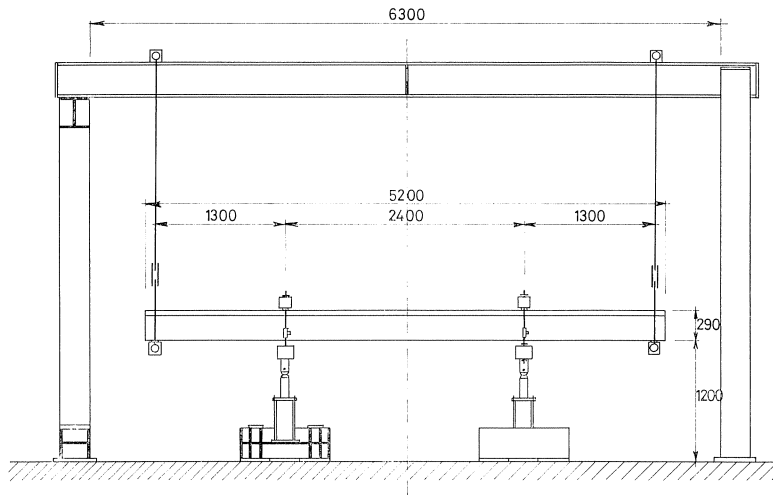


Fig. 4.7. Testing frame.

point loading. The beams stayed in the room with controlled climatological conditions for more than one year.

During this time measurements were carried out on

- concrete strain at midspan
- deflection at midspan and quarter span
- prestressing force in the tendon of beam 2.2
- creep and shrinkage behaviour of testprisms.

After the long term test the beams were loaded to failure. The data, concerning the test-results are compiled in the tables (A4.2, A4.3, A4.4, A4.5 and A4.6).

After the tests under sustained load the four beams were loaded till failure with a four point loading test. Testframe see Fig. 4.7. Crack distribution in beam 2.1 and 2.2 see Fig. 4.8. Testresults in table A4.7.

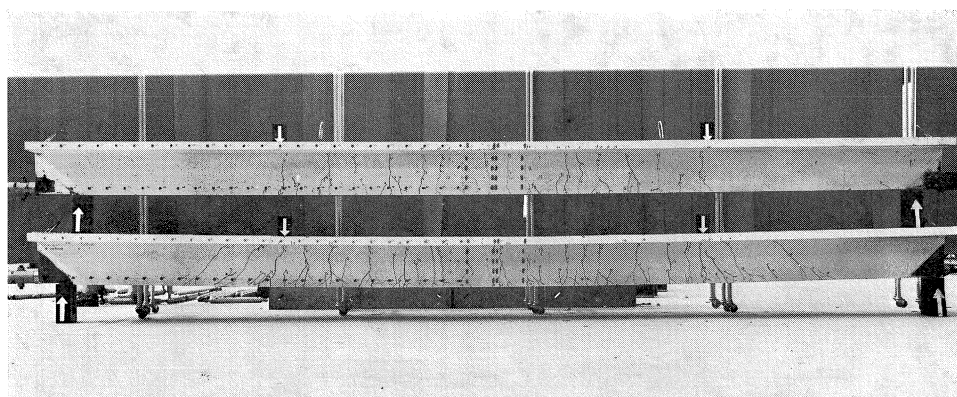


Fig. 4.8. Crack distribution.

4.4 Analysis of experimental results

4.4.1 Deflections at mispan under short term loading

Beam	1.1	1.2	2.1	2.2
	1.9 mm	5.0 mm	2.2 mm	2.3 mm

The rigidity of beam 1.1 with an uncracked tensile zone is higher than that of beam 2.1 and 2.2 with a cracked tensile zone. The differences between the deflections of the beams 2.1 (grouted duct) and 2.2 (ungouted duct) are very small. It can be concluded that – as already known – the rigidity of concrete beams with an uncracked tensile zone is large in comparison with beams with tension cracks.

Due to cracking of a part of the tensile zone the rigidity of a beam with the same cross-section is decreased by 30%–40%. This decrease is relatively small because only a part of the tensile zone of the beams 2.1 and 2.2 is cracked and the crack width is

small. The rigidity of the reinforced concrete beam (1.2) is decreased by more as 50% in relation to beam 1.1.

This is so because the tension stiffening of the tensile zone beam 1.2 is only of minor importance. The tensile force in the reinforcement must be built up to carry the sustained load. Therefore considerable elongation of the reinforcement is necessary.

4.4.2 Increase in deflection at midspan under sustained load

beam	1.1	1.2	2.1	2.2
increase in deflection	0,5 mm	5,9 mm	1,9 mm	2,6 mm
time	361 days	361 days	681 days	524 days

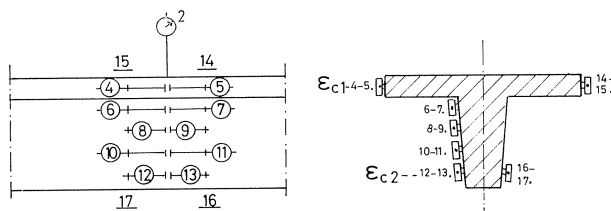


Fig. 4.9. Measurements of concrete strains at midspan.

The increase in deflection of beam 1.1 was very small, being only 20% of that measured in the short-term loading test. This low value can be explained by the nearly uniform distributed (compressive) stresses in the cross-sections.

The increase in deflection of beam 2.1 (grouted duct) is 85% of that measured in short-term loading and that of beam 2.2 is 115%. This difference in increase of deflection between beam 2.1 and 2.2 shows the influence of the grouted duct. The height (length) of the cracks in beam 2.1 was smaller in relation to that in beam 2.2, because in the latter case there were only two 6 mm diameter bonded bars across the cracks. Therefore the compressive stresses at the top of beam 2.2 were higher, causing more creep shortening of the concrete.

The increase in deflection of beam 1.2 was considerable, but in relation to the short-term deflection it was “only” 120%, assuming no tension stiffening.

The deflection of this beam can be calculated with the formulae

$$\delta_{\text{mid}} = \frac{1}{8} x_{\text{mid}} l_t^2$$

$$x_{\text{mid}} = \frac{\epsilon'_{cs}}{c \cdot h}$$

With $\epsilon'_{cs} = 0,365 \times 10^{-3}$, $h = 250$ mm and $l_t = 5000$ mm, we find – assuming $C = 0,9$ – $\delta_{\text{mid}} = 5,1$ mm.

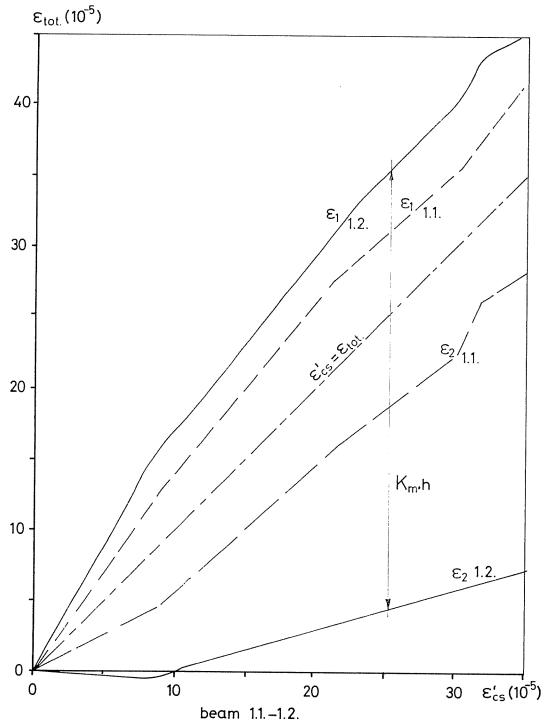


Fig. 4.10. Strain distribution in beams 1.1 and 1.2.

This value shows that only a small part of the time-dependent deflection of this beam is caused by loss of tension stiffening of the tensile zone and creep of the compression zone.

4.4.3 Deformation of the tensile zone under sustained load

beam	1.1	1.2	2.1	2.2
deformation	$-30,6 \times 10^{-5}$	$-7,8 \times 10^{-5}$	$-15,3 \times 10^{-5}$	$-13,8 \times 10^{-5}$
shrinkage (prisms)	$-36,5 \times 10^{-5}$	$-36,5 \times 10^{-5}$	$-32,0 \times 10^{-5}$	$-28,1 \times 10^{-5}$

In all cases a *shortening* of the tensile zone was found. This shortening was lowest in the reinforced concrete beam (1.2) causing widening of cracks (Fig. 4.10).

The number of cracks (45) with a spacing of nearly 100 mm on a reinforcing bar of $\varnothing 22$ makes it clear that tension stiffening could only be of minor importance. That in this case a shortening of the tensile zone occurred can partly be explained by the influence of the bond of the two small diameter bars and bond slip of the main bar allowing the surrounding concrete to shrink. The difference in shortening of beams

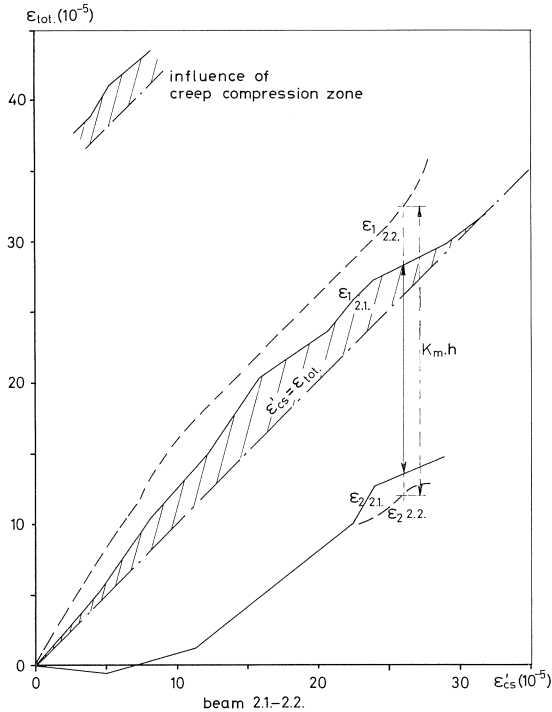


Fig. 4.11. Strain distribution in beams 2.1 and 2.2.

2.1 and 2.2 in relation to beam 1.1 can be explained by the influence of the stress distribution over the cross-section (Fig. 4.11).

Due to higher compressive stresses, caused by the prestressing force, the creep deformations in the bottom of beam 1.1 are of greater importance than those in beams 2.1 and 2.2.

The reduction of the tensile zone shortening of beams 2.1 and 2.2 with regard to the shrinkage deformations measured on prisms, over the same period, is due to the influence of tensile stresses in the concrete between two cracks and to that of bonded reinforcement.

Assuming φ to be 2, n to be 6 and $A_c = 90 \times 100 = 9000 \text{ mm}^2$ we obtain for $|\bar{\epsilon}_{cs}|$ a value between $0,14$ and $0,16 \times 10^{-3}$ or, “translated” into steel stresses, a value between 29 and 34 N/mm^2 . Beam 1.2 – reinforced concrete – had a steel stress in the cracks of approx. 170 N/mm^2 , i.e., a relatively high value of concrete strain between two cracks.

Therefore more cracks were developed in course of time, causing a relaxing of tension stiffening. Beams 2.1 and 2.2 underwent an increase in steel stress (after reaching zero stress in the concrete of the tensile zone) of 10 to 15 N/mm^2 .

Therefore no extra cracks appeared as time went by. This effect resulted in shortening of the tensile zone.

4.5 Summary of experimental results

The experimental results can be summarized as follows:

1. With low percentages of reinforcement, tension stiffening in the short-term test is likely to be considerable. This effect is also considerable in a long term test. Therefore the shrinkage shortening of the cracked tensile zone will be greater than the crack widening due to shrinkage of concrete between the cracks. The time-dependent deflections are reduced in comparison with a beam with a normal percentage of reinforcement.
2. The phenomenon mentioned in 1. is enhanced by the effect of prestressing, because the prestressing force “increases” the shrinkage shortening force.
3. In P.P.C. beams with straight tendons in the tensile zone this zone is cracked only in the part of the beam with high bending moments.

In statically determinate beams the parts of the beams near the supports are uncracked.

Therefore the overall flexural stiffness of the P.P.C. beam is only slightly reduced in relation to the stiffness of the P.P.C. beam with an uncracked tensile zone.

From this point of view the influence of prestressing on deflections (and time-dependent deflections) is also favourable, especially if the increase in steel stress (after the bending moment with zero stress at the bottom of the concrete) is limited to 150 N/mm^2 or less.

4. The failure load of beams, prestressed with unbonded tendons, can be considerably reduced if the reinforcement has not enough uniform distributed elongation before failure.
5. The influence of time-dependent deformations over the depth of a beam is such that Bernoulli's law “plane sections remain plane” is not adequate.
This can be concluded from the strain measurements on beams 2.1 and 2.2.

4.6 Conclusions

1. Generally speaking, the tests have shown that the behaviour of the tendons in practice was indeed as expected.
2. It is not easy to predict the real values of the time-dependent deflection of P.P.C. beams. The test series has not given enough information for establishing design rules.
3. It can be assumed that, generally speaking, the prestress reduces the time-dependent deformations in relation to normally reinforced concrete.
4. The chosen type of beam, the magnitude of the prestressing force and the load made it possible to compare the test results with one another. Agreement between these beams and many practical solutions is not particularly good.

5. It is of no use to continue the tests without more knowledge of the time-dependent behaviour of a cracked and uncracked concrete “tendon”. With tests on concrete “tendons” a new theory for this behaviour, which has yet to be developed, can be checked.

The new experiments could be as follows:

1. Tensile tests on symmetrical reinforced concrete columns of square cross-section with variable percentages of reinforcement.
2. Creep tests on these columns with a cracked concrete section and observation of the time-dependent deformations of the steel and concrete near the cracks.
3. Relaxation tests on such columns with a cracked concrete section and the same observation mentioned in 2.

5 References

1. BRUGGELING, A. S. G.: Het gedrag van betonconstructies, T.H.-Delft, 1975.
2. THÜRLIMANN, B. et al.: Biege- (Schub-)versuche an teilweise vorgespannten Betonbalken, ETH-Zürich, Berichte Nr. 6504-1 trough – 5.
3. WALTHER, R., BHAL, N. S.: Teilweise Vorspannung. DAFStb Heft 223, Berlin 1973.
4. Commissie Uitvoering Research (CUR): Gedeeltelijk voorgespannen beton, Report 87, 1977.
5. BRUNEKREEF, S. H.: Gedeeltelijk voorgespannen beton op buiging belast, Stevin lab., T.H.-Delft, No. 5-76-8, Delft 1976.
6. THÜRLIMANN, B.: Shear strength of reinforced and prestressed concrete beams CEB-approach Paper, distributed at the ACI-symposium 1976, Philadelphia U.S.A.
7. THÜRLIMANN, B., GROB, J.: Bruchwiderstand und -bemessung von Stahlbeton- und Spannbetontragwerken. Erläuterungen zu Richtlinie 34 der Norm SIA 162. Bericht Nr. 66 Institut für Baustatik ETH-Zürich, Sept. 1976.
8. BRAESTRUP, M. W., NIELSEN, M. P., FINN BACH, JENSEN, B. CHR.: Shear tests on reinforced concrete T-beams. Seris T Rapport Nr. R 72 1976. Afdelingen for Baerende konstruktioner, Danmarks Tekniske Højskole.
9. NIELSEN, M. P., BRAESTRUP, M. W., Plastic shear strength of reinforced concrete beams Rapport Nr. R 73 1976. Structural Research Laboratory, Technical University of Danmark.
10. BRAESTRUP, M. W., Plastic analysis of shear in reinforced concrete. Rapport No. 70, Juli 1974. Technical University of Danmark.
11. LYNGBERG, B. S.: Ultimate shear resistance of partially prestressed reinforced concrete beams. Journal of the ACI. April 1976.
12. BENNETT, E. W., BALASOORIYA, B. M. A.: Shear strength of prestressed beams with thin webs failing in inclined compression. Journal of the ACI-March 1971.
13. LEONHARDT, F., KOCH, R., ROSTÁSY, F. S.: Schubversuche an Spannbetontragern. Deutscher Ausschuss für Stahlbeton – Heft 227 – Berlin 1973.
14. JUNGWIRTH, D.: Elektronische Berechnung des in einem Stahlbetonbalken im gerissenem Zustand auftretenden Kräftezustandes unter besonderes Berücksichtigung des Querkraftbereiches. Deutscher Ausschuss für Stahlbeton, Heft 211, 1970.
15. PLACAS, A., REGAN, P. E.: Shear failures of reinforced concrete beams. Proceedings, ACI, Okt. 1971.
16. CEDERWELL, K., HEDMAN, O., LOSBERG, A.: Shear strength of partially prestressed beams with pretensioned reinforcement of high grade deformed bars. ACI-Special Publication SP-42. pp. 215–230.
17. KUPFER, H., HILSDORF, H. K., RÜSCH, H.: Behaviour of concrete under biaxial stresses. Journal of the ACI – August 1969.
18. NELISSEN, L. J. M.: Biaxial testing of normal concrete. Heron, Vol. 18, No. 1, 1972 – Stevin Laboratory, Technical University Delft.
19. CEB – Bulletin d'Information No. 117-F 1977, pp. 66–67.
20. FENWICK, R. C., PAULAY, T.: Mechanisms of shear resistance of concrete beams. Journal of the structural division, ASCE, Vol. 94, No. ST. 10, Proc. Paper 2345, Okt. 1968, pp. 2325–2350.
21. HOUDE, J., MIRZA, M. S.: A finite element analysis of shear strenght of reinforced concrete beams. ACI – Special Publication SP – 42.
22. BAUMANN, T., RÜSCH, H.: Versuche zum Studium der Verdübelungswirkung der Biegezugbewehrung eines Stahlbetonbalkens. Deutscher Ausschuss für Stahlbeton, Berlin 1970, Heft 210.
23. BRUGGELING, A. S. G.: De constructieve beïnvloeding van de tijdsafhankelijke doorbuiging van betonbalken. (Dutch with english summary). Stevinrapport 5-74-2/3. 2-72-04. February 1974.
24. BRUGGELING, A. S. G.: Are cracks in partially prestressed concrete permitted? Meeting Budapest F.I.P. Commission "Prestressing Steel and Systems". April 1973.
25. BENNET, E. W., VEERASUBRAMANIAN, N.: Behaviour of non-rectangular beams with limited prestress after flexural cracking. Journal of the ACI (1972) Sept.–(1973) March.

26. BENNETT, E. W., CHANDRASEKHAR, C. S.: Supplementary tensile reinforcement in prestressed concrete beams. *Concrete* (1972) October.
27. HEIMGARTNER-KRAUS-BACHMAN: Langzeitversuche an teilweise vorgespannten Leichtbetonbalken. Bericht ETH-Zürich 6504-5. Oktober 1972.
28. CEDERWALL, K.: Time-dependent behaviour of reinforced concrete structures. Document National Swedish Building Research D3. 1971.
29. BRUGGELING, A. S. G.: Kritische beschouwing van enige grenstoestanden bij gedeeltelijk vorgespannen beton. Tijdschrift der Openbare Werken van België (1973–1974) no. 4.
30. KRÜGER, W.: Kriech und Schwindberechnungen an Stahlbetonplatten im Zustand II. *Bauplanung – Bautechnik* 25 (1974) Heft 6.
31. BACHMAN, H., FLÜCKIGER, P.: 5 Jahresresultate der Langzeitversuche an teilweise vorgespannten Leichtbetonbalken. Bericht ETH-Zürich 6504-7.
32. BRUGGELING, A. S. G.: Time-dependent deflection of partially prestressed concrete beams. Stevinrapport 5-77-1/3. 2-74-12. March 1977.
33. BIRKENMAIER, H.: Berücksichtigung der Einflüsse Kriechen und Schwinden bei der Berechnung von Betonkonstruktionen. Bericht ETH-Zürich 62. Mai 1976.
34. CORLEY, W. G., SOZEN, M. A.: Time-dependent deflections of reinforced concrete beams. Paper 63-17. *Journal of the ACI* (1966) March.
35. STEVENS, R. F.: Deflections of reinforced concrete beams. *Proceedings of the Institution of Civil Engineers (England)* 53 (1972) Sept.; Part 2: Research and Theory.
36. NEVILLE, A. M., DILGER, W.: *Creep of concrete: Plain, reinforced and prestressed*. Amsterdam, North-Holland Publishing Co., 1970.
37. BEDNÁR, J.: Spannungsumlagerung infolge Schwinden und Kriechen in zentrische belasteten Stahlbetonprismen. *Heron* 21 (1976) no. 2 pp. 83–85.
38. PAUW, A., MEYERS, B. L.: Effect of creep and shrinkage on the behaviour of reinforced concrete member. Symposium on creep of concrete; 60th Annual ACI Convention, Houston, Texas, 1964. ACI Special Publication SP-9. pp. 129–158.
39. BAŽANT, Z. P., OSMAN, E., THONGUTHAI, W.: Practical formulation of shrinkage and creep of concrete. *Matériaux et Constructions* 9 (1976) no. 54 pp. 395–406.
40. PAUW, A.: Notes, written on effective modulus method during Sabbatical year at Delft University of Technology (not published).
41. DISCHINGER, F.: Elastische und plastische Verformungen der Eisenbetontragwerke. *Bauingenieur* (1937) nr. 18, (1939) nr. 20.
42. WITTMANN, F. R., ROELFSTRA, R.: Quantitative determination of the total deformation of concrete under load and simultaneous drying. To be published in *Cement and Concrete Research*.
43. SCHADE, D.: Einige eindimensionale Ansätze zur Berechnung des Kriechens und der Relaxation von Betontragwerken. *Beton- und Stahlbeton* 67 (1972). pp. 63–67.
44. ROSEMEIER, G.-E.: Zum zeitabhängigen Spannungs-Dehnungsverhalten von Beton. *Beton- und Stahlbetonbau* 7 (1976), pp. 223-226.

6 Notation

Symbols

A	cross-section
E	Young's modulus
F	prestressing force
I	moment of inertia
M	bending moment
$M_{cr,fl}$	flexural cracking moment
$M_{u,fl}$	ultimate flexural moment
N	normal force
V	shear force
a	distance
b	width of flange
b_0	width of web
c	concrete cover
d	total depth of beam
e	eccentricity of the reinforcement
f	strength
h	effective depth of beam
n	ratio E_s/E_c
k	height of kern
s	distance of stirrups
y	distance from center of gravity of concrete
w	crack width
z	inner lever arm
α	effective equivalent initial reinforcement ratio
ε	strain
ξ	coefficient – see below
η	coefficient – see below
κ	curvature
λ	degree of prestressing
σ	stress
φ	creep coefficient
ω	reinforcement ratio A_s/A_c
$\Delta\sigma$	stress loss in prestressing steel
ρ	reduction factor in creep calculations
\varnothing	diameter of reinforcing bar

Indices

<i>c</i>	compression
<i>c</i>	concrete
<i>cs</i>	concrete shrinkage
<i>i</i>	initial (just before testing)
<i>l</i>	longitudinal normal reinforcing steel
<i>m</i>	average value
<i>p</i>	prestressing steel
<i>r</i>	cracking
<i>s</i>	steel
<i>t</i>	time
<i>u</i>	ultimate
<i>x</i>	refers to uncracked part of concrete section
<i>y</i>	yield
<i>R</i>	reference
0,2	0,2% limit strain
<i>cr</i>	cracked
<i>un</i>	uncracked
0	at zero time
∞	at infinite time
1	upper surface of concrete
2	bottom surface of concrete
'	refers to compression – or shortening

Coefficients

$$\xi = 1 + \frac{A_c \cdot e^2}{I_c} = \frac{\sigma_{cs}}{\sigma_{cm}}$$

$$\alpha = \frac{n\omega}{1+n\omega}$$

$$\eta = \frac{n\omega\xi \cdot \varphi_t}{1+n\omega\xi}$$

$$k = \frac{I_c}{A_c \cdot y_1}, \quad k' = \frac{I_c}{A_c \cdot y_2}$$

$$\lambda = \frac{A_{sp} \cdot f_{0,2}}{A_{sl} \cdot f_y + A_{sp} \cdot f_{0,2}}$$

7 Appendices

Table 1. Reinforcement, theoretical and measured results. All moments are *exclusif* the dead load moment.

beam nr.	A_{st} mm ²	A_{sp} mm ²	λ	theor.			meas.			theor.			meas.		
				F_{Rt} kN	M_{Rt} kNm	M_r kNm	κ_r 10 ⁶ mm ⁻¹	M_y kNm	κ_y 10 ⁶ mm ⁻¹	M_y kNm	κ_y 10 ⁶ mm ⁻¹	M_u kNm	M_{max} kNm		
programme 1	0	186	1	137.9	33.5	47.6	1.61	42.9	1.46	66.6	10.6	66.6	10.7	100.6	103.0
1	57	186	0.93	130.7	31.7	43.3	1.44	45.8	1.57	74.9	11.4	74.9	11.4	107.4	116.5
3	101	186	0.89	126.5	30.6	41.7	1.38	49.0	2.35	82.4	11.8	82.4	11.8	114.0	125.5
4	158	186	0.83	118.2	28.8	40.9	1.38	44.0	1.16	87.9	11.1	87.9	11.1	131.8	134.5
5	201	186	0.78	116.3	28.1	40.6	1.31	43.9	1.21	95.9	11.8	95.9	11.8	137.9	139.0
6	259	186	0.74	112.1	26.9	38.5	1.24	43.7	1.05	100.1	11.5	100.1	11.5	133.1	143.5
7	308	186	0.73	108.2	26.2	38.6	1.21	40.5	1.35	101.1	10.5	101.1	10.5	137.3	143.5
8	359	186	0.69	102.9	24.9	38.7	1.17	42.2	0.63	112.7	11.0	112.7	11.0	145.9	152.5
9	402	186	0.68	101.4	24.9	40.2	1.22	43.7	1.45	116.2	10.7	116.2	10.7	152.5	152.5
10	452	186	0.64	97.1	23.2	34.7	1.11	34.6	0.95	118.6	11.2	118.6	11.2	154.8	157.0
programme 1	1005	-	0	-	-	14.9	1.12	17.4	1.83	87.1	11.7	87.1	11.7	90.9	96.6
2	804	93	0.35	49.4	8.8	22.4	1.77	22.5	1.75	99.7	15.2	99.7	15.2	111.1	114.0
3	534	93	0.45	59.4	10.5	22.8	1.93	24.5	2.90	80.6	15.7	80.6	15.7	86.7	96.5
4	402	93	0.52	60.6	11.8	23.3	2.05	26.0	2.32	69.3	15.0	69.3	15.0	74.8	87.0
5	308	93	0.59	59.5	11.5	22.5	2.04	23.7	1.76	58.8	14.1	58.8	14.1	66.3	75.0
6	402	186	0.69	123.6	23.9	35.0	2.97	42.5	3.32	103.1	19.1	103.1	19.1	113.3	124.5
7	308	186	0.74	130.8	25.1	35.6	3.12	40.5	3.32	91.6	18.7	91.6	18.7	104.8	111.5
8	226	186	0.80	124.7	23.8	34.0	3.06	37.0	2.98	83.1	18.4	83.1	18.4	97.4	107.5
9	101	186	0.90	124.7	23.5	33.2	3.11	36.8	3.08	66.4	18.1	66.4	18.1	86.1	91.6

It isn't possible to notice a measured M_y while the tests are stopped in the beginning of the plastic stage (see Fig. 1.21).

Table 2. Concrete and reinforcement data.

All values are the average of 3 test values.

The tensile strength is calculated from the splitting test.

Sizes: cubes: $150 \times 150 \times 150 \text{ mm}^3$; prisms: $100 \times 100 \times 300 \text{ mm}^3$ (E-modulus).

Creep value: after 28 days $\varphi_t = 2.06$; after 21 days 1.70.

Shrinkage: $\varepsilon_{cs}/\varphi_t = -10^{-4}$.

Relaxation: 1.39% (1.74%).

beam nr.	concrete 3 days			concrete 28 days			hardening conditions			reinforcement		
	cube strength N/mm ²	tensile N/mm ²	E-modulus N/mm ²	cube strength N/mm ²	tensile N/mm ²	E-modulus N/mm ²	R.H. %	temperature °C	failure stress N/mm ²	σ_y N/mm ²	d mm	σ_{p0} N/mm ²
programme 1	1	26.3	2.4	26400	38.3	3.4	35.2±3.8	18.5±3.5	—	—	—	896
	2	22.7	2.2	24500	37.7	2.7	36.2±4.3	19.2±4.2	442	620	6	898
	3	24.5	2.1	25500	40.5	2.6	36.5±4.0	19.2±4.2	469	696	8	898
	4	21.1	2.0	23600	35.3	2.9	36.5±4.0	19.4±3.2	443	627	10	898
	5	24.0	2.2	25200	38.9	2.8	35.8±4.7	19.9±3.7	468	729	8	901
	6	25.0	2.2	25700	38.6	2.5	33.5±6.2	20.0±3.8	456	620	10	899
	7	25.7	2.4	26100	37.5	2.5	31.8±5.7	20.4±4.2	409	558	14	897
	8	23.6	2.4	25000	36.7	2.9	32.8±7.2	21.2±4.5	410	551	16	897
	9	28.6	2.5	27500	39.5	3.0	35.2±4.8	22.1±3.7	425	557	16	900
	10	23.1	1.9	24800	35.2	2.4	37.4±3.9	22.1±3.7	429	597	12	898
programme 2	4 days						21 days					
	1	34.2	—	27300	47.9	3.3	—	—	402	550	16	—
	2	42.3	—	29550	54.5	3.8	—	—	403	545	16	1297
	3	38.5	3.0	28300	50.8	3.9	32700	—	444	595	12	1280
	4	38.9	2.9	—	51.7	3.6	—	—	410	565	14	—
	5	40.2	2.9	—	56.5	3.5	—	35%±5% 20±4	407	560	16	1177
	6	42.3	3.1	—	50.8	3.8	—	—	410	560	14	1068
	7	44.3	3.6	—	52.6	3.8	—	—	423	540	16	1190
	8	45.8	3.4	—	53.5	3.9	—	—	405	540	14	1173
9	41.7	3.5	—	53.2	4.1	—	—	444	595	12	1053	

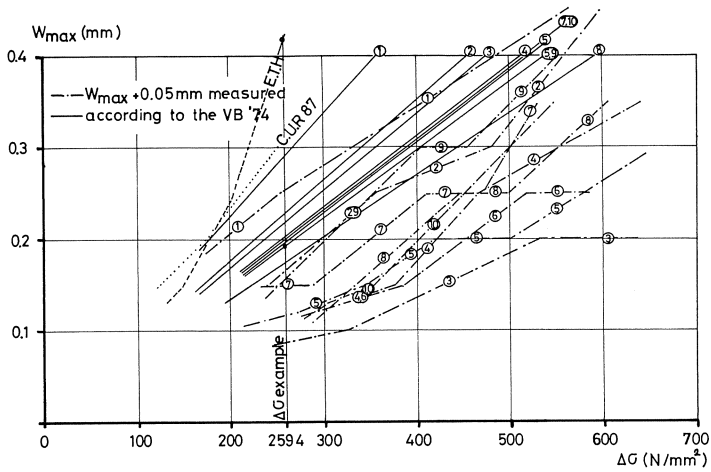


Fig. 1.15. Crack widths of the beams due to $\Delta\sigma$ (prog. 1).

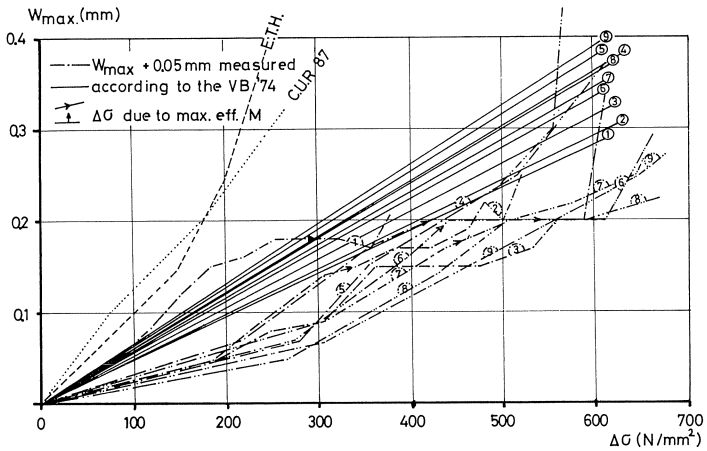


Fig. 1.16. Crack widths of the beams due to $\Delta\sigma$ (prog. 2).

Example of a calculation Beam nr. 9 programme 1.

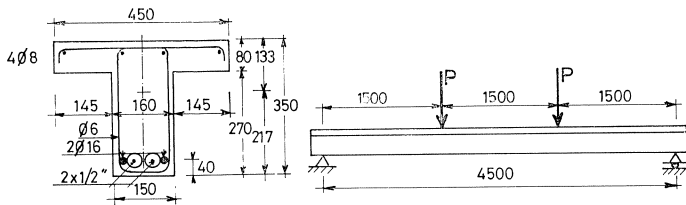


Fig. 1.17. Cross-section and loading scheme.

Main data:

– Cross-section: $d = 350$ mm

$$y_2 = 217 \text{ mm} \quad y_1 = 133 \text{ mm}$$

$$A_c = 77850 \text{ mm}^2$$

$$W = 395 \cdot 10^5 \text{ mm}^3 \quad W' = 642 \cdot 10^5 \text{ mm}^3$$

$$I_c = 856 \cdot 10^5 \text{ mm}^4$$

$$k = 83 \text{ mm} \quad k' = 51 \text{ mm}$$

– Concrete: compression strength: $f_c = 0.8 \times 39.5 = 31.6 \text{ N/mm}^2$, used 30 N/mm^2

tensile strength: $f_t = 1.5 \times 3 = 4.5 \text{ N/mm}^2$, for bending.

The other data are given in Table 2 and in Fig. 1.17.

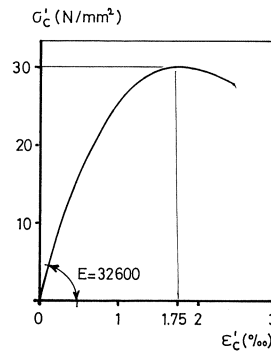


Fig. 1.18. Stress-strain relation of the concrete.

– Reinforcement: $A_{st} = 402 \text{ mm}^2$

$$f_y = 425 \text{ N/mm}^2$$

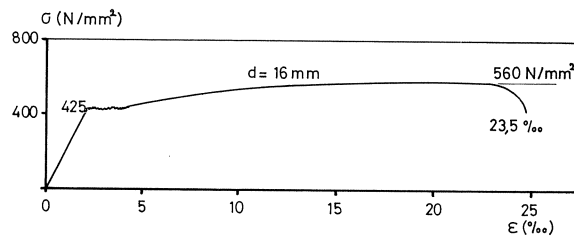


Fig. 1.19. Stress-strain relation of the normal reinforcing steel.

A1.4

- Prestressing: $A_{sp} = 186 \text{ mm}^2$
 $f_{0,2} = 1830 \text{ N/mm}^2$

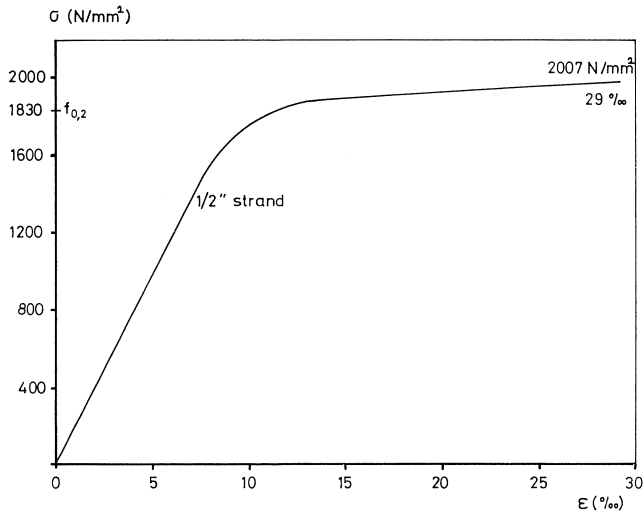


Fig. 1.20. Stress-strain relation of the prestressing steel.

A. Calculation of the uncracked stage

1. Dead load: $g = 25 \times 0.07785 = 1.95 \text{ kN/m}'$
 $M_g = \frac{1}{8} \times 1.95 \times 4,5^2 = 4.93 \text{ kNm}$
2. Inferred data: $M_p = 1.5 \times P$ (see Fig. 1.9)
 $e = 217 - 40 = 177 \text{ mm}$
 $\xi = 3.85$
 $n_3 = 7.64$ (after 3 days) $n_{28} = 6.36$ (after 28 days)
 $\omega_1 = 0.52\% \omega_p = 0.24\% \omega = 0.7\%$
 $n_3 \omega = 0.0581$ $n_{28} \omega = 0.0483$
 $n_3 \omega f = 0.2235$ $n_{28} \omega f = 0.1861$
 $\sigma_{p0} = 900 \text{ N/mm}^2$ (measured)
 $\Delta \sigma = 1.39 \cdot 10^{-2} \cdot 900 = 12.5 \text{ N/mm}^2$

relaxation

$$\eta = \frac{0.2235 \cdot 2.06}{1.2235} = 0.3763 \rightarrow e^{-\eta} = 0.6864$$

$$1 - e^{-\eta} = 0.3136$$

$$\frac{M_g e}{I_c} + \frac{\epsilon_{cst} \cdot E_c}{\varphi_t} = \frac{4.93 \cdot 10^6 \cdot 177}{856 \times 10^6} - 10^{-4} \cdot 27500 =$$


$$= -1.73 \text{ N/mm}^2$$

3. Reference force: $F_{R0} = 186 \cdot (900 - 12.5) = \underline{165100 \text{ N}}$

formula 1: $F_{Rt} = 165100 \cdot 0.6864 - 1.73 \cdot \frac{77850}{3.85} \cdot 0.3136 =$
 $= \underline{102300 \text{ N}}$

formula 2: $M_{Rt} = 102300 \cdot 177 \cdot \frac{3.85}{2.85} = \underline{24.46 \text{ kNm}}$

The stresses due to M_{Rt} are:



$$\sigma_{c1} = - \frac{102300 \cdot 310}{77850 \cdot 177} = -2.30 \text{ N/mm}^2$$

$$\sigma_{c2} = + \frac{102300 \cdot 40}{77850 \cdot 177} = +0.30 \text{ N/mm}^2$$

$$\sigma_l = (102300 - 165100) / (186 + 402) = -106.7 \text{ N/mm}^2$$

$$\sigma_p = \left(102300 + 165100 \cdot \frac{0.52}{0.24} \right) / 558 = +780.8 \text{ N/mm}^2$$

$$\varepsilon_{Rt} = \frac{(102300 - 165100) \cdot 177}{32600 \cdot 856 \cdot 10^6 \cdot 0.2235} +$$

$$+ \frac{4.93 \cdot 10^6 \cdot 0.3136}{32600 \cdot 856 \cdot 10^6 \cdot 0.2235 \cdot 3.85} =$$

$$= \underline{-1.72 \cdot 10^{-6} \text{ mm}^{-1}}$$

4. Decompression Moment: $M_0 = 102300 \cdot 217 \cdot \frac{228}{217 + 0.0483 \cdot 40} = \underline{23.10 \text{ kNm}}$

formula 3

5. Cracking Moment: $M_r = 23.10 + 4.5 \cdot \frac{856 \cdot 10^6 \cdot 0.1861}{217 + 0.0483 \cdot 40} = \underline{43.97 \text{ kNm}}$

formula 4

The stresses due to M_r are the stresses due to

$M_{Rt} + \Delta M$, with $\Delta M = M_r - M_{Rt}$

$\Delta M = 43.97 - 24.46 = 19.51 \text{ kNm}$

$\sigma_{c1} = -2.10 - \frac{19.51 \cdot 10^6 \cdot (133 + 0.0483 \cdot 310)}{856 \cdot 10^6 \cdot 1.1861} =$

$= -2.30 - 2.84 = -5.14 \text{ N/mm}^2$

$\sigma_{c2} = +0.30 + \frac{19.51 \cdot 10^6 \cdot (217 + 0.0483 \cdot 40)}{856 \cdot 10^6 \cdot 1.1861} =$

$= +0.30 + 4.20 = +4.50 \text{ N/mm}^2$



$$\begin{aligned}\sigma_l &= -106.7 + \frac{19.51 \cdot 10^6 \cdot 6.36 \cdot 177}{856 \cdot 10^6 \cdot 1.1861} = \\ &= -106.7 + 21.6 = -85.1 \text{ N/mm}^2 \\ \sigma_p &= +780.8 + 21.6 = +802,4 \text{ N/mm}^2\end{aligned}$$

The measured value of M_r is $43.7 + 4.93 = 48.63 \text{ kNm}$.

$$\begin{aligned}\varkappa_r &= -1.72 \cdot 10^{-6} + \frac{102300 + 4.5 \cdot 1.0483 \cdot 77850}{32600 \cdot 77850 \cdot (217 + 0.0483 \cdot 40)} = \\ &= -0.88 \cdot 10^{-6} \text{ mm}^{-1}\end{aligned}$$

Measured is the curvature due to the moment

$$\Delta M = 43.97 - 4.93 = 39.04 \text{ kNm}$$

$$\varkappa = \frac{39.04 \cdot 10^6 \cdot 1.0483}{32600 \cdot 856 \cdot 10 \cdot 1.1861} = 1.22 \cdot 10^{-6} \text{ mm}^{-1}$$

The difference between the theoretical curvature and the measured curvature $\Delta \varkappa = 2.10 \cdot 10^{-1} \text{ mm}^{-1}$.

The reason for the difference in curvature is that between fabrication of the beam and starting the measurement the beam have already a curvature due to dead load, prestressing, relaxation, shrinkage and creep. For comparison of the results of tests and theory, this difference has to be taken into account.

B. Calculations of the cracked stage

6. Crackwidth control: In this example, the crackwidth is calculated for a chosen value of the depth of the concrete compression zone.

$$\begin{aligned}\text{Take } h_x &= 80 \text{ mm} \rightarrow A_{cx} = 36000 \text{ mm}^2 \\ y_x &= 40 \text{ mm} \\ k'_x &= 13.3 \text{ mm}\end{aligned}$$

formula 6: $h_x = 80 \text{ mm}$ due to a moment M_w :

$$M_w = 102300 \cdot \frac{36000 \cdot 40 \cdot 283.3}{36000 \cdot 40 - 6.36 \cdot 588 \cdot 230} = \underline{72.0 \text{ kNm}}$$

The stress in A_l due to this moment is:

$$\text{formula 7: } \sigma_l = \frac{72 \cdot 10^6}{588 \cdot 283.3} - \frac{165100}{588} = +151.2 \text{ N/mm}^2$$

The stress in A_l due to M_0 is:

$$\sigma_l = -106.7 - 1.5 = -108.2 \text{ N/mm}^2$$

The increase of the stress in A_l from M_0 to M_w is:

$$\Delta\sigma = 151.2 - -108.2 = \underline{259.4 \text{ N/mm}^2}$$

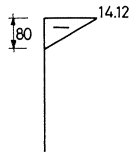
formula 8: Using the E.T.H. relation between $\Delta\sigma$ and w_{\max} :

$$w_{\max} = \sim \underline{0.42 \text{ mm.}}$$

formula 9: Using the Dutch standards $w_{\max} = 0.19 \text{ mm}$.

The measured crackwidth due to $\Delta\sigma = 259.4 \text{ N/mm}^2$ is $\sim 0.16 \text{ mm}$ including a possible fault of 0.05 mm (Fig. 14). The reasonable difference between the theoretical and measured crackwidth has two main reasons:

1. *Tension stiffening*: the (measured) average strain of the reinforcement differs from the strain of the reinforcement in a crack.
2. *Measuring faults*: in measuring of the crackwidth. Due to $M = 72 \text{ kNm}$ the stresses in the concrete are:



$$\sigma_{c1} = -\frac{72 \cdot 10^6 \cdot 80}{36 \cdot 10^3 \cdot 40 \cdot 283.3} = -14.12 \text{ N/mm}^2$$

In the prestressing steel:

$$\sigma_p = 151.2 + 887.5 = +1038.7 \text{ N/mm}^2$$

The curvature is:

$$\kappa = -1.72 \cdot 10^{-6} + \frac{14.12}{32600 \cdot 80} = +3.69 \cdot 10^{-6} \text{ mm}^{-1}$$

7. Yield moment:

M_u is reached as $\sigma_l = 425 \text{ N/mm}^2$

then $\sigma_p = 425 + 887.5 = 1312.5 \text{ N/mm}^2$

$$N_s = A_{sl}f_y + A_{sp}f_{0,2} = 402 \cdot 425 + 186 \cdot 1312.5 = 414975 \text{ N.}$$

If $h_x < 80 \text{ mm}$:

$$N'_c = 414975 \cong \frac{7}{12} h_x b \sigma'_{c1} = 262.5 h_x \sigma'_{c1}$$

The strain of the concrete at the level of the centre of gravity of the reinforcement

$$\frac{\sigma_{c,s}}{E_c} = \varepsilon_{c,s}$$

is *not* the same as the strain of the reinforcement

$$\frac{\sigma_l}{E_s} = \varepsilon_{sl}$$

Due to $M = 72 \text{ kNm}$:

$$\varepsilon_{c,s} = \varepsilon'_{c1} \frac{h-hx}{h_x} = \frac{14.12}{32600} \cdot \frac{310-80}{80} = 1.25\text{‰}$$

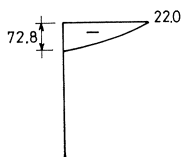
$$\varepsilon_{sl} = \frac{151.2}{210000} = 0.71\text{‰}$$

If $\varepsilon_{sl} = \frac{425}{210000} = 2.02\text{‰}$ then

$$\varepsilon_{c,s} = (2.02 + 1.25 - 0.72)\text{‰} = 2.55\text{‰}$$

$$\varepsilon'_{c1} = \frac{h_x}{h-h_x} \cdot \varepsilon_{ba} = \frac{h_x}{310-h_x} \cdot 2.55\text{‰}$$

ε'_{c1} is so great that the relation between σ and ε is not longer linear. Therefore a semi-parabolic relation is used.



Then is found $\varepsilon'_{c1} = 0.78\text{‰}$, $\sigma'_{c1} = 22.0 \text{ N/mm}^2$ and

$$h_x = 72.8 \text{ mm. } M_u = 414.975 \cdot 0.282 = \underline{117.0 \text{ kNm.}}$$

$$\kappa = -1.72 \cdot 10^{-3} + \frac{0.78 \cdot 10^{-3}}{72.8} = 8.99 \cdot 10^{-6} \text{ mm}^{-1}$$

$$\Delta\kappa = \frac{2.10 \cdot 10^{-6} \text{ mm}^{-1}}{11.09 \cdot 10^{-6} \text{ mm}^{-1}}$$

8. The ultimate stage:

$$z_u = \sim 310 - 20 = 290 \text{ mm (estimated)}$$

formula 10: $A_{sl} \cdot f_u + A_{sp} \cdot f_{0,2} = 402 \cdot 425 + 186 \cdot 1830 = 511230 \text{ N}$

$$M_u = 0.29 \cdot 511.23 = \underline{148.3 \text{ kNm.}}$$

This moment is less than the real moment of failure.

$\varepsilon'_{cu} = 2.5\text{‰}$ is reached if $h_x = 62 \text{ mm}$ and the concrete will fail.

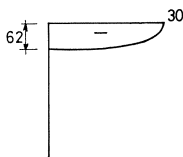
Then $\varepsilon_{sl} = 9.5\text{‰}$ and $\varepsilon_{sp} = 13.7\text{‰}$.

With the stress-strain relation of the reinforcement and prestressing steel the real values of σ_l and σ_p can be taken into account.

$$\text{Then } N'_{cu} = \frac{2}{3} \cdot 62 \cdot 450 \cdot 30 = 558000 \text{ N}$$

$$z_u = 310 - \frac{3}{8} \cdot 62 = 286.7 \text{ mm}$$

$$M_u = 558 \cdot 0.2867 = \underline{160.0 \text{ kNm}}$$



$$\kappa_u = \frac{2.5 \cdot 10^{-3}}{62} = 40.3 \cdot 10^{-6} \text{ mm}^{-1}$$

9. The deflection:

The stiffness in the uncracked stage is:

$$E_c I_0 = 32600 \cdot 856 \cdot 10^6 \cdot \frac{1.1861}{1.0483} = 31.57 \cdot 10^{12} \text{ Nmm}^2$$

The stiffness in the cracked stage is:

$$E_c I_{cr} = \frac{M_e - M_r}{\kappa_e - \kappa_r} = 7.40 \cdot 10^{12} \text{ N/mm}^2$$

$$\frac{E_b I_0}{E_b I_{cr}} = 4.27$$

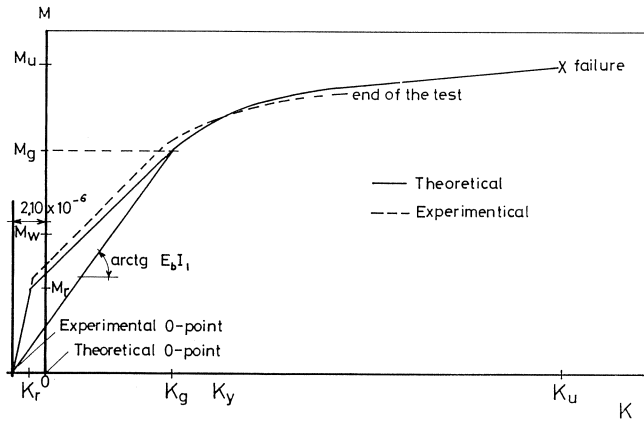


Fig. 1.21. M - κ -diagram (theoretical and measured).

$$E_c I_1 = \frac{M_{\max} E_c I_0}{M_r + (M_{\max} - M_r) \frac{E_c I_0}{E_c I_{cr}}} = \frac{117.0 \cdot 31.57 \cdot 10^{12}}{43.97 + 73.03 \cdot 4.27} = 10.39 \cdot 10^{12} \text{ Nmm}^2$$

A sufficient approximation of the deflection can be found if $E_c I_1$ is taken into account for the whole length of the beam.

Then:

$$\delta_{\max} = \frac{23 M_{\max} \cdot l_t^2}{216 E_c I_1}$$

$$\text{For } M_{\max} = M_u: \delta_{\max} = 24.3 \text{ mm}$$

$$\text{Measured is } \delta_{\max} = 22.4 \text{ mm}$$

It is possible that these results will show little differences with the results in Table 2, because Table 2 is calculated with the *real* beam sizes.

Fig. 2.21

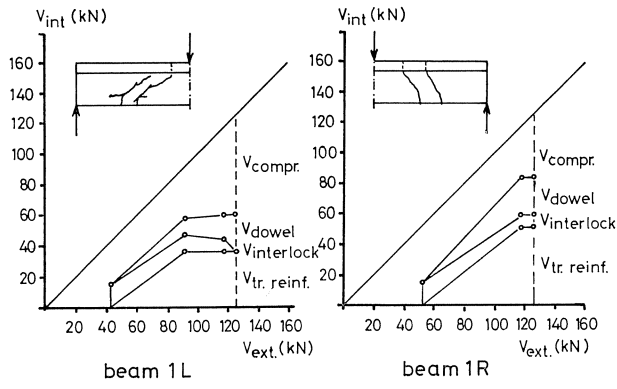


Fig. 2.22

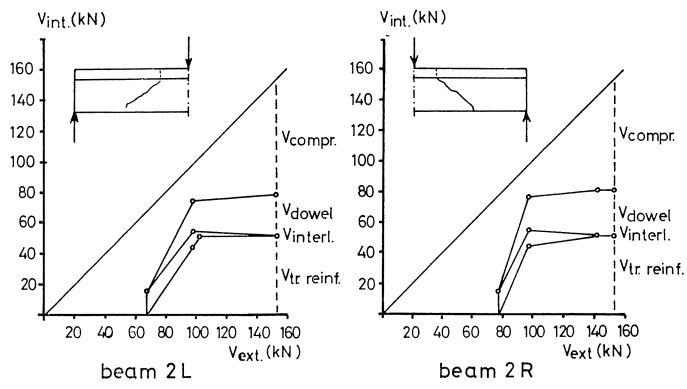


Fig. 2.23

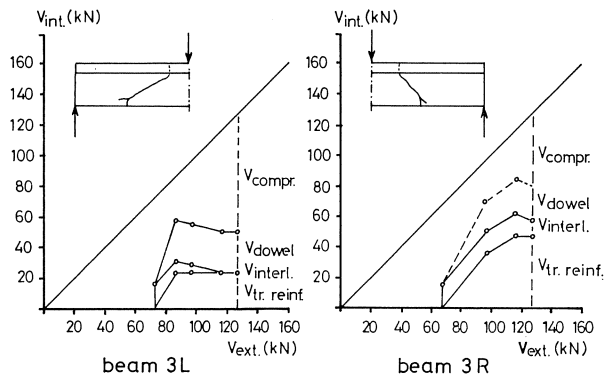


Fig. 2.24

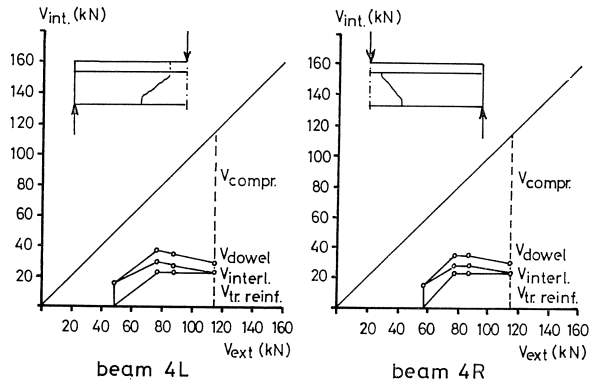


Fig. 2.25

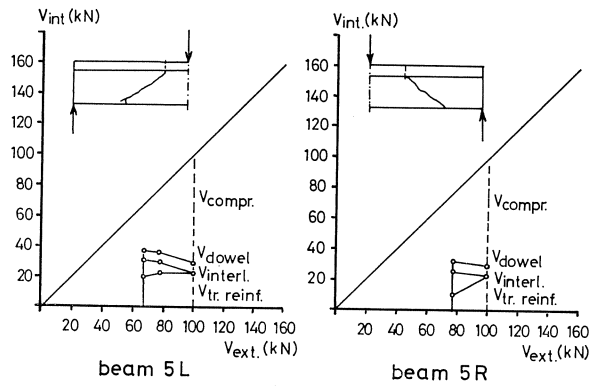


Fig. 2.26

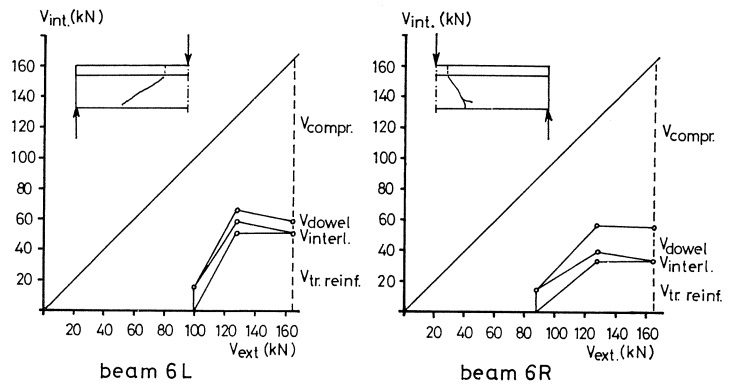


Fig. 2.27

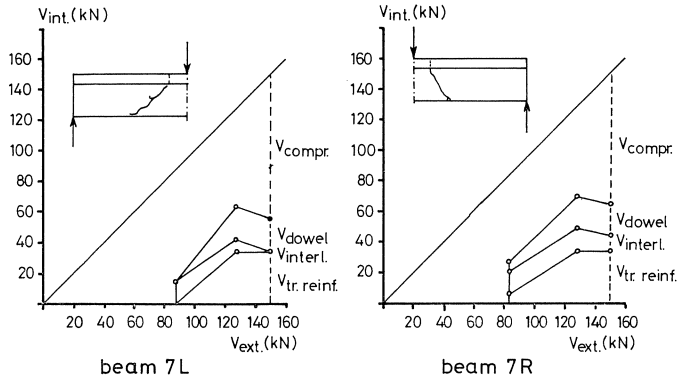


Fig. 2.28

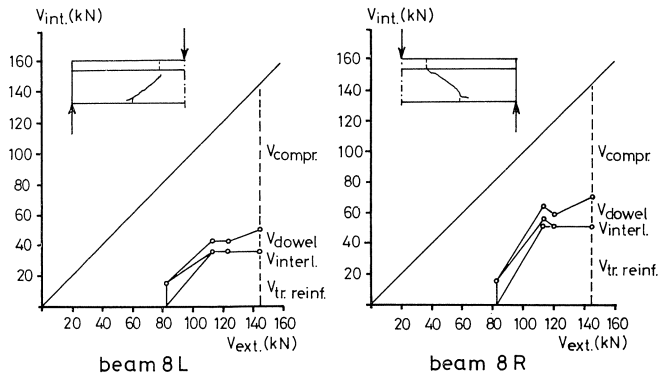
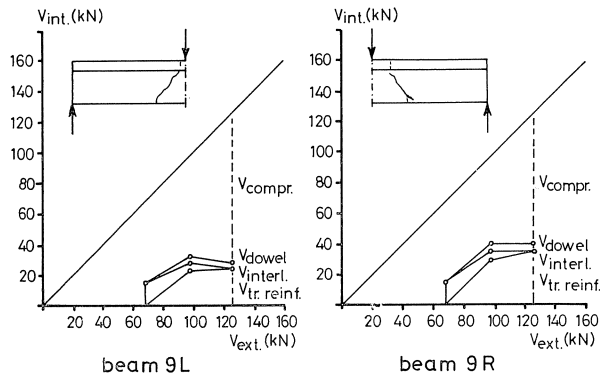


Fig. 2.29



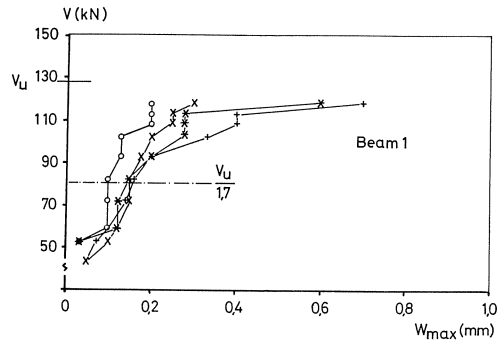


Fig. 2.30

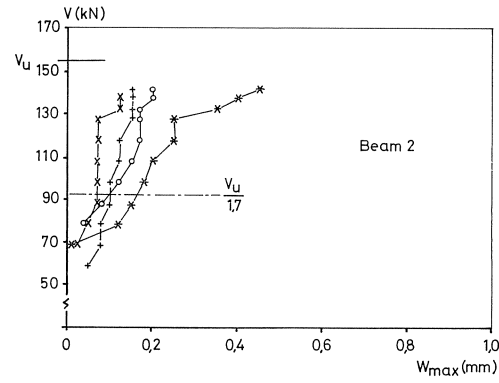


Fig. 2.31

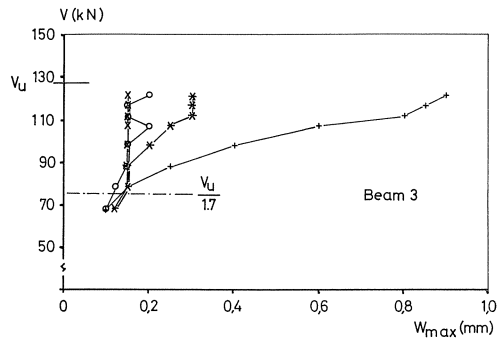


Fig. 2.32

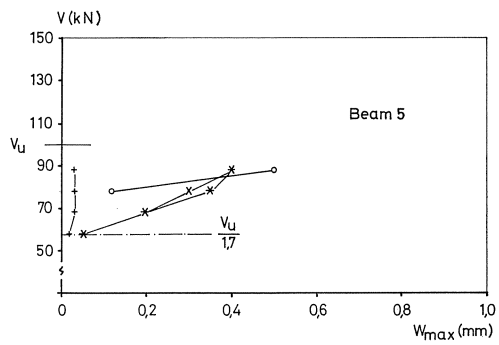


Fig. 2.33

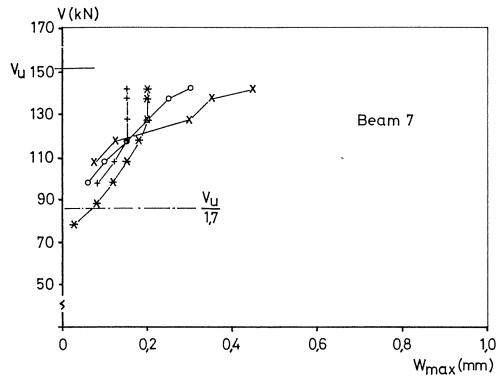


Fig. 2.34

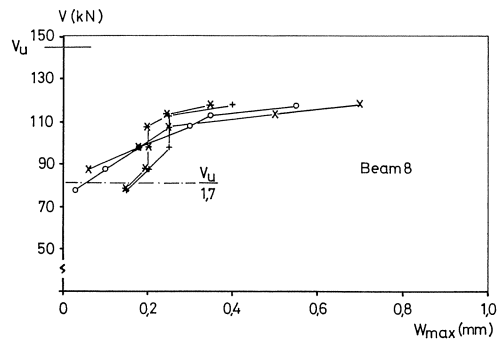


Fig. 2.35

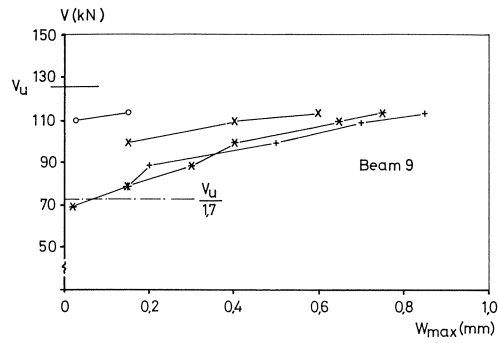


Fig. 2.36

	pour and date			
	I 6-11-74	II 13-11-74	III 20-11-74	IV 6-8-75
Cube strength (C)				
7 days after concreting	22,6	23,1	18,4	19,6
14 days after concreting	28,4	30,4	25,1	25,9
28 days after concreting	36,0	35,7	28,8	30,7
182 days after concreting	44,0	45,8	39,7	37,0
365 days after concreting	41,5	44,7	39,1	39,9
Prism strength (P and P.S)				
14 days	17,8	19,3	15,1	17,2
28 days	22,4	23,4	19,7	21,1
Youngs modulus (P.S)				
14 days	28,2 × 10 ³	30,5 × 10 ³	28,1 × 10 ³	25,5 × 10 ³
28 days	29,7 × 10 ³	32,4 × 10 ³	29,9 × 10 ³	29,3 × 10 ³
182 days				32,8 × 10 ³
Tensile splitting strength (C)				
28 days	27,3	32,7	33,1	39,6

Loss of weight in time in kg/m ³ by evaporation of water		Series P Prism's 150 × 150 × 600 mm				
		7	33	91	182	364
days after loading of columns*						
P ₀	pour I	9,4	18,5	27,7	35,0	41,4
P ₁		10,2	20,1	30,9	39,8	47,9
A		9,7	19,5	29,4	37,9	45,5
B		9,2	18,1	27,4	35,2	47,1
P ₂	pour II	8,0	16,1	24,6	32,1	38,9
P ₃		8,5	16,9	25,7	33,3	40,1
C		9,0	17,8	27,1	34,9	41,9
D		8,7	17,4	26,3	33,9	38,4
P ₄	pour III	12,4	23,1	33,7	42,9	51,3
P ₅		12,5	22,6	33,4	43,0	50,1
E		10,6	20,0	29,9	38,4	46,3
F		10,8	20,8	30,8	39,6	47,1
P ₁₀	pour IV	6,3	17,0	27,7	35,0	43,2
P ₁₁		6,6	17,1	27,3	34,2	42,2
P ₁₂		6,3	17,4	28,2	35,2	42,8
P ₁₃		6,9	17,9	28,7	35,7	43,8
P ₁₄		6,9	18,0	29,0	36,6	44,8
P ₁₅		6,5	17,8	28,8	36,0	44,0
G		6,7	17,9	29,1	36,8	45,2
H		6,5	17,2	28,0	35,2	43,4
I		6,2	16,6	27,0	31,1	42,5
J		6,0	16,2	26,6	33,8	41,7
mean value		8,36	18,36	28,51	36,16	44,07
standard deviation		2,05	1,91	2,24	3,07	3,32
variation coeff.		24%	10%	8%	8%	8%

* During the time between demoulding and loading the specimen were stored in a curing room (95% RH).

Redistribution of stresses – Non loaded prism's $150 \times 150 \times 600$ mm deformations due to shrinkage only

	P ₀	P ₁	P ₂	P ₃	P ₄	P ₅	P ₁₀	P ₁₁	P ₁₂	P ₁₃	P ₁₄	P ₁₅
A_e (meas.)	22786	22809	22811	22561	22183	21450	22670	22717	22859	22608	21915	21442
A_s (theor.)	-	113	201	452	905	1608	-	113	201	452	905	1608
$\omega = A_s/A_e$	-	0,49	0,88	2,00	4,08	7,50	-	0,50	0,88	2,00	4,13	7,50
bars	-	4∅6	4∅8	4∅12	4∅12	8∅16	-	4∅6	4∅8	4∅12	8∅12	8∅16
after loading												
ϵ'_c	0,135	0,088	0,093	0,067	0,083	0,058	0,087	0,095	0,082	0,088	0,050	0,052
σ'_s	-	-18,5	-19,5	-14,0	-17,4	-12,2	-	-20,0	-17,2	-18,5	-10,5	-10,9
σ'_c	-	+0,09	+0,17	+0,28	+0,71	+0,91	-	+0,10	+0,15	+0,37	+0,44	+0,82
91 days												
ϵ'_c	0,223	0,158	0,158	0,133	0,133	0,093	0,170	0,171	0,150	0,153	0,092	0,082
σ'_s	-	-33,2	-33,2	-27,9	-27,9	-19,5	-	-35,9	-31,5	-32,1	-19,3	-17,2
σ'_c	-	+0,16	+0,29	+0,56	+1,14	+1,46	-	+0,18	+0,28	+0,64	+0,78	+1,29
182 days												
ϵ'_c	0,288	0,216	0,206	0,185	0,150	0,108	0,235	0,231	0,208	0,204	0,119	0,106
σ'_s	-	-45,4	-43,3	-38,9	-31,5	-22,7	-	-48,5	-43,7	-42,8	-25,0	-22,2
σ'_c	-	+0,22	+0,38	+0,78	+1,29	+1,70	-	+0,24	+0,38	+0,86	+1,03	+1,66
364 days												
ϵ'_c	0,338	0,263	0,226	0,211	0,183	0,123	0,299	0,291	0,263	0,251	0,154	0,131
σ'_s	-	-55,2	-47,5	-44,3	-38,4	-25,8	-	-61,1	-55,2	-52,7	-32,3	-27,5
σ'_c	-	+0,27	+0,42	+0,89	+1,57	+1,93	-	+0,30	+0,49	+1,05	+1,33	+2,06
calculated values 364 days with the use of test results												
364 days												
D		0,281	0,304	0,270	0,198	0,149		0,275	0,259	0,218	0,161	0,115
T		0,274	0,287	0,255	0,176	0,129		0,267	0,247	0,200	0,141	0,099
E		0,271	0,291	0,248	0,167	0,120		0,264	0,258	0,192	0,133	0,092

	K ₀	K ₁	K ₂	K ₃	K ₄	K ₅	K ₁₀	K ₁₁	K ₁₂	K ₁₃	K ₁₄	K ₁₅
A _c (meas.)	22880	22727	22859	22628	22195	21422	22670	22707	22779	22448	22025	21342
A _s (theor.)	-	113	201	452	905	1608	-	113	201	452	905	1608
ω = A _s /A _c	0	0,49	0,88	2,00	4,08	7,51	-	0,50	0,88	2,01	4,11	7,53
bars	-	4∅6	4∅8	4∅12	8∅12	8∅16	-	4∅6	4∅8	4∅12	8∅12	8∅16
cube strength												
14 days after concr.		28,4		30,4		25,1				25,9		
28 days after concr.		36,0		35,7		28,8				30,7		
6 month's		44,0		45,8		39,7				37,0		
12 month's		41,5		44,7		39,1				39,9		
loading												
	0 days = 14 days after concreting											
N'	175	175	192	212	205	238	230	235	245	255	270	322
ε' _c	0,270	0,261	0,251	0,257	0,247	0,242	0,399	0,401	0,402	0,403	0,403	0,399
σ' _s	-	54,8	52,7	54,0	52,0	50,9	-	84,3	84,5	84,7	84,8	83,7
σ' _c	7,65	7,42	7,94	8,29	7,12	7,29	10,10	9,93	10,10	9,66	8,77	8,78
E _{c0} = $\frac{N'}{A_c \cdot \epsilon'_c} - \frac{A_s}{A_c}$ 210000	283,3	284,3	317,5	323,6	287,6	293,1	253,6	247,6	249,0	239,6	217,1	219,9
	34 days											
ε' _c	0,650	0,618	0,608	0,592	0,544	0,482	0,890	0,932	0,924	0,883	0,726	0,649
σ' _s	-	130,0	127,7	124,4	114,3	101,3	-	195,8	194,1	164,7	152,5	136,3
σ' _c	7,65	7,05	7,28	6,88	4,58	3,51	10,10	9,37	9,04	8,04	5,99	4,81
	91 days											
ε' _c	0,916	0,811	0,780	0,752	0,631	0,594	1,13	1,17	1,13	0,970	0,867	0,751
σ' _s	-	170,3	163,9	157,9	132,7	124,8	-	247,0	238,6	203,8	182,2	157,9
σ' _c	7,65	6,85	6,96	6,21	3,82	1,74	10,10	9,12	8,65	7,25	4,77	3,19
	182 days											
ε' _c	1,09	0,975	0,939	0,886	0,731	0,673	1,27	1,32	1,27	1,06	0,939	0,797
σ' _s	-	204,8	197,2	186,2	153,7	141,5	-	278,1	268,4	224,4	197,4	167,4
σ' _c	7,65	6,68	6,67	5,65	2,97	0,49	10,10	8,96	8,38	6,84	4,15	2,46
	364 days											
ε' _c	1,23	1,12	1,04	0,978	0,824	0,728	1,45	1,47	1,42	1,17	1,01	0,856
σ' _s	-	235,6	219,6	205,6	173,2	153,1	-	309,6	299,9	246,3	213,8	179,9
σ' _c	7,65	6,52	6,47	5,26	2,17	+0,38	10,10	8,81	8,11	6,40	3,47	1,53

(tension!)

unloading at 364 = 0

unloading

deformation at unloading

 E_{cu} calcul.

	$N/mm^2 \times 10^2$	-0,22	-0,23	-0,23	-0,28	-0,66	-0,50	-0,29	-0,31	-0,34	-0,68	-0,80	-0,76
		347,6	324,3	346,7	293,6	cr	cr	349,8	323,3	297,9	cr	cr	cr
ε'_c	0 days	1,01	0,89	0,81	0,70	0,16	0,23	1,16	1,16	1,08	0,49	0,21	0,10
σ'_c	10^{-3}	0	+0,93	+1,50	+2,93	cr	cr	0	+1,21	+2,00	cr	cr	cr
	N/mm^2	1,00	0,86	0,78	0,66	0,09	0,21	1,12	1,11	1,02	0,42	0,16	0,08
ε'_c	1 day	0	+0,90	+1,44	+2,76	cr	cr	0	+1,16	+1,89	cr	cr	cr
σ'_c	10^{-3}	0,99	0,85	0,77	0,65	0,07	0,19	1,11	1,10	1,01	0,40	0,15	0,07
	N/mm^2	0	+0,89	+1,42	+2,73	cr	cr	0	+1,15	+1,87	cr	cr	cr
	14 days	0,98	0,84	0,77	0,64	0,06	0,17	1,11	1,09	1,00	0,39	0,14	0,07
ε'_c	10^{-3}	0	+0,88	+1,42	+2,68	cr	cr	0	+1,14	+1,85	cr	cr	cr
σ'_c	N/mm^2	0,97	0,83	0,76	0,63	0,06	0,15	1,08	1,08	0,99	0,37	0,14	0,06
	28 days	0	+0,87	+1,40	+2,64	cr	cr	0	+1,13	+1,83	cr	cr	cr
ε'_c	10^{-3}												
σ'_c	N/mm^2												

Relationship – Creep – Shrinkage – evaporation of water with time.
 Values 364 days after loading are 100%.

time after loading	K ₀		P _I		K ₁₀		P _{IV}		φ _t	
	ε' _c	ε' _{est}	ev. water	ε' _c	ε' _{est}	ev. water	ε' _{cst}	ev. water	K ₀	K ₁₀
0 days	0%	0%	0%	0%	0%	0%	0%	0%	0	0
1 days	6,0	1,1	3,9	13,0	1,4	3,1	1,4	3,1	0,25	0,33
2 days	16,1	2,4	8,8	17,3	4,9	5,5	4,9	5,5	0,33	0,42
9 (7) days	22,4	13,3	22,8	24,9	10,4	14,7	10,4	14,7	0,65	0,57
14 (12) days	26,4	17,4	29,1	30,7	13,9	21,5	13,9	21,5	0,75	0,70
21 (23) days	34,6	25,3	34,5	39,0	21,7	32,3	21,7	32,3	0,96	0,86
34 (33) days	39,8	35,4	44,6	46,7	29,1	39,4	29,1	39,4	1,02	1,00
56 (63) days	52,2	47,9	55,2	59,1	45,1	53,9	45,1	53,9	1,33	1,21
91 (98) days	67,4	63,6	66,8	69,9	56,9	64,1	56,9	64,1	1,69	1,40
133 days	76,1	77,4	77,0	75,3	66,9	69,6	66,9	69,6	1,86	1,48
182 days	85,5	83,9	84,5	82,9	78,6	81,0	78,6	81,0	2,12	1,59
252 days	94,0	92,4	92,6	93,3	88,0	90,3	88,0	90,3	2,37	1,79
364 days	100	100	100	100	100	100	100	100	2,47	1,89
values 364 days	0,963 × 10 ⁻³	0,305 × 10 ⁻³	41,4 kg/m ³	1,05 × 10 ⁻³	0,299 × 10 ⁻³	43,2 kg/m ³	0,299 × 10 ⁻³	43,2 kg/m ³	-	-

() column K₁₀ and prism P₁₀

Relationship. Creep – shrinkage – loss of weight due to evaporation of water. To determine whether the relationships between creep, shrinkage, loss of weight and time is the same for the three values the relative proportion between

$$\frac{\epsilon'_{ct}}{\epsilon'_{c\ 364}}; \frac{\epsilon'_{cst}}{\epsilon'_{c\ 364}} \text{ and } \frac{\Delta W_t}{\Delta W_{364}}$$

is given. In Fig. 3.12 this relationship is presented graphically.

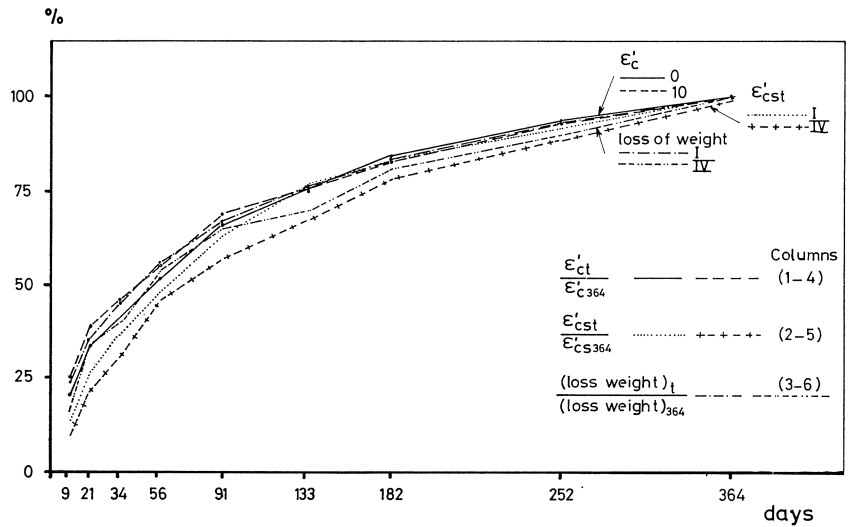


Fig. 3.12

Values of ε'_c measured and calculated with 3 methods. ε'_c values in 10^{-2} .

	K_1	K_2	K_3	K_4	K_5	K_{11}	K_{12}	K_{13}	K_{14}	K_{15}
Loading 0 days										
Measured	261	251	257	247	242	401	402	403	403	399
9 days after loading										
Measured	458	466	446	416	382	749	719	627	604	558
Dischinger	463	443	437	396	361	709	698	665	615	561
Trost	461	441	432	389	353	706	693	656	603	548
Eff. modulus	460	438	429	386	355	704	692	660	598	543
14 days after loading										
Measured	492	498	494	452	396	791	782	677	627	575
Dischinger	498	470	462	427	385	772	759	717	655	589
Trost	496	468	457	418	375	768	751	715	638	572
Eff. modulus	495	465	429	414	376	765	750	708	631	566
21 days after loading										
Measured	544	544	534	484	435	857	843	729	669	604
Dischinger	571	511	499	455	407	841	824	772	696	619
Trost	568	507	492	443	394	835	814	755	674	598
Eff. modulus	566	504	488	438	394	832	811	757	666	589
34 days after loading										
Measured	618	608	592	544	482	932	924	883	726	649
Dischinger	617	574	556	510	448	913	892	830	739	650
Trost	613	569	546	492	429	906	880	808	711	623
Eff. modulus	611	564	541	485	427	902	876	808	700	612
91 days after loading										
Measured	811	780	752	631	594	1170	1130	970	867	751
Dischinger	858	740	704	625	530	1150	1110	1010	871	740
Trost	846	729	685	591	497	1130	1090	974	823	697
Eff. modulus	841	722	675	578	490	1120	1080	968	804	680
182 days after loading										
Measured	975	939	886	731	673	1320	1270	1060	939	797
Dischinger	1010	868	816	705	585	1300	1250	1120	948	791
Trost	997	851	787	658	541	1270	1220	1070	888	739
Eff. modulus	989	841	773	639	530	1270	1200	1060	863	717
271 days after loading										
Measured	1050	995	938	774	698	1410	1370	1130	994	839
Dischinger	1090	918	860	737	608	1390	1340	1190	993	819
Trost	1070	898	826	686	561	1370	1300	1130	924	761
Eff. modulus	1060	887	810	666	548	1350	1280	1110	896	736
364 days after loading										
Measured	1120	1040	978	824	728	1470	1420	1170	1010	856
Dischinger	1140	969	904	773	631	1460	1400	1240	1020	842
Trost	1110	946	865	716	580	1420	1360	1170	953	779
Eff. modulus	1100	934	848	692	565	1420	1340	1150	922	753
Values calculated with $1,2\varepsilon'_{eS\infty}$										
364 days after loading										
Measured	1120	1040	978	824	723	1470	1420	1170	1010	856
Dischinger	1195	1021	948	805	654	1516	1460	1294	1060	872
Trost	1163	996	905	744	600	1485	1417	1221	988	824
Eff. modulus	1153	986	886	719	583	1474	1398	1200	955	779
Values calculated with $E'_c = 32000 \text{ N/mm}^2$; $\varphi_{364} = 2,6$ and $\varepsilon'_{eS364} = 270 \times 10^{-6}$										
Measured	1120	1040	978	824	728	1470	1420	1170	1010	856
Dischinger	1100	1050	940	790	650	1610	1550	1380	1170	970
Trost	1080	1020	880	730	590	1520	1490	1300	1080	890
Eff. modulus	1070	1000	860	700	570	1560	1470	1270	1040	850

Mean values of measured and calculated deformation of loaded columns

time after loading in days	$\frac{\varepsilon'_{bt} - \varepsilon'_{bt=0}}{\varepsilon'_{b\ 364} - \varepsilon'_{bt=0}}$ measured in %	difference between measured and calculated deformations in %		
		Dischinger	Trost	Eff. E modulus
9 days	29	-3,6	-6,6	- 7,4
14 days	34	-2,0	-5,5	- 7,3
21 days	41	-1,6	-5,5	- 6,7
34 days	50	-1,6	-5,5	- 6,7
91 days	71	-2,3	-7,6	- 9,6
182 days	86	-3,1	-9,0	-11,2
271 days	94	-3,7	-9,7	-12,3
364 days	100	-3,3	-9,6	-12,1

A3.9

Table A.4.1.

Concrete strength – Creep and shrinkage values
Beams 2.1 and 2.2

1.1. Concrete compressive strength in N/mm² Testcubes 150³ mm³ after

days	7	28	month 3	6	12
beam 2.1	38,7	48,0	53,3	54,8	58,9
beam 2.2	37,5	47,0	49,5	53,4	53,6
beam 1.1 and 1.2	-	53,2	-	-	59,3

Concrete mix 325 kg Cement per m³
water-cement ratio 0,46

1.2. Shrinkage ε'_{cst}
RH 50% $\pm 2\%$
Temp 20°C $\pm \frac{1}{2}^{\circ}\text{C}$
Values in 10⁻³, after

days	7	28	month 3	6	12
beam 2.1	0,06	0,12	0,21	0,26	0,31
beam 2.2	0,05	0,12	0,20	0,26	0,30

1.3. Creep φ_t Constant compressive stress 9,5 N/mm²
RH 50% $\pm 2\%$
Temp 20°C $\pm \frac{1}{2}^{\circ}\text{C}$

days	7	28	month 3	6	12
beam 2.1	0,49	0,80	1,27	1,58	2,12
beam 2.2	0,37	0,78	1,43	1,85	2,09
	$\frac{\varepsilon'_{cst}}{\varphi_t}$ in 10 ⁻³				
beam 2.1	0,122	0,150	0,165	0,165	0,146
beam 2.2	0,135	0,154	0,140	0,141	0,144

A3.9/A4.1

Table A.4.2. Cracks in the tensile zone

beam	duration of sustained loading	shrinkage shortening over that period	cracks in the tensile zone	bending moment at midspan
1.1	361 days	$0,365 \times 10^{-3}$	no	15.0 kNm
1.2	361 days	$0,365 \times 10^{-3}$	45	15.8 kNm
2.1	686 days	$0,320 \times 10^{-3}$	17	15.5 kNm
2.2	524 days	$0,281 \times 10^{-3}$	6	15.5 kNm

Table A.4.3. Beam 1.1 – Pretensioned

Deformations measured from start of prestressing till start of measurements under sustained load.

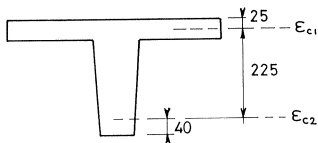
Shrinkage $\epsilon'_{cs} = -5,0 \times 10^{-5}$
 $\epsilon_{c1} = -15,7 \times 10^{-5}$
 $\epsilon_{c2} = +3,3 \times 10^{-5}$
 $\kappa_{mid} = 0,84 \times 10^{-6} \text{ 1/mm}$
 $\delta_{mid} = -1,87 \text{ mm}$

Stresses at start of measurements $\sigma'_{c1} = +1,0 \text{ N/mm}^2$ $\sigma'_{c2} = -6,7 \text{ N/mm}^2$ $F = 108,8 \text{ kN}$
 (Fig. 4.11).

Development of deformations under constant load. $M = 14,94 \text{ kNm}$

time days	$\epsilon'_{cs} \times 10^{-5}$	$\epsilon'_{c1} \times 10^{-5}$	$\epsilon'_{c2} \times 10^{-5}$	$\kappa_{mid} \times 10^{-6} \text{ 1/mm}$	$\delta_{mid} \text{ mm}$	$f/\kappa \text{ 10}^6 \text{ mm}^2$
0	0	0	0	0	0	
18	-9,0	-13,0	-4,8	0,36	0,69	1,9
75	-21,7	-27,7	-15,7	0,53	0,95	1,8
166	-29,8	-35,8	-22,7	0,59	0,85	1,4
229	-31,7	-38,0	-26,3	0,53	0,76	1,4
286	-35,5	-42,5	-28,5	0,50	0,68	1,4
361	-36,5	-42,0	-30,6	0,42	0,48	1,1

Beam loaded with tiles – loading frame supported by rollers.



Graphical display ϵ_{c1} , ϵ_{c2} and ϵ'_{cs} on Fig. 4.11.

Table A.4.4. Beam 1.2 – reinforced concrete

Deformations measured from start of prestressing beam 1.1 till start of measurements under sustained load.

Shrinkage: $\epsilon'_{cs} = -5,0 \times 10^{-5}$
 $\epsilon_{c1} = -19,3 \times 10^{-5}$
 $\epsilon_{c2} = +16,5 \times 10^{-5}$
 $\kappa_{mid} = 1,59 \times 10^{-6} \text{ 1/mm}$
 $\delta_{mid} = 5,02 \text{ mm}$

Stresses at start of measurements $\sigma'_{c1} = -4 \text{ N/mm}^2$ $\sigma_s = +178 \text{ N/mm}^2$ (Fig. 4.10)

Development of deformations under constant load. $M = 14,94$ kNm

time days	ε'_{cs} $\times 10^{-5}$	ε_{c1} $\times 10^{-5}$	ε_{c2} $\times 10^{-5}$	κ_{mid} $\times 10^{-6}$ 1/mm	δ_{mid} mm	f/κ $\times 10^6$ mm ²
0	0	0	0	0	0	–
18	– 9,0	–15,5	–0,2	0,68	2,30	3,4
75	–21,7	–31,7	–4,0	1,23	4,25	3,5
166	–29,8	–40,3	–6,0	1,53	5,32	3,5
229	–31,7	–43,3	–6,8	1,63	5,58	3,4
286	–35,5	–45,7	–7,2	1,71	5,84	3,4
361	–36,5	–47,8	–7,8	1,74	5,93	3,4

Beam loaded with tiles – loading frame, supported by rollers.
Graphical display ε_{c1} , ε_{c2} and ε'_{cs} on Fig. 4.11.

Table A4.5. Beam 2.1 – Grouted duct – bounded tendon.

Deformations measured from prestressing till start of measurements under sustained load.

Shrinkage: $\varepsilon'_{cs} = - 3,1 \times 10^{-5}$
 $\varepsilon_{c1} = -12,5 \times 10^{-5}$
 $\varepsilon_{c2} = - 1,7 \times 10^{-5}$
 $\kappa_{mid} = - 0,39 \times 10^{-6}$ 1/mm
 $\delta_{mid} = + 0,40$ mm

Stresses at start of measurements $\sigma'_{c1} = -1,6$ N/mm² $\sigma'_{c2} = 0$ (cracked) $F = 64,6$ kN

Development of deformations under constant load. $M = 15,48$ kNm (14,80 kNm)

time days	ε_{kr} $\times 10^{-5}$	ε_b $\times 10^{-5}$	ε_0 $\times 10^{-5}$	κ $\times 10^{-6}$ 1/mm	f mm	f/κ $\times 10^6$ mm ²
0	0	0	0	0	0	–
7	– 4,5	– 4,7	+ 0,5	0,23	0,64	2,8
18	– 7,7	–10,0	– 0,3	0,43	1,07	2,5
35	–11,7	–14,8	– 1,8	0,58	1,51	2,6
72	–16,2	–20,8	– 5,3	0,69	1,69	2,4
beam replaced in new loading frame, therefore discontinuity in deflexion values δ_m possible						
114	–20,5	–23,8	– 8,5	0,68	2,02	3,0
150	–22,7	–26,3	–10,5	0,71	2,22	3,1
240	–24,0	–27,2	–12,8	0,64	1,91	3,0
317	–27,4	–28,7	–14,0	0,65	2,00	3,1
394	–28,9	–29,8	–14,7	0,68	2,05	3,0
533	–29,2	–30,7	–14,2	0,73	1,86	2,5
686	–32,0	–31,3	–15,3	0,71	1,93	2,7

Graphical display of relationship ε_{c1} , ε_{c2} and ε'_{cs} on Fig. 4.11.

Table A4.6. Beam 2.2 – non grouted duct – unbonded tendon.

Deformations measured from prestressing till start of measurements under sustained load.

Shrinkage: $\varepsilon'_{es} = - 4,2 \times 10^{-5}$
 $\varepsilon_{c1} = -11,3 \times 10^{-5}$
 $\varepsilon_{c2} = - 5,2 \times 10^{-5}$
 $\kappa_{mid} = 0,27 \times 10^{-6} \text{ 1/mm}$
 $\delta_{mid} = + 0,65 \text{ mm}$

Stresses at start of measurements $\sigma'_{c1} = -3,9 \text{ N/mm}^2$ $\sigma'_{c2} = 0$ (cracked) $F = 69,9 \text{ kN}$

Development of deformations under constant load. $M = 15,48 \text{ kNm}$.

time days	ε_{kr} $\times 10^{-5}$	ε_b $\times 10^{-5}$	ε_0 $\times 10^{-5}$	κ $\times 10^{-6} \text{ 1/mm}$	f mm	f/κ $\times 10^6 \text{ mm}^2$	F kN
0	0	0	0	0	0	–	69,9
10	– 3,9	– 7,0	– 0,2	0,33	0,97	2,9	
31	– 8,6	–14,2	– 1,0	0,59	1,51	2,6	
45	–11,0	–17,2	– 2,3	0,66	1,68	2,5	
73	–14,6	–20,8	– 4,0	1,02	1,87	1,8	67,7
155	–20,8	–27,3	– 8,3	1,12	2,03	1,8	66,6
243	–23,8	–30,0	–10,5	1,14	2,00	1,8	65,8
279	–23,2	–29,2	–10,0	1,13	1,87	1,7	65,5
370	–26,1	–32,4	–12,2	1,17	2,62	1,4	
524	–28,1	–33,9	–13,8	1,16	2,55	2,2	

Graphical display ε_{c1} , ε_{c2} and ε'_{es} on Fig. 4.11.

Table A4.7.

beam	M_u ultimate bending moment	type of failure
1.1	56,9 kNm	rupture compression zone
1.2	46,4 kNm	yielding of reinforcement
2.1	54,4 kNm	yielding of reinforcement
2.2	39,8 kNm	rupture of normal reinforcement